Mechanistic Studies into Interfacial Interactions via Chemical Vapor Deposition Polymerization

by

Xiaoyang Zhong

A dissertation submitted in partial fulfillment
of the requirements for the degree of
Doctor of Philosophy
(Materials Science and Engineering)
in the University of Michigan
2023

Doctoral Committee:

Professor Joerg Lahann, Chair
Professor Zhan Chen
Professor Jinsang Kim
Professor Anish Tuteja

Xiaoyang Zhong

xyzhong@umich.edu

ORCID iD: 0000-0003-1259-8452

Acknowledgments

This work would not be possible without the support and inspiration of many talented people. Firstly, I would like to thank my research advisor, Professor Joerg Lahann, for granting me opportunities, support, patience, and guidance to conduct research. From him, I have learned more than experimental work. He taught me how to nurture entrepreneur ideas, develop collaborations and be creative as a scientist and an engineer. I would like to also thank Dr. Jeffery Raymond, my life mentor. Jeff not only taught me how to scientifically think, how to present my works and ideas, and to aspire towards the best of what I can do, but also cheered for my success and pointed out the direction for my future. I am so grateful to have him as a mentor and a friend. Furthermore, I would like to thank my committee members, Professor Zhan Chen, Professor Anish Tuteja, and Professor Jinsang Kim, who shaped my dissertation by inspired discussions.

In addition, I would like to express my thanks to many people with that I had the pleasure to work over the past five years. I would like to specifically thank my Intel mentors, Jiun-Ruey Chen and Rob Jordan, who have given me many opportunities to experience industrial projects and thoughts during my time in graduate school. I would like to thank Jeffrey Horowitz, my first collaborator, for his help and patient on not only the collaboration project but also many of my works. I would also like to thank Merjem Mededovic who has allowed me to branch my skills out into a different area. She is a wonderful collaborator, who is hardworking, and efficient.

Moreover, I would also like to thank all the amazing Lahann lab members for their support and encouragement throughout my PhD. In particular, I would like to thank Albert Chang for being

a great friend and office mate who encouraged me when I felt defeated. I am grateful to have built valuable friendships with Ava Mauser, Isabel Waibel, Dr. Michael Triebwasser, Arit Patra, Yuxuan Deng, Chris Kim, Fjorela Xhyliu, Dr. Seongjun Moon, Anthony Berardi, Julio Zelaya, Josh Flint, Yao Yao, John Kim, and Zane Zhang. Thank you for all the support, encouragement, and cheer during my interview, data meeting, and defense. I would also like to thank Prof. Yeongun Ko for being an old brother, a great friend, and a wonderful research mentor. It has been such a joyful and rewarding journey to be in Lahann lab with all of you. I would like to thank Jieming Fu, who worked with me during her summer visit in Lahann Lab. I would also like to thank the Lahann lab at Karlsruhe Institute of Technology, especially Dr. Meike Konig, Katharina Cu, Marvin Klaiber, Dr. Tahereh Mohammadi Hafshejani, Martina Plank, Bahar Dadfar and Safoura Vaez.

On a personal note, I would like to express my thanks to my best friends, Yu Zhao, Zhongning Tang, Qian Cao, Hankun Jin, and many others for their invaluable support over the past years. Most importantly, I would like to express my sincere gratitude to my parents, Hui Zhong and Lei Wang, for their unconditional love, care, and support. My deepest thanks to my loving family, my grandma Bizhen Chen, my aunts Ning Wang, Yanmei Xu, and Xiaohong Yang, and uncles Ying Zhong, Jian Zhong, and Zhongwei Chen, and my cousins Xiaoyu and Bailin Zhong. To my beloved grandma Guiqin Jin and grandpas Shouxian Zhong and Chenjian Wang, I will always miss you. I would also like to thank my boyfriend, Chris Kim, for everything he has done for me. I will always treasure and cherish every second I spend with you. Last but not least, my lovely cats, Fanta and Coke, thanks for all the joy you bring to me.

Table of Contents

List of Tables

List of Figures

List of Schemes

List of Acronyms

CVD	Chemical Vapor Deposition
FT-IR	Fourier transform infrared spectroscopy
XPS	X-ray photoelectron spectroscopy
STEM	Scanning transmission electron microscopy
AFM	Atomic force microscopy
ASD	Area-selective deposition
ALD	Atomic layer deposition
PPX	Poly-para-xylylene
PCP	[2.2]paracyclophane
PEGMA	Polyethylene glycol methacrylate
PDMS	Polydimethylsiloxane
ATRP	Atom transfer radical polymerizations
OVJP	Organic vapor jet printing
VTE	Vacuum thermal evaporation
DBP	Dibutyl phthalate
CBP	4,4′-Bis(N-carbazolyl)-1,1′-biphenyl
ECM	Extracellular matrix
PBS	Phosphate-buffered saline
μCP	Microcontact printing

Cx43	Connexin-43
GFP	Green Fluorescence protein
MSCs	Mesenchymal stem cells

Abstract

Chemical vapor deposition (CVD) polymerization is a widely used fabrication method for preparing substrate-independent thin film polymer coatings for a broad range of applications. Functional poly(*p*-xylylene) (PPX) coatings are specific examples of CVD polymer coatings, and they can be applied for surface functionalization and bio-conjugation. The first portion of this dissertation serves to explore the fundamental mechanism of area-selective CVD polymerization, which has a high potential to be utilized as one of the bottom-up processes. In this dissertation, we report a systematic study into the impact of thermodynamic processes on the area-selectivity of chemical vapor deposition (CVD) polymerization of functional [2.2]paracyclophanes (PCP). Adhesion mapping of pre-closure CVD films by atomic force microscopy (AFM) provided a detailed understanding of the geometric features of the polymer islands that form under different deposition conditions. Our results suggest a correlation between interfacial transport processes, including adsorption, diffusion, and desorption, and thermodynamic control parameters, such as substrate temperature and working pressure. This work culminated in a kinetic model that predicted both area-selective and non-selective CVD parameters for the same polymer/substrate ensemble (PPX-C + Cu). These findings are corroborated by STEM results indicating extensive reorientation of continuous CVD thin films on deposition-prohibited substrates at temperatures above 120 ^{o}C. Moreover, deposition on patterned substrates (Ru patterns on Si substrates) suggests that the area-selectivity is not affected by the surface geometry of hybrid substrates, such as the structure of patterns and feature/spacing sizes of patterns, supporting the application of area-selective CVD polymerization on 3-D materials. While limited to a focused subset of CVD

polymers and substrates, this work provides an improved mechanistic understanding of area-selective CVD polymerization and highlights the potential for thermodynamic control in tuning area-selectivity. The second portion of this dissertation serves to extend the use of CVD-based reactive PPX coatings as a surface modification strategy to enhance biomolecule and biomaterial interaction. In this dissertation, we report a precise cell attachment method using CVD-initiated atom transfer radical polymerizations (ATRP), which provides a convenient access route to controlled radical polymerization on a wide range of different materials, to grow polyethylene glycol methacrylate (PEGMA) polymer brushes. This antifouling material shows the resistance of both protein and cell, promoting a high yield of cell attachment to the targeted sites. Moreover, this dissertation also demonstrates the use of CVD-based co-polymer coatings as intermediate layers to immobilize multiple biomolecules on substrates. CVD copolymer coating with designed functional groups was deposited on the biomaterial surface to selectively conjugate both viral vectors and peptides through chemical reactions. The ability to tether lentiviral vectors together with a mesenchymal stem cell (MSC)-binding peptide enhances cell communication among MSCs and increases cell binding and differentiation, providing a safe and efficient gene therapy delivery strategy.

Chapter 1 Introduction

The materials shown in this section were adapted from the following peer-reviewed journal article with permission:

- Mohammadi Hafshejani, T., **Zhong, X.**, Kim, J., Dadfar, B., Lahann, J., "Chemical, biological and topological control of surfaces using functional parylene coatings". Organic Materials 2022, under review.

1.1 Background of CVD Polymerization

Chemical vapor deposition (CVD) was first developed to produce inorganic thin films and materials and applied to industrial production.[1] Recently, CVD has been shown to have a high potential for creating and engineering polymer thin films.[2], [3] Back in the 1960s, the polymerization of functional poly-*p*-xylylene (PPX) via CVD was first developed by Gorham.[4] After that, this method has been widely used to develop reactive polymer coatings for biosensors,[5] energy storage,[6] photovoltaics,[7] and advanced printing,[1] due to the fact that CVD polymerization is a solvent-free and low-temperature/pressure process to form pinhole-free, ultra-thin, and conformal polymer layers. Moreover, the large library of substituted [2,2]paracyclophane (PCP) (PPX precursors) enables a diverse range of surface modifications with high chemical specificity, as shown in Scheme 1-1.[8] These functional groups also enable the widespread use of CVD polymers in biomaterials design to immobilize different biomolecules by controlling the biological response to specific biomaterials.[8]–[11]

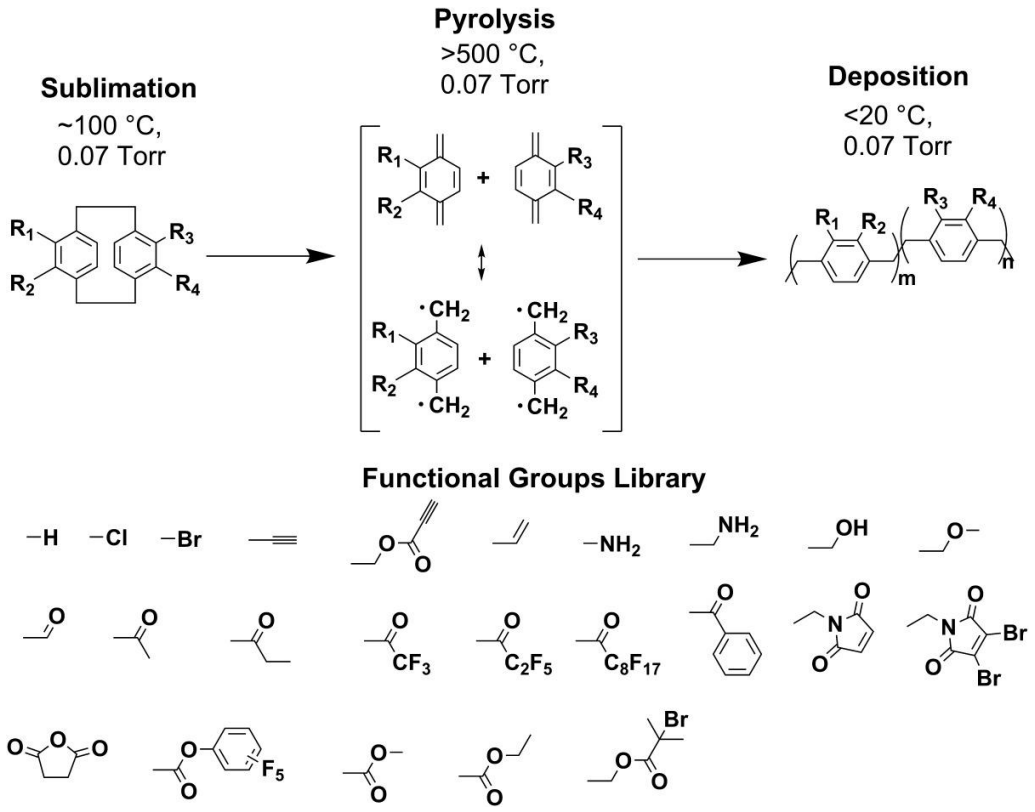

Scheme 1-1**:** Scheme for the CVD polymerization process of different functionalized [2.2]paracyclophanes and the established and constantly updating functional group library. The functionalized [2.2]paracyclophanes (the precursors or dimers) sublimate around 100°C in vacuum, flow with the argon carrier gas to the pyrolysis zone (>500°C) and break into radicals. The radicals adsorb on the substrates placed on the cooled deposition stage (<20°C) and form the functionalized polymer coatings. Reproduced from [8] with permission. (Copyright 2014 Wiley Periodicals, Inc.)

1.2 Area-selective Deposition in CVD Polymerization

As summarized above, CVD polymerization is an essential fabrication process of conformal thin films. Recently, area-selective deposition was found in CVD polymerization, offering another possibility for the formation of nanostructures.

In order to generate arrays of nanoscale features at high densities, a lot of methods are developed to perform multiple stages of surface preparation and treatment. Microcontact printing (μCP) is one of the most commonly exploited patterning methods, which uses elastomers with designed patterns to stamp reactive substances on polymer-modified substrates.[12] Another common patterning technique is by applying a photomask to vapor deposit polymer films on ideal substrates. Both of these two methods are based on photo- or soft-lithographical methods.[12], [13] However, due to the limitation of photomasks or elastomeric stamps, these techniques are limited to conventional two-dimensional surfaces.[14]

Nanolithography,[15] e-beam lithography,[16] and two-photon laser[17] are combined with vapor-deposited polymer films to achieve micro- or nanostructures on substrates with complex geometry. This is because vapor-deposited polymer films have the advantages of conformal coverage, controllable ultra-thin (<20nm) thickness, pinhole-free, and tunable topology and chemistry.[1], [18] They are not only applied to the patterning process on three-dimensional structures but also widely used in electronics as a tunable organic dielectric layer,[19] or biotechnology for localized surface modification[20]. However, these processes suffer from being expensive, time-consuming, chemically demanding on the environment, material wastes, and hazardous.

To this extent, ASD is a more appropriate strategy for pursuing this goal.[21], [22] Gladfelter quantified selectivity for area-selective CVD with Equation 1-1.[23]

$$S = \frac{\theta_1 - \theta_2}{\theta_1 + \theta_2} \quad (1\text{-}1)$$

Instead of using the number of nuclei on the surface, Gladfelter used the easy-measured nuclei coverage to compare the preference of deposition during initial deposition. By comparing the deference between the nuclei coverage on surface 1, θ_1, and surface 2, θ_2, the overall selectivity, S, can be defined.

Vaeth and Jensen found that Iron and its salt have important implications for the prevention of poly(*p*-phenylene vinylene) (PPV) polymerization on the substrate surface during CVD, by controlling polymer nucleation and propagation steps of monomer.[24] They further expanded the polymerization inhibition to transition metals, transition metal salts, and organo-transition metal complexes.[25] PPX-N and PPX-C, as the most common PPX CVD polymers, also have area-selective deposition properties. Suh et al. combined μCP with selectively deposited CVD polymerization to perform nano-scale structures.[26] Their methods (Figure 1-1A) consist of fabricating PDMS stamps with photolithographic-made structures, depositing inhibitor layers with titanium and iron films only on flat top and bottom surfaces via e-beam evaporation, and depositing PPX by means of CVD polymerization. The PPX was only deposited on the walls of PDMS stamps because of the inhibition of iron. Further, SEM (Figure 1-1B) measurement was utilized to identify the high aspect ratio structures. The technical usefulness of the modified stamp was further tested using μCP, Figure 1-1C and D demonstrate successful pattern transfer.

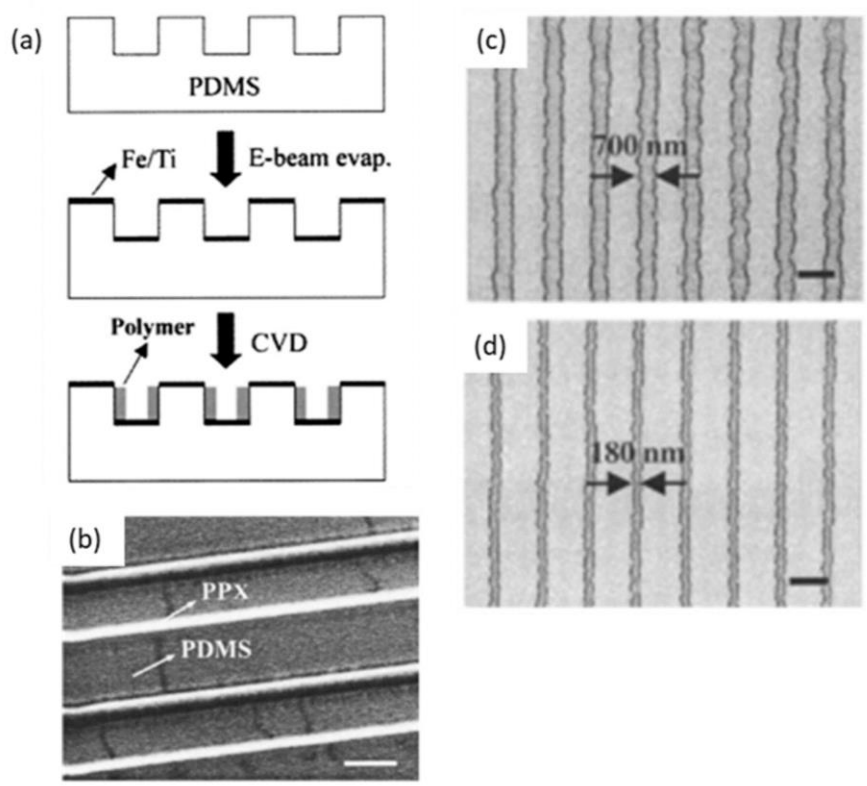

Figure 1-1: (a) A schematic diagram of the experimental procedure. (b) An SEM image of a PDMS stamp with a selectively grown PPX film along the sidewall. Note the sharp difference in colors between PDMS and PPX. The lateral thickness of the PPX layer is 100 nm, which gives an increased aspect ratio of 1.9. The bar scale indicates 500 nm. (d)-(e) SEM images of Au lines obtained by μCP onto a gold substrate followed by wet etching. The bar scales indicate 1 μm. Reproduced from [26] with permission. (Copyright 2003 American Institute of Physics)

Chen et al. systemically investigated the selective inhibition of CVD polymerization by a series of metals, as shown in Figure 1-2.[27] They extended the selective inhibition to reactive polymer coatings, such as functionalized PPX. For substituted PPX containing oxygen or nitrogen, no area-selective property was found on transition metals. It suggested attractive interaction between the metal and the heteroatoms due to the chelation effect. Moreover, not all metals showed selectivity with the same polymer, which indicated the inhibition of polymer deposition occurred only on substrates with high surface energy. This may be because the high surface energy

deactivates the reactive monomer species that are absorbed on the surface and prevents further initiation and propagation for polymer form.

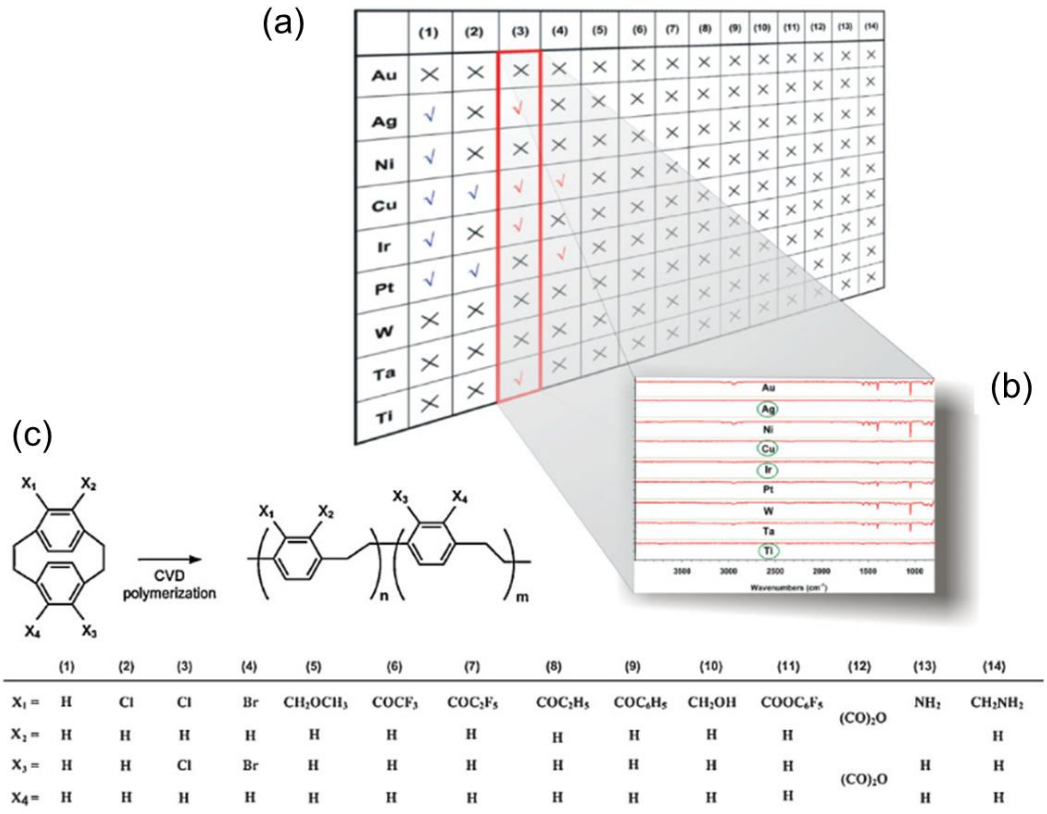

	(1)	(2)	(3)	(4)	(5)	(6)	(7)	(8)	(9)	(10)	(11)	(12)	(13)	(14)
X_1 =	H	Cl	Cl	Br	CH_2OCH_3	$COCF_3$	COC_2F_5	COC_2H_5	COC_6H_5	CH_2OH	$COOC_6F_5$	$(CO)_2O$	NH_2	CH_2NH_2
X_2 =	H	H	H	H	H	H	H	H	H	H	H			H
X_3 =	H	H	Cl	Br	H	H	H	H	H	H	H	$(CO)_2O$	H	H
X_4 =	H	H	H	H	H	H	H	H	H	H	H		H	H

Figure 1-2: (a) Inhibition behavior of nine different metals (Au, Ag, Ni, Cu, Ir, Pt, W, Ta, and Ti) for poly-p-xylylenes deposited via CVD polymerization. (b) Typical spectra for poly(dichloro-p-xylylene) (3) on Au, Ag, Ni, Cu, Ir, Pt, W, Ta, and Ti. The spectra are dominated by characteristic C–Cl stretches at 1030–1100 cm^{-1}, which were present on Au, Ni, Pt, W, and Ta surfaces, but not on Ag, Cu, Ir, or Ti surfaces. (c) Schematic illustration shows the CVD polymerization process of [2.2]paracyclophanes that yields nonreactive (1–4) as well as reactive (5–14) poly-p-xylylenes. Reproduced from [27] with permission. (Copyright 2008 WILEY-VCH)

Besides, Chen et al. first reported a deposited reactive CVD coating, functionalized PPX (poly[4-vinyl-*p*-xylylene-*co*-*p*-xylylene]), which selectively inhibited by the presence of Titanium, and demonstrated its reactivity in cross-metathesis reactions.[27] With its functional groups, this

selectively deposited reactive coating may provide an extremely simple patterning method of micro- and nano-structured bio-interfaces.

1.3 Kinetic Model of CVD Polymerization

Poly(*p*-xylylene) CVD is the process of depositing molecules onto a substrate, typically via physisorption or simple collision. This can be done with the intent to initiate further chemistry after physical contact with the substrate, either with the substrate itself or with other molecules on the substrate. Physisorption first drives the gas-phase reactive monomers to be adsorbed on the substrate surface, then chemisorption happens after overcoming an energy barrier.[28] Specifically, CVD polymerization is the process by which activated monomers are deposited for either reaction with the substrate or other monomers, with subsequent chain growth. During the initial deposition stage, during which the homogeneous polymer film has not formed, the absorbed reactive species will diffuse on the substrate surface to bind.[29] This diffusion process is ended by either desorption from the surface or a reaction with active ends of existing polymer chains. Based on this, a kinetic model was developed by Fortin et al. where the precursor species adsorption on the surface was treated as the rate-limiting step of polymer form.[28]

In the Fortin model,[28] the sticking coefficient, which is determined by the energetics of the monomer-substrate interaction, is defined as the probability of a precursor species adsorbing or reacting each time it strikes the surface and is typically varied by controlling the substrate temperature. It is important to note that the sticking coefficient is only meaningful concerning chemisorption processes. In the absence of significant coverage, each of the initial monomers that chemisorb will result in a new radical chain end (similar to nucleation in crystallization). In Figure 1-3A, the experimental data clearly shows that the sticking coefficient of *p*-xylylene reactive species is proportional to temperature, in this case, the deposition rate also functions to the

deposition temperature. Typically, the deposition rate of poly(*p*-xylylene) increases as substrate temperature decreases, which indicates that species adsorption is the limiting step, as shown in Figure 1-3B. Working pressure within the CVD system is another critical parameter of deposition rate which shows in Figure 1-3C, as it affects the concentration of gas-phase precursor species and their strike possibility. Hence, the deposition rate is increasing as working pressure increases.

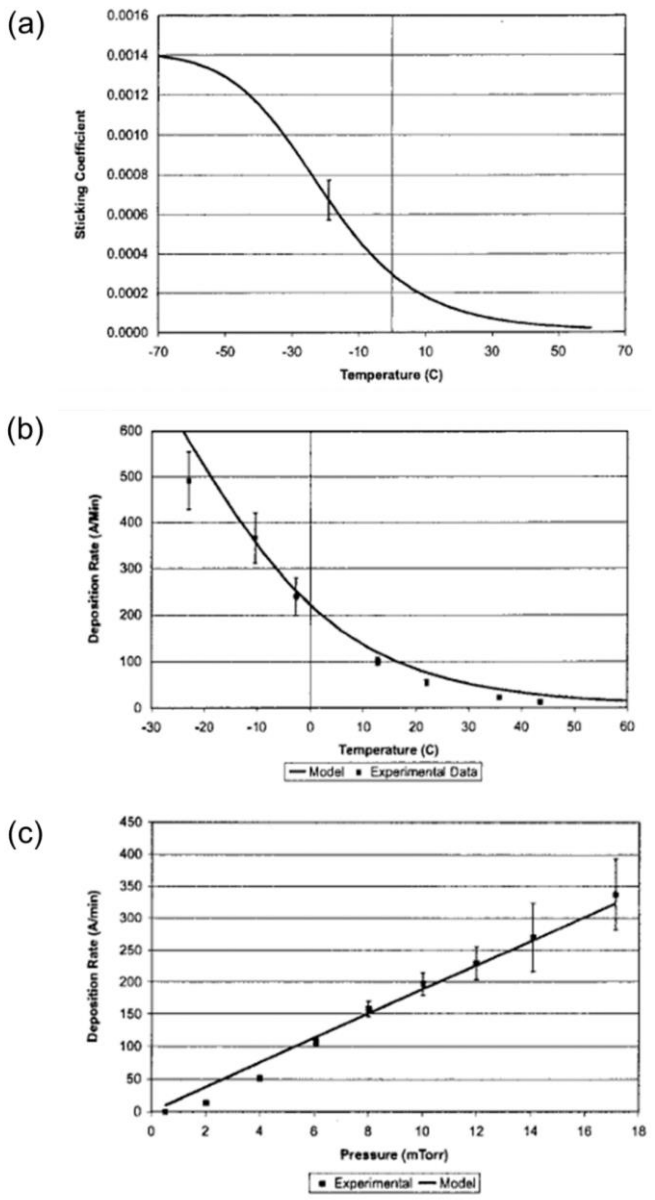

Figure 1-3: (a) Sticking coefficient of p-xylylene reactive species as a function of temperature. (b) deposition rate as a function of temperature at pressure = 4.0 mTorr. (c) deposition rate as a function of pressure at temperature = 22 °C. Adapted with permission from [28]. (Copyright 2002 American Chemical Society)

Although the exact fundamental mechanism of area-selectivity in CVD polymerization is still unknown, it is believed that the metal-treated surface suppresses both the initiation and

propagation by deactivating the interacts. The higher surface energy substrates, such as iron, copper, silver, platinum, and the salts of these metals, are more likely to prevent deposition or polymerization than substrates with lower surface energy.[27]

1.4 Potential Applications of Area-selective CVD Polymerization

Nowadays, it is an aim to scale down electronic devices, especially semiconductors and microchips, to get faster performance with smaller sizes. That makes complex three-dimensional structures and thin film materials favored, leading to rapid advances described by Moore's law.[30], [31] Commonly used 'top-down' techniques, including e-beam lithography,[32] laser ablation,[33] template electrodeposition,[34], [35] and molecular beam epitaxy[36] have disadvantages of being expensive, time-consuming, chemically demanding on the environment, and hazardous. In this case, 'bottom-up' methods, as another explore direction, to form nano-scale structures are more favorable in manufacturing. This bottom-up technology can help to perform nanomaterials with well-defined shapes, sizes, and chemical compositions that are formed through the growth and self-assembly of atoms and molecules as their building blocks.[37], [38]

ASD as one of the bottom-up methods is promising in applications such as thermoelectric devices, inverted organic photovoltaic devices (OPV), and asymmetric supercapacitor (ASC) devices owing to its unique characteristics, including molecular-scale chemical sensitive, augmenting traditional patterning methods, and less number of masking steps required in device preparation.[21], [39] However, the most common ASD method is using atomic layer deposition (ALD) for inorganic materials, and it needs cycles of etching process due to the deposition on the non-target area. On the other hand, CVD polymer films have been widely used as conductive polymers.[6], [21], [22], [40] Kim et al have fabricated amorphous In-Ga-Zn-O thin film transistors (a-IGZO TFTs) using four different types of PPX as gate dielectrics.[41] The PPX layer

exhibited excellent dielectric properties and can act as a passivation layer as well. This whole process can be easily applied to various types of electronic devices and the functionalized PPX is expecting to introduce different side functional groups into the gate layers, which can tune the sensor applications to environmental changes. In this case, CVD polymerization with its area-selectivity is willing to be used as one of the ASD methods. To achieve this goal, it needs to explore more on the fundamental mechanism of area-selective CVD polymerization.

1.5 Polymer Brushes Prepared by CVD Polymerization for Interfacial Engineering

Polymer brushes are assemblies of polymer chains which are achieved through grafting or grafting from approaches. With tailored chemical and biological functionalities, polymer brushes can be created and engineered for desired interfacial properties.[42], [43] Previous research has revealed the application of polymer brushes to either prevent non-specific protein adsorptions[44] or precisely recognize and bind to specific proteins[45], [46] by controlling the brush composition. In this case, the formation of polymer brushes is essential for its function. The common methods are through polymerization, such as atomic transfer radical polymerization (ATRP),[42], [44] ring open polymerization (ROP),[47] and nitroxide-mediated polymerization (NMP).[48] ATRP is a living polymerization process to prepare block co-polymers by controlling molecular weight and molecular weight distribution.[42] The ATRP initiators are always immobilized on the substrate surface, followed by desired monomers propagating to the imitation sites to form densely tethered polymer chains through the ATRP process.

CVD polymerization as a substrate-independent method can be utilized as a strategy to create a polymeric initiator coating through surface chemistries for further ATRP process, as shown in Scheme 1-2.[49] The non-fouling properties after ATRP were proved by a protein adsorption study, that the proteins only adhesive to non-polymer brushes area.[49] Given that, the

combination of CVD polymerization and ATRP provides a novel surface modification method, which can form non-fouling surface coatings on various substrates for generic surface engineering applications.

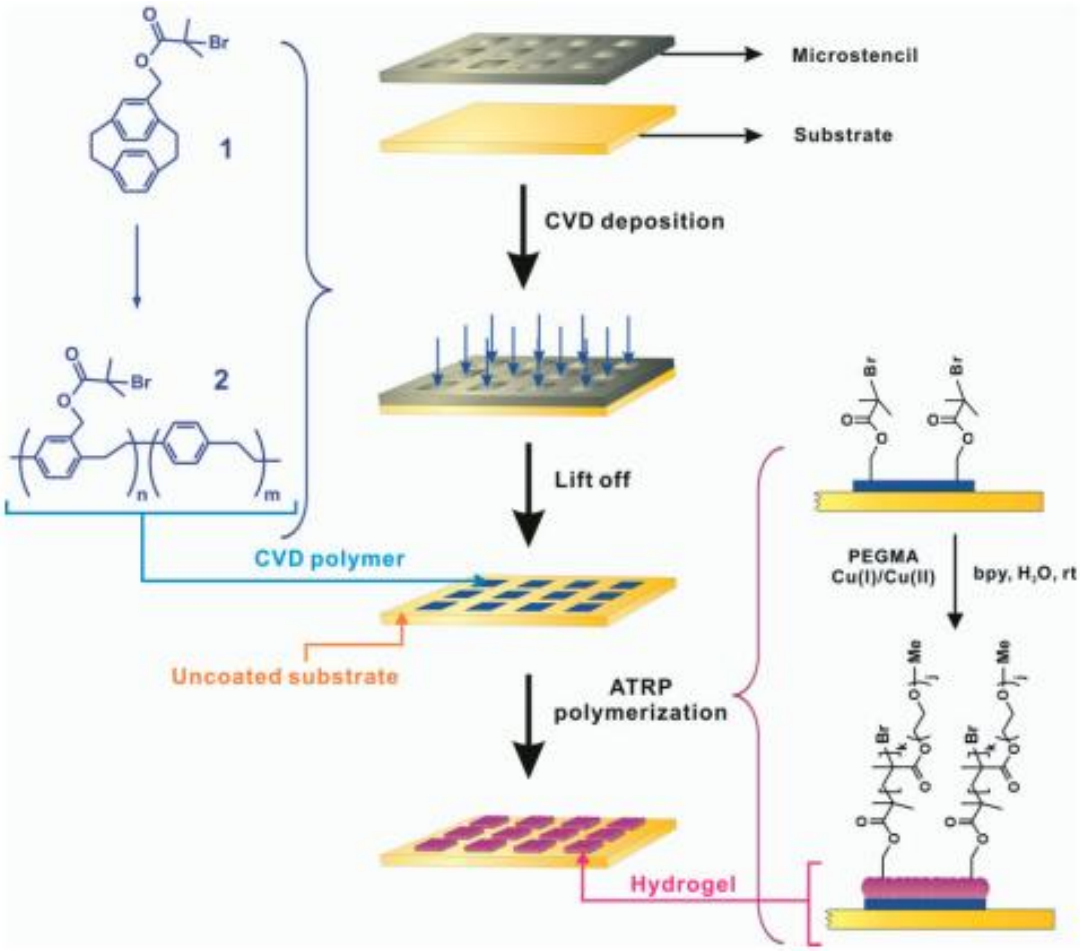

Scheme 1-2: CVD polymerization approach to prepare the vapor-based initiator coating 2 for subsequent poly(OEGMA) modification via ATRP. A micro stencil is used during CVD polymerization to direct the reactive initiator coating to defined surface areas only. Using surface initiated ATRP, a poly(OEGMA)film is then selectively prepared at areas, where the initiator coating 2 has been deposited. The result is a micro-structured hydrogel surface with potential for protein or cell patterning. (j, k, m, n denote repeating units of the corresponding structures.) Adapted with permission from [49]. (Copyright 2008 Wiley-VHC)

1.6 Bio-orthogonally CVD Coatings for Biomolecules Conjugation

To mimic the complex and dynamic extracellular environment where cells reside,[50] it is essential to immobilize more than one functional biomolecule on the surface simultaneously.[9] Both physical and covalent methods have been carried out to achieve the co-presentation and manipulation of multiple biomolecules.[8], [51] However, compared with weak physical adsorption, covalent binding is more stable and controllable. Under these circumstances, reactive CVD co-polymer coatings have been applied for surface functionalization to different bioconjugation chemistries with adjustable surface densities and ratios of different functional groups or immobilized biomolecules.[8]–[11], [52]

Scheme 1-3 presents a typical example of CVD co-polymerization process to conjugate both growth factor and adhesion peptides.[8] Two [2,2]paracyclophanes with different functional groups were introduced into the CVD system with a 1:1 molar ratio to prepare multifunctional PPX coating. In a previous study,[53] surface characterizations, such as x-ray photoelectron spectroscopy (XPS), Fourier transform infrared spectroscopy (FT-IR), and X-ray Diffraction (XRD) were utilized to confirm the chemical composition of different copolymers. It demonstrated that the copolymer coatings with different functional groups ratios can also be designed and prepared by changing the ratios of the two precursors.[53] Here, the two functional groups (PFP ester and ethynyl groups) were picked based on the special surface chemistry of bioconjugations.[8] This bio-orthogonal surface was then applied to immobilize the epidermal growth factor by the highly efficient reaction of PFP ester and amine groups. Moreover, an azide-ethynyl click reaction was also utilized to immobilize the RGP peptide with an azide end group on the material surface. The biomolecules remained bioactive after co-conjugation on the bio-orthogonal surface.

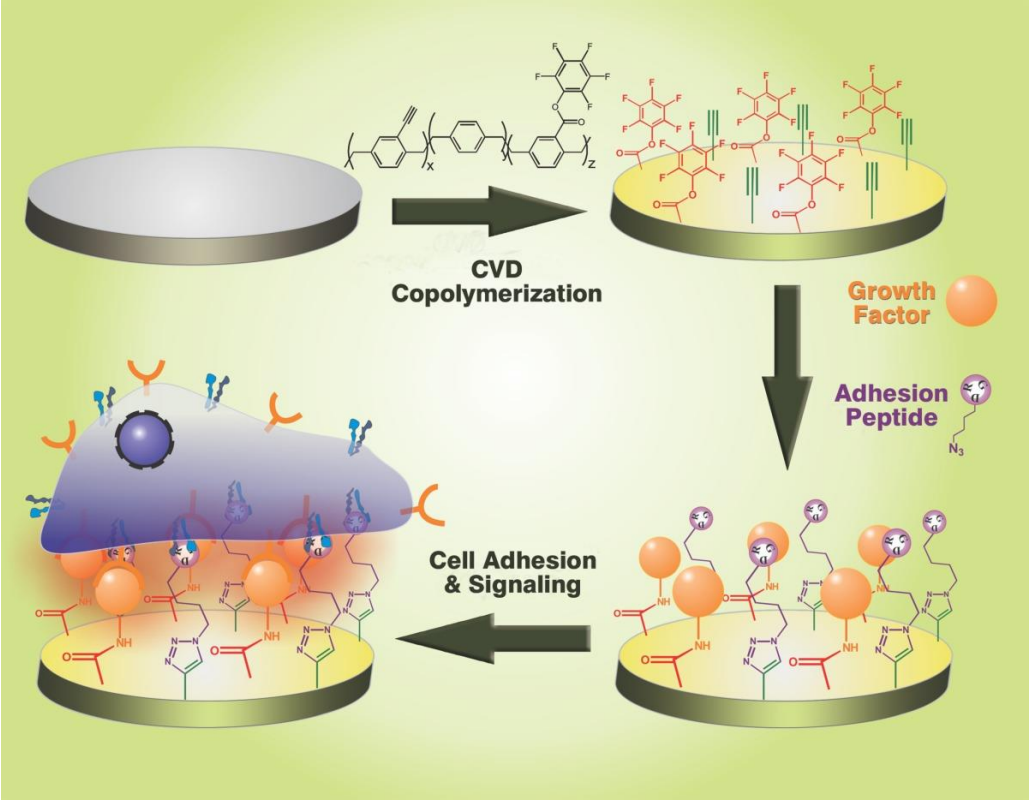

Scheme 1-3: Scheme of orthogonally immobilizing two different biomolecules on the CVD polymer surface with both alkyne and PFP-ester functional groups. Adapted with permission from [8]. (Copyright 2014 Wiley Periodicals, Inc.)

1.7 Thesis Outline

The work described in this dissertation can be divided into two parts: The first part of the dissertation (Chapter 2 and 3) develops the fundamental mechanism of area-selective chemical vapor deposition that was observed in previous work [27]. Chapter 2 demonstrates the important engineering parameters of the CVD system (deposition temperature and working temperature) that we can control to affect the area-selectivity of specific polymer-substrate pairs. Based on these findings, Chapter 3 further establishes the fundamental mechanism and explores the potential use of area-selective CVD in the semiconductor industry as one of the bottom-up strategies by operating Ru-patterned Si substrates to mimic the real industry fabrication process.

The second part of the dissertation (Chapter 4) explores the using of reactive functional poly(*p*-xylylene) coatings prepared by CVD polymerization for biological applications. Different polymer coatings can be engineered according to the requirements of biomaterials. Chapter 4 demonstrates two different applications of CVD polymer coatings. The first one describes a designed substrate that can control the adhesion point of cells by applying CVD polymerization and organic vapor jet printing (OVJP) together based on previous works [44], [54]. The second application is also built on previous work [9] on utilizing a co-polymer coating prepared by CVD polymerization to precisely bind two different biomolecules and demonstrates the benefits of this polymer layer in improving the efficiency of gene therapy.

Chapter 5 summarizes the key findings of this dissertation and outlines future directions and potential applications.

Chapter 2 Mechanistic Studies into the Area-selectivity of Chemical Vapor Deposition Polymerization

2.1 Introduction and Background

It is routine in the semiconductor and microchip industry to perform multiple stages of surface preparation and treatment, often under harsh conditions, to generate arrays of nanoscale features at high densities.[55] Bottom-up strategies present a high potential to eliminate defects in the fabrication of current electronic devices, which are only several nanometers in size.[38], [56] However, to achieve bottom-up growth of nanofeatures on a substrate, precise spatial control of chemical reactions is required. When the desired nanofeatures are sought by way of small molecule chemistries on a surface, the spatial patterning resolution can be hampered by the mobility of the small molecules.[21] One strategy is to seek out paired material-substrate systems that allow for reactions to occur only in a designated region, often by limiting the mobility of the reactants to the desired region.[57] Additionally, the number of materials that can be utilized in these processes is often relegated to semiconductor, metal, metal oxide, metalloid, and semi-metal species.[58]–[62] It is therefore of interest to identify organic material-substrate systems that allow for the inclusion of various polymeric structures at these scales while also avoiding the workload and harsh chemistries involved in the conventional fabrication spaces. To this extent, area selective deposition (ASD) may be an appropriate strategy for pursuing this goal.[39], [57] Generally, ASD is a chemical process in which a substrate possesses various regions with differing degrees of interaction with the presented materials.[39] The basis is selective adsorption, absorption, or chemical reaction with the target/highly interacting regions and low or no deposition in the low

interacting regions.[39] Ultimately, this can result in structured or patterned depositions without the need for lift-off, etching, or other engineering regimes in which something is later added or taken away from the substrate.[57] In this case, the use of area-selective materials is critical to bottom-up nano-manufacturing.

ASD uses the chemical interactions between the reactants and the exposed surface to guide the creation of the desired material design,[39] and chemical vapor deposition (CVD) polymerization is one of the common methods of ASD.[63]–[66] CVD polymerization is a process of depositing molecules onto a substrate, typically via physical adsorption or simple collision to form nucleation sites, followed by initiation and propagation that result in continuous polymer films.[67] Specifically, CVD polymerization involves activated monomers deposited for either reaction with the substrate or other monomers, with subsequent chain growth.[68] The as-deposited polymer coatings typically are pin-hole free, homogeneous, and subject to excellent thickness control.[1], [10], [68], [69] Furthermore, by using different functional polymers, the CVD coatings have tunable chemistry properties and can be utilized for surface modification of electronic materials or biomaterials.[8], [70], [71] Among many applications of CVD, what attracts our attention is that it can make high-performance electric devices by reducing potential damages since CVD is a solvent-free process under low-temperature process conditions.[68], [69]

Poly-p-xylylene (PPX or parylene) is one of the common CVD polymers. Previous works[3], [9], [72]–[75] established a series of functionalized PPX with different chemical groups for further covalent immobilization or surface modification, based on CVD polymerization following the Gorham process[76]. The CVD polymerization of these functionalized PPX precursors can be either monomer-substrate or monomer-monomer initiated[52], [68], [69]. Jensen's group[65], [66] reported selective inhibit properties of poly(para-xylylene) (PPX-N), poly(chloro-p-xylylene)

(PPX-Cl), and poly (p-phenylene vinylene) (PPV) by iron and iron salts and created a wide range of patterns via selective CVD polymerization. They hypothesized that the metal-treated substrates inactive the adhesive reactive species, which made them easy to desorb, which left no or less deposition on those metal substrates. Our group [77] has studied the selective inhibition of a library of functionalized PPX containing a wide range of different functional groups that are either nonreactive or reactive and extended the polymerized substrates to nine different metal surfaces. We observed that several transition metals, metal salts, and organometallic complexes exist that can inhibit the growth of PPX-N and PPX-Cl. However, even though the selective inhibition of functionalized poly-p-xylylene, especially PPX-N and PPX-Cl, has been the focus of past studies, the fundamental mechanism of this area-selective property is still unknown.

Herein, we thus embarked on a systematic study to elucidate the effects of deposition conditions on area-selective chemical vapor deposition. Silicon (Si) and Copper (Cu) were used in this study as the two main substrates because a previous study showed that Si has the property of a non-inhibitor, while Cu is a good inhibitor.[77]

2.2 Experimental Methods

Substrate Preparation:

Si and Cu substrates with natural oxidation were prepared by Intel Co. Electron-beam evaporation was performed to deposit 7.7 ± 0.1 nm thick Cu films onto Si substrates. A biopsy punch was utilized to cut 2.5 mm radius holes in 1 cm^2 PDMS squares. TEM grids were placed over these holes and fastened to the Si surface, allowing for the 400 mesh TEM grids (Ted Pella, Inc., United States) to act as deposition masks. Cu was evaporated in a vacuum with a base pressure below 4 x 10^{-6} torr (Scheme 2-2). All substrates were pre-cleaned by 0.5 wt% Potassium hydroxide

(KOH) solution at room temperature for 5 minutes, then sonicated by 70% ethanol solution (Fisher Scientific, United States) and DI water respectively for 10 minutes.

CVD polymerization:

Poly-*p*-xylene (PPX) derivatives are synthesized via a custom-built chemical vapor deposition setup following a previously reported routine.[77] As shown in Scheme 2-1A and B, the monomer was sublimed under vacuum at 86.5 ℃ and converted into free radical in the furnace by pyrolysis under 450/550/560 ℃, then transported into the deposition chamber. Constant argon with a 5.0 sccm flow rate was operated as a carrier gas for the chemical reaction process. Subsequently, the polymerization occurred on a rotating sample holder ensuring uniform polymer deposition. The sample holder was maintained by a temperature controller, while the wall of the deposition chamber was maintained at 90 ℃ to prevent any residual deposition on the chamber wall. The CVD system is linked with a vacuum pump through a butterfly valve. By modifying the opening degree of this butterfly valve, the pressure of the system can be precisely controlled.

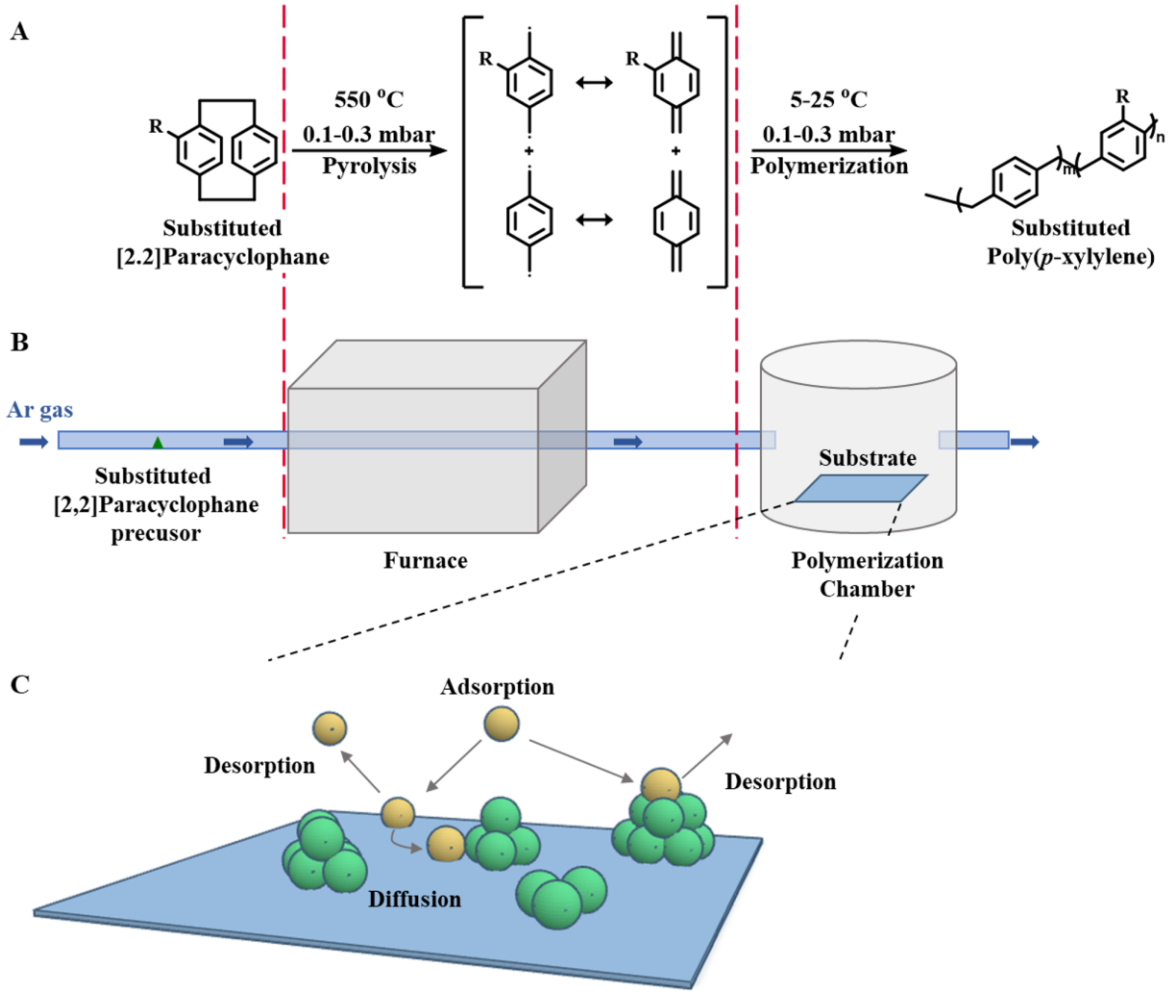

Scheme 2-1: Chemical vapor deposition (CVD) polymerization of substituted [2,2]paracyclophane precursors. (a) The chemical reaction of [2,2]paracyclophane polymerization in the CVD system. (b) Scheme of CVD system. (c) Deposition model of the CVD process in the polymerization chamber.

Atomic Force Microscopy:

AFM measurement was performed by Veeco Dimension Icon Atomic Force Microscope (Bruker, United States) operated in PeakForce Quantitative Nanoscale Mechanical (PF-QNM) mode. The Scanasyst-Air probe was operated with a spring constant of about 0.4 N/m and an

effective tip radius of about 2 nm. The probe oscillated along the vertical axis at a frequency of 70 kHz near the sample surface. The size of the scan area was 500 × 500 nm with a resolution of 256 × 256 points. The analysis of the AFM data was performed by Nanoscope Analysis software.

Focused Ion Beam Electron Microscopy:

All Scanning Transmission Electron Microscopes (STEM) samples were prepared by Helios G4 PFIB UXe (Thermo Fisher Inc., United States). A 0.2 μm-thick layer of carbon was deposited by a gas injector of electron beam source on the region of interest on the sample surface. Followed by the deposition of a 2 μm-thick mixed layer of platinum and carbon by the gas injector of the ion beam source. Both carbon and platinum-carbon mixed layer were protective layers of the region of interest. Rough trench milling by argon ion beam was performed to achieve the cross-section lamella which was then attached to a lift-out TEM grid (Ted Pella Inc., United States). To achieve electron transparency for subsequent STEM analyses, a further thinner was performed with a lower beam voltage.

Transmission Electron Microscopes:

JEOL 3100R05 Transmission Electron Microscopes (JEOL Ltd., Japan) were used to perform the cross-sectional measurement of specimens. It was operated at 300 keV and employed for STEM-bright field (STEM-BF) and high annular dark field (HAADF) imaging. JEOL Double-Tilt holder was used to tilt the sample to an orientation that was parallel to the electron beam. Before STEM, the TEM samples and holder were cleaned with Oxygen and Argon mixed plasma for 1 minute by Gatan Solarus II Plasma Cleaning System (Gatan Inc., United State) Data analysis was performed using Gatan Microscopy Suite.

2.3 Results and Discussion

Monomer Precursor Screening

We initially focused on determining the nature of selective vs. non-selective behavior as it relates to the deposition of substituted PPX systems. As such, a preliminary assessment of multiple substituted PPX systems was undertaken. Six functionalized PPX precursors were used to deposit on Si and Cu substrates via CVD using known masses of precursor. For the purposes of this study, Si and Cu both possessed native oxide and should be considered as Si/SiO_x and Cu/CuO_x, respectively. The resultant thickness of each film was measured by ellipsometry and is presented in Figure 2-1 for the Si substrate. All six precursors were deposited and polymerized on Si surface with thicknesses proportional to precursor mass. Measurements of the polymer films on Cu showed that of the deposited polymers, only PPX-$COCF_3$ and PPX-CH_2NH_2 were found to be deposited on Cu surfaces, indicating the non-area selectivity of PPX-$COCF_3$ and PPX-CH_2NH_2, and the potential area-selectivity of the rest polymers compared to their deposit capabilities on Si substrates. These findings confirmed previous research that found substituted PPX with nitrogen or oxygen in their side functional group to not exhibit area-selectivity on metal substrates.[77] A potential contributor might be a chelating effect between those function groups and the metal surface. A comparison of the deposition thickness for both of these precursors is presented in Figure 2-2A, indicating nearly identical deposition on both substrates. In the case of the Si and Cu substrates observed, PPX-Cl can be considered to be area-selective (Si >> Cu) (Figure 2-2B), while PPX-CH_2NH_2 is a non-area selective polymer (Si = Cu) (Figure 2-2A).

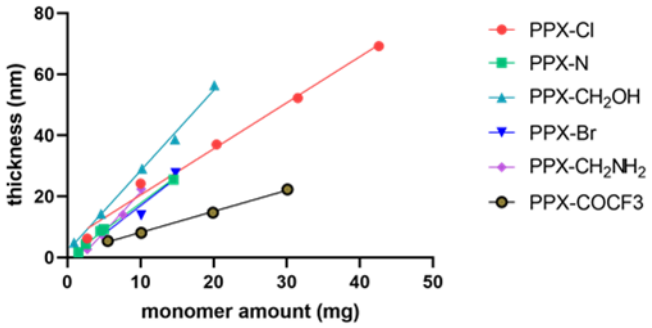

Figure 2-1: Average polymer film thickness as a function of the feeding amount of precursor on Si substrate. Slopes are polymer dependent.

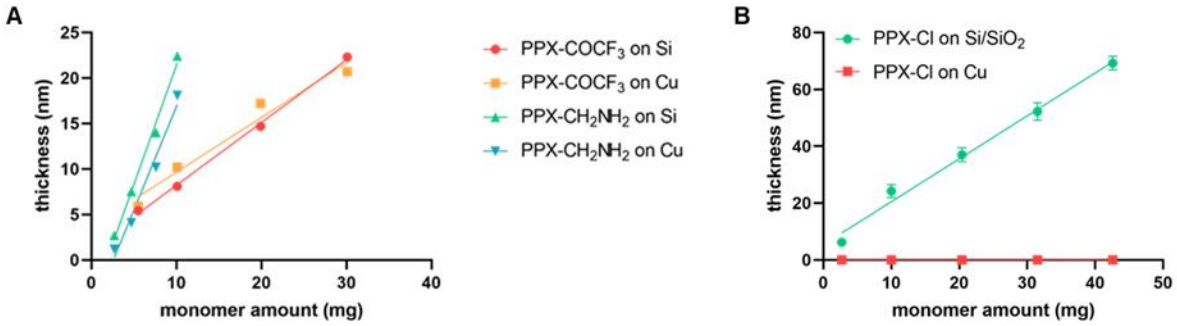

Figure 2-2: Average polymer film thickness on Si and Cu substrates of (a) non-area selective polymers (PPX-$COCF_3$ and PPX-CH_2NH_2) and (b) area-selective polymer (PPX-Cl).

During CVD polymerization, initial deposition of the monomers typically occurs via physisorption. The build-up of polymer film on the substrate is characteristically dictated by the competition between the rate of adsorption and the rate of desorption.[75] Prior to desorption, the monomer may diffuse across the substrate to find a reaction partner. The diffusion rate is affected by the intrinsic mobility of a monomer on the substrate. During polymerization, molecular weights quickly exceed sizes that allow for desorption under the conditions of CVD polymerization. In effect, these various rates dictate the likelihood of a particular monomer participating in the polymerization process. Theoretically, by changing the balance between adsorption, desorption,

and lateral diffusion of the monomers, a system should be switched between selective and non-selective deposition regimens.

To model for area-selective and non-area selective deposition under varied reaction conditions and on different substrates, we initially considered the chemisorption model developed by Fortin et al.[78], which only reflects the adsorption process. In the Fortin model, at deposition onset, the monomers are physically adsorbed as they impinge on the surface followed by chemisorption which involves reactions with existing chain-end radicals. The adsorption rate is treated as the limiting step and includes both physisorption and chemisorption processes.

The maximum deposition rate for any CVD process[78] can be given by

$$R_d = \frac{SPN_aV_m(60 \times 10^{10})}{(2\pi m_r RT_0)^{0.5}} \qquad 2\text{-}1$$

where the total quantity of $PN_aV_m/(2\pi m_r RT_0)^{0.5}$ is the flux of the reactant at the substrate surface in collisions; parameter S is the sticking coefficient that reflects the proportion of molecules that react after hitting the surface.

In Eq. 2.1, only the sticking coefficient (S) and working pressure (P) are variables. The sticking coefficient reflects the energetics of the monomer-substrate interaction and is typically varied by controlling the deposition temperature. At low surface coverage, each of the initial monomers that chemisorb on the substrate will also start a new radical chain. Furthermore, as we mentioned before, the diffusion process is also critical to decide if the reactive species can stay on the surface before desorption and its effects by the mobility of the reactive species which is also relative to deposition temperature. To better understand how deposition temperature affects each step of the deposition process, especially the diffusion rate, it is critical to investigate the surface geometry prior to polymer film formation under controlled deposition conditions, as it allows us to gain insight into learning how the polymer film growth and can be compared to different

depositions when controlling the amount of reactive monomer entering the deposition chamber. Besides that, pressure is another critical parameter that affects the deposition rate. In this case, we can infer from the Fortin model that the deposition rate is a function of pressure and temperature for the steady-state deposition of PPX-N.

By adjusting the fitting parameters according to the energetics of the Lennard-Jones potential of different monomer types (Table 2-1), this simple model can be applied to other PPX-substituted polymers (PPX-Cl in this paper). For these reasons, this model is used in the current work to understand and predict how system pressure and temperature affect the area-selective properties of PPX-substituted polymers.

Table 2-1: Values of the Fitting Parameters for the Chemisorption Model

Parameter	**Value**
Na	6.02×10^{23}
Vm	1.88×10^{-4} m^3/monomer
R	1.10×107 m^{-1}
T_0	823.15 K

According to Figure 2-2B, PPX-Cl expresses area-selective behavior with a strong bias towards deposition onto Si substrates (relative to Cu). We thus focused on PPX-Cl to experimentally verify the deposition model. By decreasing the temperature of the monomer below the sublimate temperature, the sublimation process was arrested. This, in turn, halted additional deposition and polymerization. In effect, polymer islands that did not merge into a film were captured in a pre-film state as identified by AFM.

Kinetic studies on pre-closure CVD films

In order to assess polymer formation on the substrates, AFM was used to analyze the surface topography. AFM can map the surface morphology during different deposition times (Figure 2-3A to D). Given that polymer islands on the substrate surface during initial deposition are only nanoscale and the substrate also has nanoscale surface roughness, QNM PeakForce AFM must identify the polymer islands and substrate based on mechanical property differences (Figure 2-3E to H). As shown in Figure 2-4A, there are two ways for monomers to be adsorbed and retained on the substrate. The first one is to be adsorbed on the substrate surface and then diffuse to an existing polymer island. This will cause the polymer islands to grow horizontally. Alternatively, the incoming monomer directly adsorbs and reacts to the substrate. This scenario will favor the vertical growth of the polymer islands. By comparing the horizontal or vertical growth, we can indirectly assess the balance between monomer-substrate and monomer-polymer interactions. For identical deposition times, the sample with fewer polymer islands but larger sizes represents the preference for horizontal growth during the initial deposition, due to the monomer-substrate interactions being more rapid and favorable compared with the monomer-polymer interactions. Moreover, the coverage within fixed deposition time is an important parameter to detect lateral diffusion during horizontal growth. Higher coverage infers a higher diffusion rate and longer lifetime on the surface before desorption. In this case, a particular focus was placed on assessing the number, average size, and average height of polymer islands and the overall coverage on the surfaces by AFM. These results were then used to validate our growth model under different conditions (Figure 2-4B).

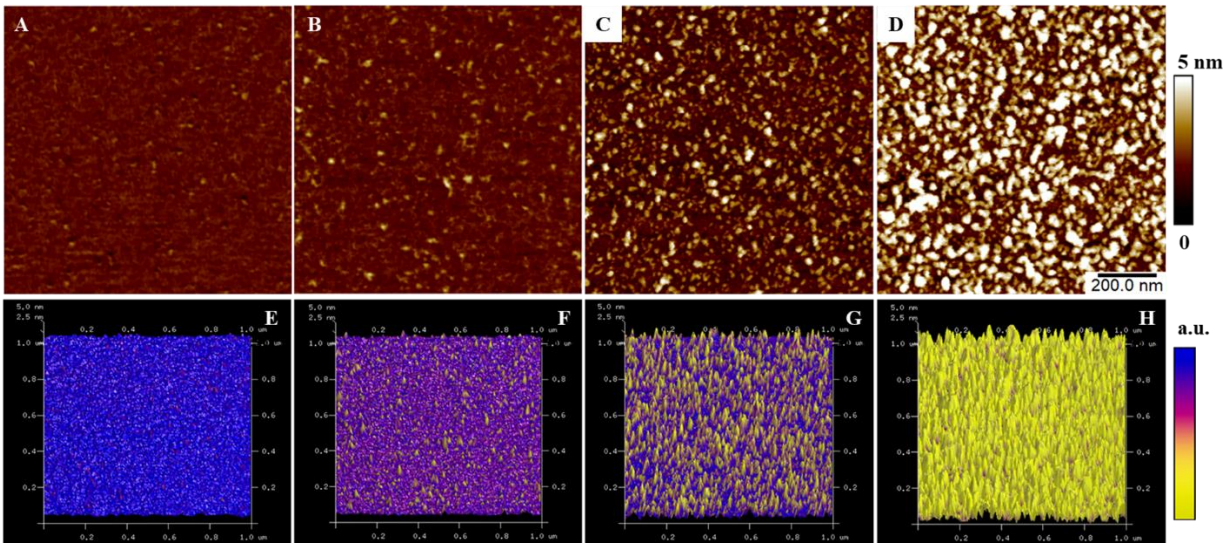

Figure 2-3: PPX-Cl deposition on Si substrates for (a & e) 0 s, (b & f) 30 s, (c & g) 120 s, and (d & h) 180 s. (a - d) are height images of AFM measurements, while (e - h) are adhesin images.

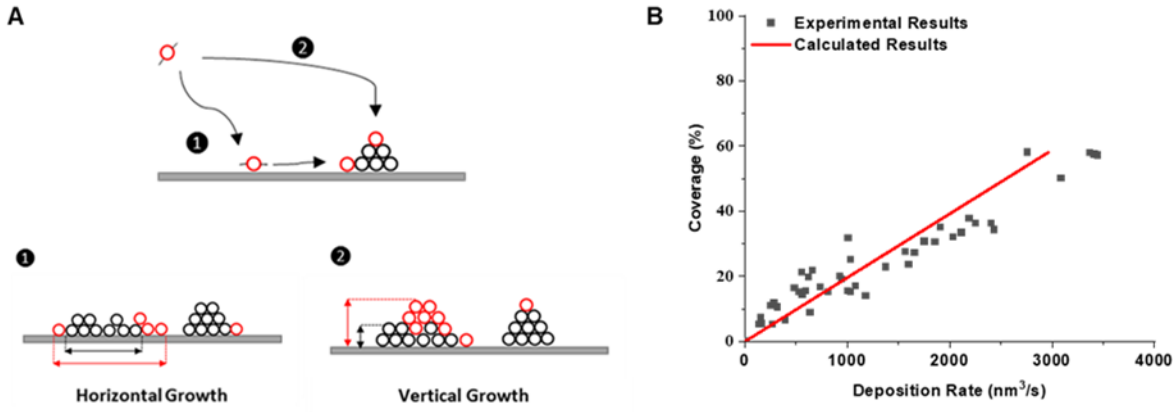

Figure 2-4: (a) Two examples of polymer deposition on a substrate surface. (b) Experimental results under different deposition conditions that were measured by AFM (dots) confirmed the linear relationship between polymer coverage and deposition rate, which is consistent with calculated results (line) based on the deposition rate model. ($R^2 = 0.90$)

Thermodynamic Studies

The results of a time series generated at substrate temperatures of 5, 15, and 25 ℃ at constant working pressure (0.1 mbar) are depicted in Figure 2-5A to C. By controlling the deposition time, the total number of incoming reactive species can be controlled. The transition of a reactive molecule from a vapor phase to a cluster on the surface includes several stages. The first stage after adsorption is the diffusion of these reactive species to a cluster (Scheme 2-1C). [79] This process can be described by a diffusion flow equation of reactive molecules to a cluster, namely[79], [80]

$$L_d = 2\pi D_a(-n_R) \times \frac{K_1(x)}{K_0(x)} \quad 2\text{-}2$$

$$n(r,0) = n_1(0), \qquad n(\infty,t) = n_1(t) \quad 2\text{-}3$$

$$n(R(t),t) = n_R \quad 2\text{-}4$$

where D_a is the diffusion coefficient of molecules and is strongly dependent on surface temperature, n(r,t) is the molecular concentration at time t; R(t) is the radius of a linear cluster boundary moved due to the cluster growth; n_R is the molecular concentration at the cluster boundary, which is assumed to be isolated and symmetrical; $x \equiv \frac{R}{\sqrt{D_a \tau}}$ and τ is the time for desorption; K_0 and K_1 are the Macdonald functions.[81] Figure 2-5A shows the relationship between coverage and deposition time at different temperatures, indicating that the lower the temperature, the higher the deposition rate. Since deposition temperature mainly affects the diffusion coefficient on the substrate surface, it is the key parameter driving island growth and further affects the final deposition rate.[79] This result experimentally demonstrates that the diffusion efficiency increases with decreasing temperature. The lifetime of molecules on the substrate surface (τ) and the time to achieve 50% surface coverage ($t_{1/2}$) at each deposition

temperature shown in Figure 2-5A reveals that the reactive molecules have lower mobility but longer diffusion lifetimes on the substrate surface. In another word, the reactive monomer has a longer stay time on the substrate surface before leaving. This made them more likely to coalesce with any existing polymer island or reactive species on the surface without desorption, compared with the diffusion process at higher deposition temperatures.

Moreover, Figures 2-5B and 2C suggest that lower temperature correlates with fewer polymer islands with larger sizes after the same deposition time. Accordingly, the reactive species are more likely to enhance the lateral growth of the islands as the temperature decreases.

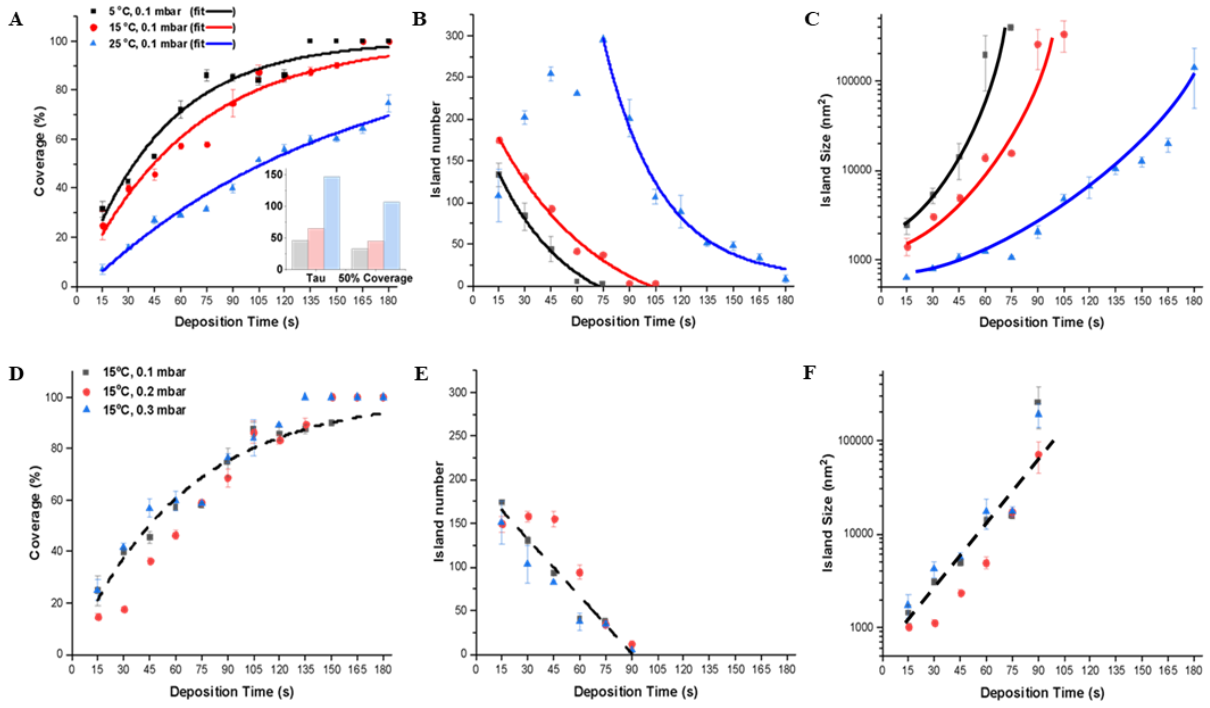

Figure 2-5: The results of a time series generated at substrate temperatures of 5 (black), 15 (red), and 25 oC (blue) at constant working pressure (0.1 mbar) of (a) coverage(lifetime of molecules on the substrate surface (τ) and the time to achieve 50% surface coverage (t1/2) are also shown in the figure with respective color to deposition temperatures), (b) island number, and (c) island size. The results of a time series were generated at a working pressure of 0.1 (black), 0.2 (red), and 0.3 mbar

(blue) at constant substrate temperature (15oC) of (d) coverage, (e) island number, and (f) island size.

Pressure Studies

Another time study was undertaken under constant temperature (15 ℃) conditions with varied working pressure (0.1 to 0.3 mbar; Figure 2-5D to F). For CVD polymerization using the Gorham process, the absolute pressure in the CVD reactor is given by the sum of the partial pressure of the precursors and the carrier gases. Since the flow rate of carrier gas was controlled at 20 sccm for all experiments. The increasing total pressure reflects the increase of partial pressure of precursors. Figure 2-5D suggests that polymer films reached full coverage faster under higher pressure. The polymer films formed under 0.3 mbar became conformal polymer films at 135 s deposition, while the 0.2 mbar samples achieved uniform polymer films at 150 s and the 0.1 mbar samples formed pin-hole free polymer layer til 165 s. This is because the surface chemistry of CVD mostly rests on the adsorption rate of the precursor, which in turn depends largely on the partial pressure of the precursor.[80] However, coverage appears to be relatively insensitive to pressure changes when compared to varying substrate temperatures. As shown in Figure 2-5E and F, the size and number of polymer islands follow a similar trend as well. These results show that pressure can affect the adsorption rate by increasing the concentration of reactive species on the substrate. However, pressure appears to have a relatively small impact on the total deposition rate, compared with temperature.

We next focused on film morphology, including the number and size of polymer islands, as a function of polymer coverage. Figure 2-6A and B show the number and size of polymer islands with varied deposition temperatures. Deposition at lower temperature resulted in a smaller number of islands, but larger island sizes, which is consistent with the above-mentioned results (Figure 2-

6B and C). Figure 2-6C and D show island morphology for various working pressure. As similar morphology trends have been shown for different pressure, it indicates that the depositions at different working pressures have the same horizontal growth rate. Hence, even if higher pressure enhanced the adsorption rate of reactive monomers onto the substrate surface, the diffusion process was not affected and the deposition of monomers was limited by the desorption step.

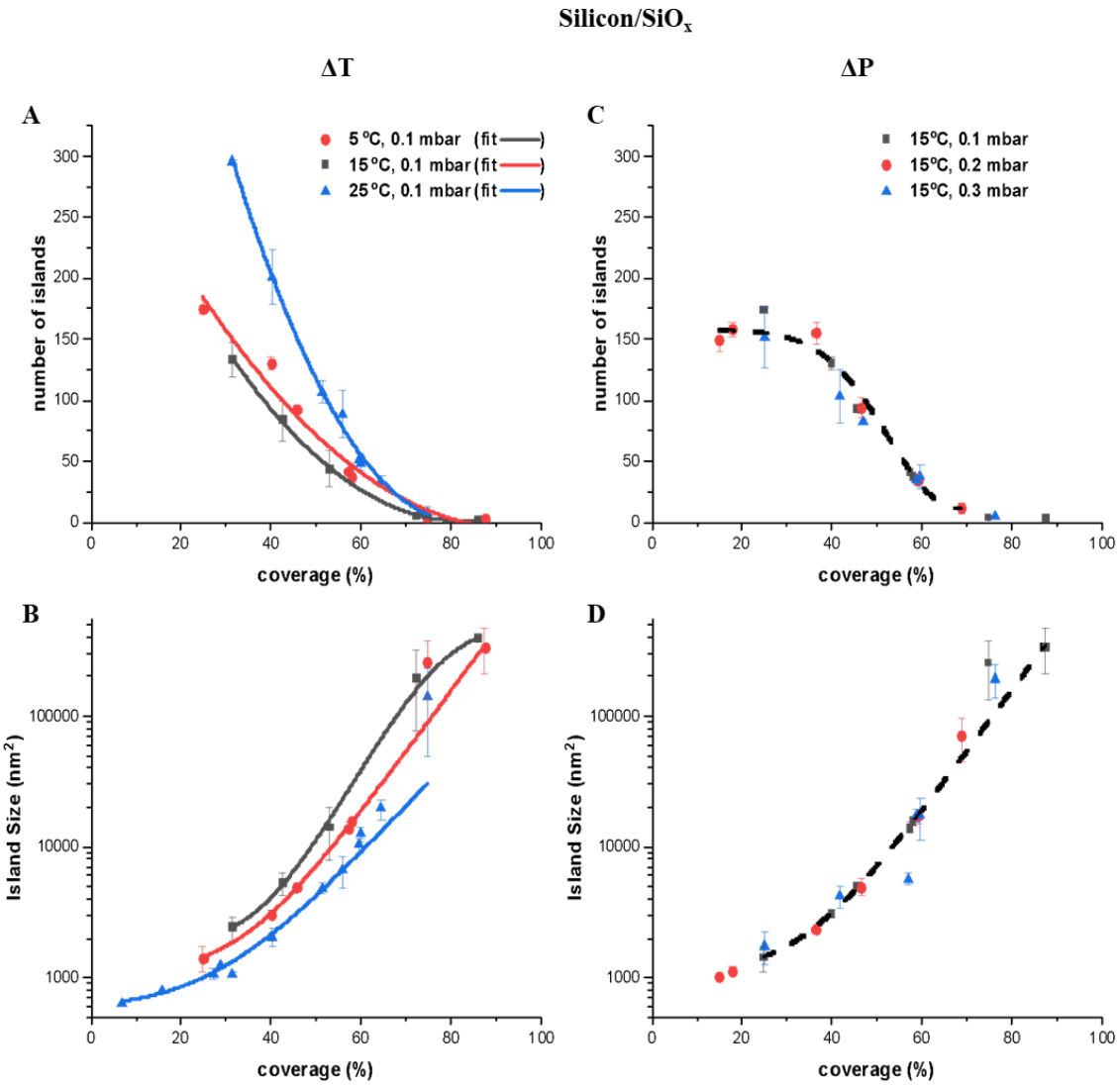

Figure 2-6: PPX-Cl deposition on Si substrates under various deposition conditions. (a) The number of islands and (b) island size with changing polymer coverages under different

temperatures (5, 15, and 25°C). (c) The number of islands and (d) island size with changing polymer coverages under different pressure (0.1, 0.2, and 0.3 mbar).

Generally, the pressure had a smaller effect on the deposition rate. However, once we decreased the deposition temperature to 5 °C, polymer deposition was easily detected on Cu substrates by FT-IR (Figure 2-7). The FTIR spectra display several bands that are characteristic of PPX-Cl.[82] Characteristic bands include 3062, 2958, and 2866 cm^{-1} (-CH stretching). They are split into three, because of the different -CH bonding in PPX-Cl unit. The band at 1612 cm^{-1} correlates with aromatic C-C stretching. Besides, due to C-H bending, there are characteristic bands at 1498, 1455, and 1403 cm^{-1}. These IR signals support the deposition of a PPX-Cl layer on Cu surface. As shown in Figure 2-8A and B, AFM was used to measure the morphology of polymer islands at a deposition temperature of 5°C. Next, the morphology of islands under the same deposition conditions on Cu and Si were compared, as shown in Figure 2-8C and D. Once the CVD polymerization is performed under suitable deposition conditions, polymers will have the analog deposition kinetics on Cu and Si substrates.

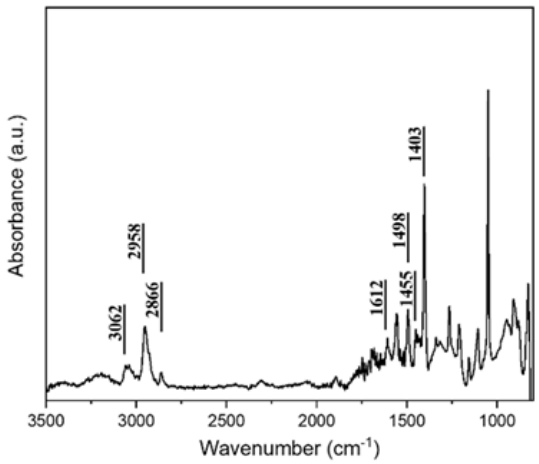

Figure 2-7: FT-IR spectra of PPX-Cl deposition on Cu under 5 °C and 0.1 mbar. C-H stretching at 3062, 2958, and 2866 cm^{-1}. Aromatic C-C stretching at 1612 cm^{-1}. C-H binding at 1498, 1455, and 1403 cm^{-1}.

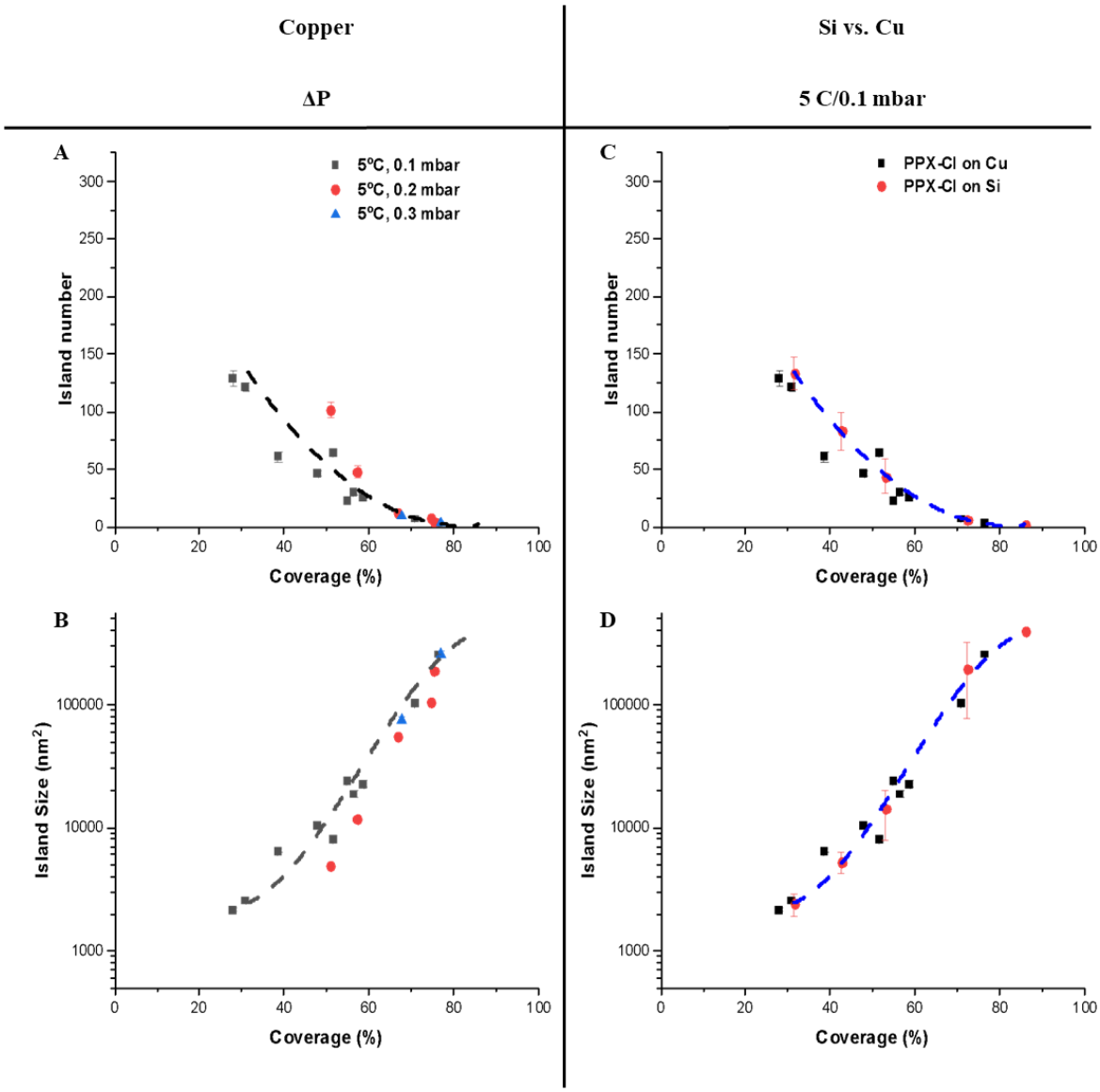

Figure 2-8: (a) Number and (b) size of PPX-Cl polymer islands on Cu substrates under various working pressure (0.1, 0.2, and 0.3 mbar), with changing coverage. Comparing PPX-Cl deposition on Si and Cu under the same deposition condition (5^{o}C and 0.1 mbar) by (c) island number and (d) island size with changing coverage.

Modification of the working conditions, such as decreasing the deposition temperature, can force the deposition of PPX-Cl onto Cu surfaces. To assess the relative stability of this process compared to a classically non-selective system, a comparison between PPX-Cl deposition and PPX-CH_2NH_2 deposition was undertaken. This comparison was made using adhesion AFM

measurements and extracting fitted peaks (gaussian) from the adhesion histograms (in mV, example in Figure 2-9). The results are presented in Figure 2-10, using data point radius as an indicator of integration intensity for multipeak extracts. Here, we use adhesion force as a proxy for surface energy. For all four samples (each polymer on a Cu and Si substrate), the surface energy increased first, then decreased to lower energy until it became stable. This change of surface energy is well-aligned with the height and coverage information provided through topographic AFM. During the early stage of the pre-closure period, less energy-minimized islands with a high surface-to-volume ratio exist, which caused increased surface energy within the region of interest. With closure transitioning to post-closure film growth, the merged polymer islands became stabilized. This is likely a combination of both a decrease in active monomers/polymer end groups, a decrease in total surface area relative to the mass/volume of the system, and bulk film stabilization as the polymer matrix achieves unity on the substrate. While these trends exist for all systems studied, a comparison of the relative intensity of the adhesion signals displays that PPX-Cl on Cu was the least stable configuration. PPX-Cl on Si possesses a higher adhesion than either of the PPX-CH_2NH_2 systems during the closure, with all three (PPX-Cl on Si, both PPX-CH_2NH_2) having comparable adhesion signal post-closure (<100 mV). This is greater than 5 times less than the PPX-Cl on Cu system. In total, this comparison aligns well with the proposed mechanism for growth on these substrates and adds credibility to the high selectivity of PPX-Cl and the low selectivity of PPX-CH_2NH_2 (e.g., non-area selective).

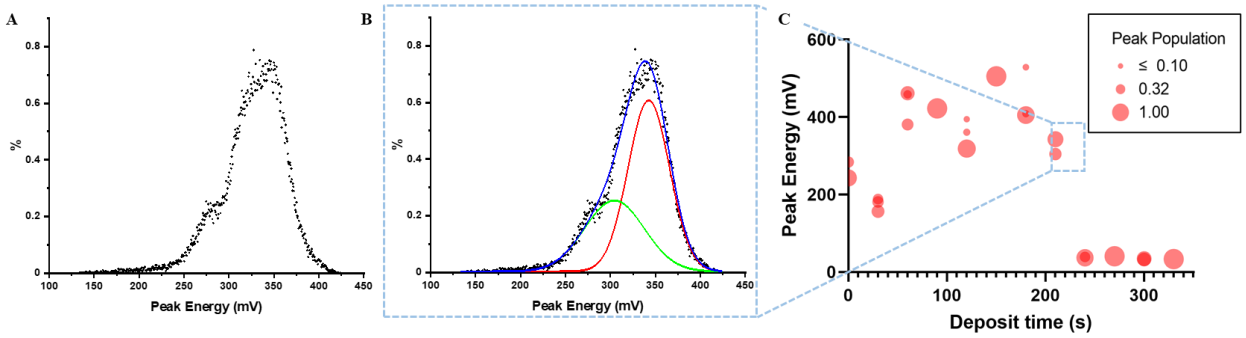

Figure 2-9: Example of Gaussian peak fitting from the AFM adhesion histogram. (a) Adhesion histogram measured by AFM. (b) Gaussian peak fitting from the adhesion histogram (R^2 = 0.89). The adhesion peak energy was separated into two sub-peaks which were plotted by deposit time. (c) Example of peak energy, changing with deposition time.

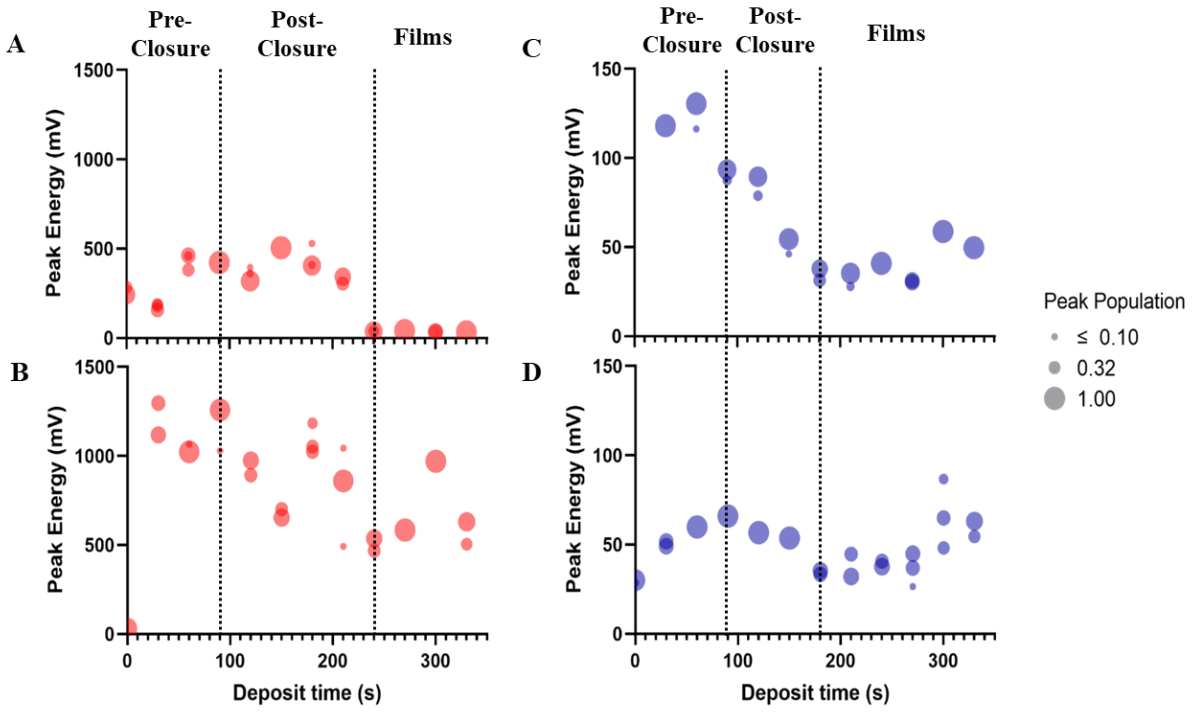

Figure 2-10: Peak Energy for PPX-Cl and PPX-CH_2NH_2 on Si and Cu substrates under 15 °C and 0.3 mbar. (a) PPX-Cl deposition on Si; (b) PPX-Cl deposition on Cu; (c) PPX-CH_2NH_2 deposition on Si; (d) PPX-CH_2NH_2 deposition on Cu. The total voltage ranges for the PPX-Cl system are about 10 times that of the PPX-CH_2NH_2 by this method.

Studies with Patterned Substrates

First, a pattern of deposited Cu (thickness 7.7 ± 0.1 nm) on a Si substrate was prepared via thermal vacuum evaporation (Scheme 2-2). These patterned substrates were then used to test the area-selective/non-area selective behavior of PPX-Cl under different deposition conditions. To investigate the property of polymer film on various substrates, cross-sectional STEM was utilized. The specimens for cross-sectional STEM were ion-milled at the boundary between the Si and Cu layer via FIB. Cross-sectional STEM revealed information about layer thickness and internal deformation, especially between layers, adding to the above-presented AFM results.

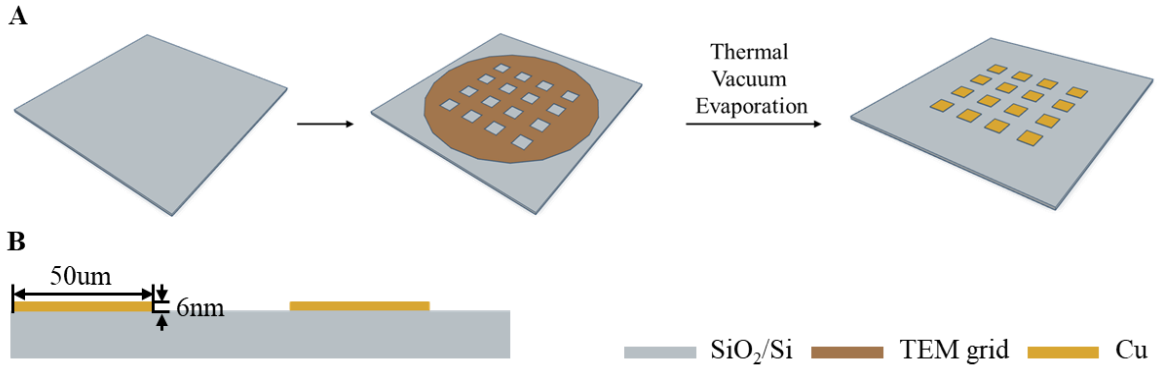

Scheme 2-2: Thermal Vacuum Evaporation of patterned Cu on SiO_2/Si substrate.

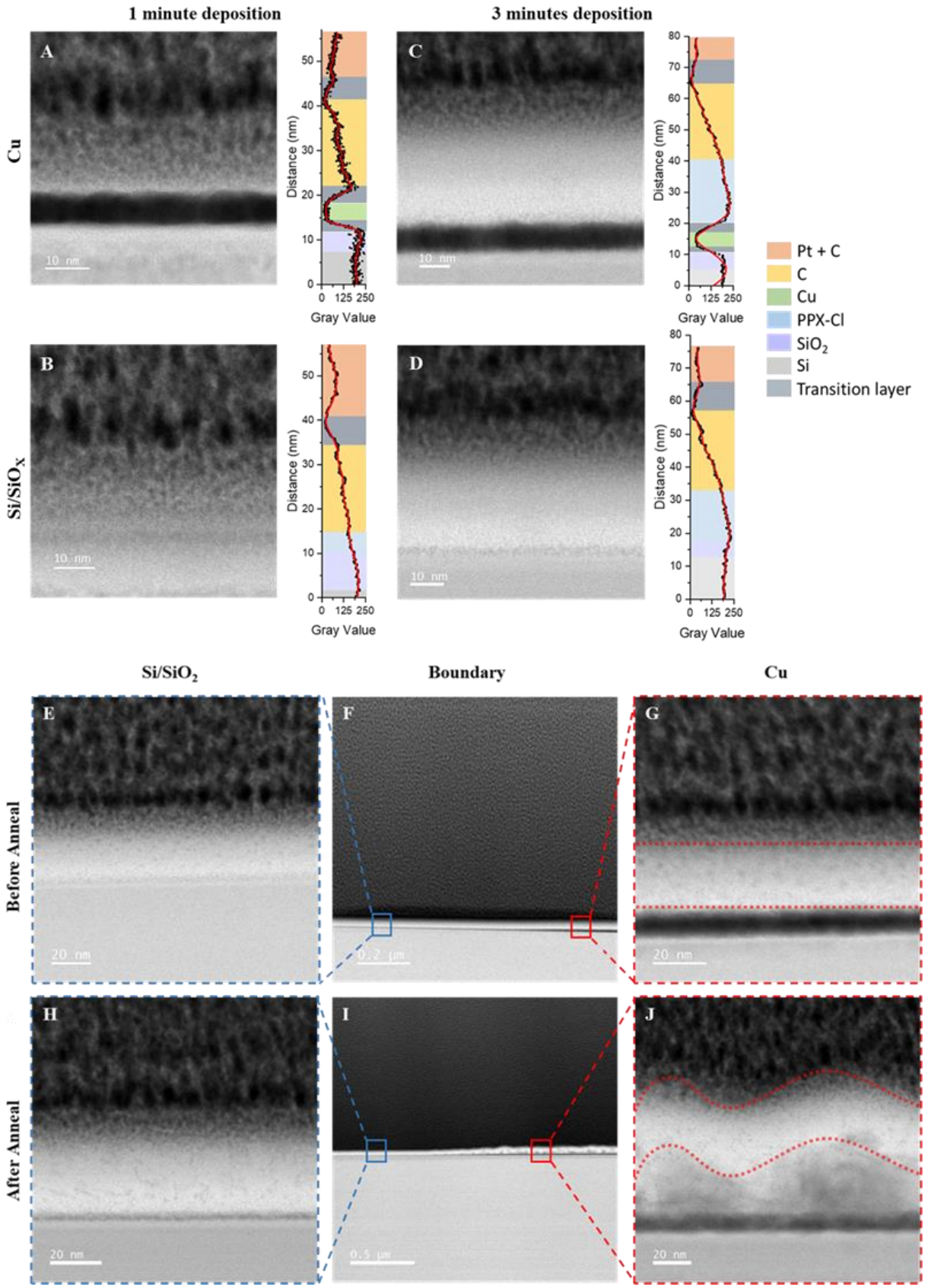
1 minute deposition
3 minutes deposition
Cu
Si/SiOX
A
B
C
D
10 nm
Distance (nm)
Gray Value
0 125 250
Pt + C
C
Cu
PPX-Cl
SiO2
Si
Transition layer
Si/SiO2
Boundary
Cu
Before Anneal
After Anneal
E
F
G
H
I
J
20 nm
0.2 μm
0.5 μm

Figure 2-11: PPX-Cl deposition on patterned Cu on Si substrates at 5 °C and 0.1 mbar. STEM images of (a) 1-minute deposition on Si area; (b) 3 minutes deposition on Si area; (c) 1-minute deposition on Cu area; (d) 3 minutes deposition on Cu area. Gray Values were used to identify each layer. STEM images of samples (f) before annealing (zoom-in images of (e) deposition on Si area and (g) deposition on Cu area) and (i) after annealing (zoom-in images of (h) deposition on Si area and (j) deposition on Cu area). The red line shows the outline of the polymer on Cu substrates.

As shown in Figure 2-11A to D, TEM was performed on Si and Cu areas after CVD coating for 1 minute and 5 minutes, respectively. The STEM images were analyzed by ImageJ, using the contrast of gray value to accurately identify the boundary between layers. There was no polymer layer identified on Cu after 1-minute deposition (Figure 2-11A), while a thin layer of 4.8 nm PPX-Cl layer was detected on the Si surface (Figure 2-11B). However, after 5 minutes of deposition, both Cu (Figure 2-11C) and Si (Figure 2-11D) were coated with a polymer film that had a thickness of around 19 nm, which supports the assumption that the deposition model that PPX-Cl becomes non-area selective under higher pressure.

To ensure that the CVD polymer films were at equilibrium, all samples were annealed at 120 °C for 8 hours. The film thickness before and after annealing was measured using STEM images and shown in Table 2-2. The results show that PPX-Cl deposition on both Si and Cu substrates under different conditions maintained the same thickness before and after annealing, indicating the stability of polymer films prepared by CVD polymerization. After annealing, no roughness change was detected for the Si samples (Figure 2-11H). However, observable surface changes occurred on thin polymer films (2 minutes deposition) on Cu samples as shown in Figure 2-11J. AFM was utilized to measure the morphology of the sample surface as shown in Figure 2-12. It shows that

before annealing, the polymer surface was smooth and uniform with an average roughness of 0.14 ± 0.05 nm (Figure 2-12A), while the samples had a higher average roughness of 1.08 ± 0.42 nm after annealing (Figure 2-12B) Previous research found that partially- and fully-oxidized Cu films can be reduced to Cu metal through vacuum annealing.[83] CuO in partially-oxidized Cu film can also be reduced to Cu_2O after annealing below 380 K. Given our heat treatment was operated at around 400K, the oxygen diffusion might be a potential reason for the observed bucking polymer film.

Table 2-2: Thickness difference (mean ± SD, n = 5) for PPX-Cl deposition on patterned substrates, before and after annealing, measured by STEM.

Deposition Time	**Temperature**	**Pressure**	**PPX-Cl film on SiO_2 area**		**PPX-Cl film on Cu area**	
			thickness before annealing (nm)	thickness after annealing (nm)	thickness before annealing (nm)	thickness after annealing (nm)
1 minute	15 ℃	0.1 mbar	3.8 ± 0.2	3.9 ± 0.3	0	0
2 minutes			8.3 ± 0.3	8.2 ± 0.2	0	0
3 minutes			11.8 ± 0.2	10.5 ± 0.3	0	0
4 minutes			16.3 ± 0.3	15.6 ± 0.1	0	0
1 minute	5 ℃	0.1 mbar	4.8 ± 0.2	4.6 ± 0.1	0	0
2 minutes			12.6 ± 0.2	10.7 ± 0.2	10.7 ± 0.2	10.3 ± 0.7
3 minutes			19.2 ± 0.3	18.9 ± 0.2	18.9 ± 0.1	17.5 ± 3.6
4 minutes			26.8 ± 0.2	25.7 ± 0.1	25.4 ± 0.3	24.0 ± 0.2

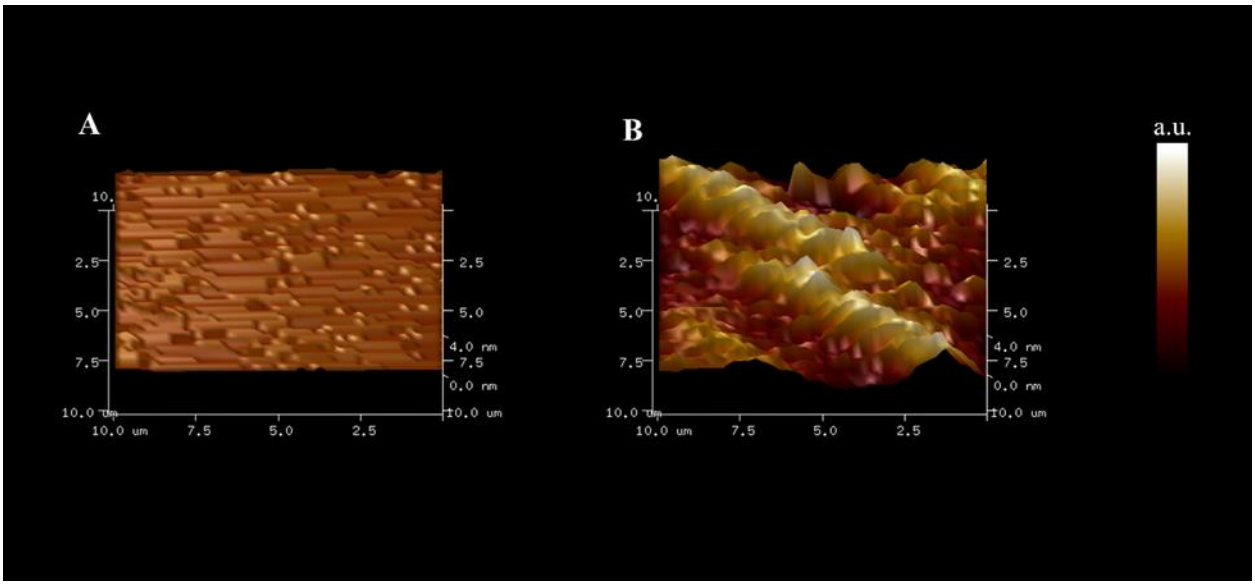

Figure 2-12: 3-D AFM surface images of PPX-Cl deposition on Cu area (a) before annealing and (b) after annealing.

2.4 Conclusions

In this work, we utilized AFM to monitor polymer growth during CVD polymerization prior to and shortly after film closure. Thermodynamic control (here: working pressure and substrate temperature) can be employed to force an area-selective polymer/substrate ensemble to undergo non-selective CVD polymerization. Initial experiments on patterned substrates suggest applicability to microfabrication processes and suggest that area-selective CVD polymerization could be a powerful bottom-up nanopatterning technology.

With further work, these findings will likely facilitate the identification of novel area-selective polymer coatings, predict optimal polymer/substrate combinations, and will contribute to a better understanding of the fundamental resolution limits that can be achieved with area-selective CVD polymerization.

Chapter 3 Area-selective Surface Manipulation on Ruthenium Patterned Substrates via Chemical Vapor Deposition Polymerization

3.1 Introduction and Background

Thin-film technologies have been widely used as the major component of electronic, biomedical, and energy related applications over the last several decades.[84], [85] This is because that two-dimensional thin films can be used to enhance surface interaction or achieve application-specific properties that are unobtainable in the substrate materials.[86] Atomic layer deposition (ALD) is one of the common methods to synthesize inorganic thin films, due to its significant advantages, such as low cost, easy fabrication, and easy integration into production lines. On this basis, chemical vapor deposition (CVD) polymerization offers a versatile platform for fabricating various polymer thin films retaining all the functionalities, which contributes to our understanding of surface chemistry.

Both organic and inorganic thin films have been applied in the semiconductor industry. According to Moore's law,[31], [87] the semiconductor industry is producing nano-scale transistors, a core element of data processing, in order to improve the performance of microchips by twofold every 2 years. Nowadays, microchips can scale down to several nanometers which makes them not only smaller, but also faster, more powerful, and more energy efficient simultaneously. Common industrial fabrication techniques can be categorized into two groups: top-down and bottom-up processes. Top-down technology is using masks to make nanostructures by removing unwanted materials through a lithography process, such as photolithography,[40], [88] electron beam lithography,[89] and extreme ultraviolet (EUV) lithography.[90], [91] The

well-developed semiconductor top-down fabrication process mainly involves nanolithography, dry/wet etch, and/or lift-off of the metal film on non-targeted patterned resists.[38], [56], [92] However, as the transistor size gets smaller, these top-down technologies are also facing their limitation. One of the key issues for dense patterns by lithography is the residual resist in between the pattern lines/spaces.[89], [93] Besides that, lithographic technologies also have other drawbacks that cannot be ignored, such as the device being expensive, and the whole process can only be conducted in clean room, as they have to be avoided airborne particulate or chemical contaminants. Unlike top-down technology, the bottom-up process uses designed substrates to grow nanostructures on the surface based on different material-substrate interactions, such as area-selective deposition (ASD). Ideally, this method can grow nanostructures with limited chemistry/process steps and avoid the residuals simultaneously.[22], [59] However, there is a lack of understanding of the fundamental mechanisms underlying bottom-up fabrication, especially for polymer synthesis.

In the current ASD process, although it shows significant potential for larger than 5 nm technology, alignment for sub-5 nm technology nodes is one of the biggest challenges, especially during the fabrication of multilayered device structures.[61], [94] Another disadvantage of ASD is that there always has residuals deposited on untargeted substrate areas. To avoid unwanted deposition, the fabrication process needs to contain an extra cleaning process, losing the advantages of the bottom-up process, which supposes to contain limited chemical/process steps. For the sake of understanding deeply the fundamental mechanism of ASD and its potential application in semiconductor industries, area-selective CVD polymerization has been used to understand the relationship/interaction between substrates and deposit polymers. CVD coatings have been widely used in either electronic materials or biomaterials due to their advantages of pin-

hole free, confocal, controllable thickness, and tunable chemistry.[75], [95] In previous works, people found that metal substrates with relatively high surface energy, such as Copper (Cu), Titanium (Ti), and Iron (Fe), together with their salts can prevent deposition on their surface.[27] Moreover, the side functional groups of deposited polymers also played a critical role in area-selective deposition.[27] For example, the functional groups consisting of oxygen and nitrogen can still deposit on those metal inhibitor surfaces because of the chelation effect. Our previous research also shows that there were no residuals on unfavored metal substrates after CVD polymerization.

In this chapter, we systematically investigated the selective inhibition of Ruthenium (Ru), a common metal used in the semiconductor industry, with a series of functionalized poly-*p*-xylylene (PPX) deposited by CVD polymerization to detect the influence of functional groups to surface interaction. After that, different metal substrates have been utilized to measure the effect of substrates with constant polymer precursors. In the meantime, we demonstrated that mass is another input effect of area-selective deposition which can switch the deposition from area-selective to non-selective. Further deposition was done on Ru patterned substrate to mimic the real industrial fabrication process. The cross-section scanning transmission electron microscopy (STEM) was demonstrated on area-selective deposition and non-selective deposition on these patterned substrates to compare the developed nanostructure. As no residual has been found on the top of Ru patterns after area-selective deposition, the potential use of CVD in fabrication can be validated. Moreover, it has been found that the feature size of Ru patterns does not affect the area-selectivity of CVD polymer coatings. Those two facts demonstrate that area-selective CVD polymerization may provide an extremely simple access route toward nanostructure development on designed substrates.

3.2 Experimental Methods

CVD polymerization:

The precursors of polymer **1-12** were all synthesized following the previously reported route.[70], [71], [96] They were polymerized via CVD process with 20 mg of each precursor. The precursors were put in the sublimation zone in the CVD system which was about 100 ℃. Then they were sublimated into the gas phase and transferred into the pyrolysis zone by the inert carrier gas, Argon, which was setting at the constant flow rate of 20 sccm. The pyrolysis regime was kept at 550 ℃ and converted the precursors into the corresponding quinodimethanes. These reactive species were further carried into the deposition chamber, which had a rotating cool stage at 15 ℃ with the ideal substrates on it, and spontaneously polymerized onto the cooling substrates while condensation. The patterned substrates were fabricated by Intel Co. The wall of the deposition chamber was maintained at 90 ℃ to prevent any residual deposition on it. The pressure of the whole system was 0.1 mbar.

Surface Characterization:

Thickness data of the polymer films was collected by a M-2000 Ellipsometer (J.A.Woollam, United States). The M-2000 provides simultaneous measurements at light wavelengths from 193 nm to 1700 nm through a continuously rotating compensator and using a CCD spectrometric detector.[97] The incidence angles in this work were, 60°, 70°, and 80°. Axis Ultra X-ray Photoelectron Spectroscopy system (Kratos Analytical Ltd, United Kingdom), which is equipped with a monochromatized Al source, was used to measure all XPS data. During the experiments, the lens mode was hybrid, while the x-ray power was 150kW. The pass energy was kept at 160.0 eV for survey acquisition and 20.0 eV for high resolution acquisition (Ru and specific elements on

side functional groups of polymers). All spectra were calibrated with respect to non-functionalized aliphatic carbon with a binding energy of 285 eV using CasaXPS software. The patterned substrates were confirmed by SEM after etching. The SEM images were taken under SE mode using 50 pA current and 2.00 kV Hz. The lift-out sample for scanning transmission electron microscopy (STEM) was prepared by Helios G4 PFIB UXe (Thermo Fisher Inc., United States) equipped with Schottky field emitter and inductively coupled Xe gas plasma as electron and ion beam source, respectively. A 0.2 μm-thick layer of carbon was deposited first by the gas injector of the electron beam source. Following by a 2 μm-thick carbon and platinum mixed layer with an ion beam source. An Argon ion beam was performed at a higher beam current (starting at 0.5 μA and decreasing to 15 nA once it was closing to the region of interesting materials) to roughly mill the sample surface with two trenches and leave a wall of material. This cross-section lamella was then attached on a lift-out TEM grid (Ted Pella Inc., United States) by carbon and platinum mixed materials and further thinning by 1.0 nA beam current. STEM data was collected by Talos F200X G2 S/TEM (Thermo Fisher Inc., United States), using a double-tilt holder for simultaneous STEM HAADF/DF4/DF2/BF acquisitions.

3.3 Results and Discussion

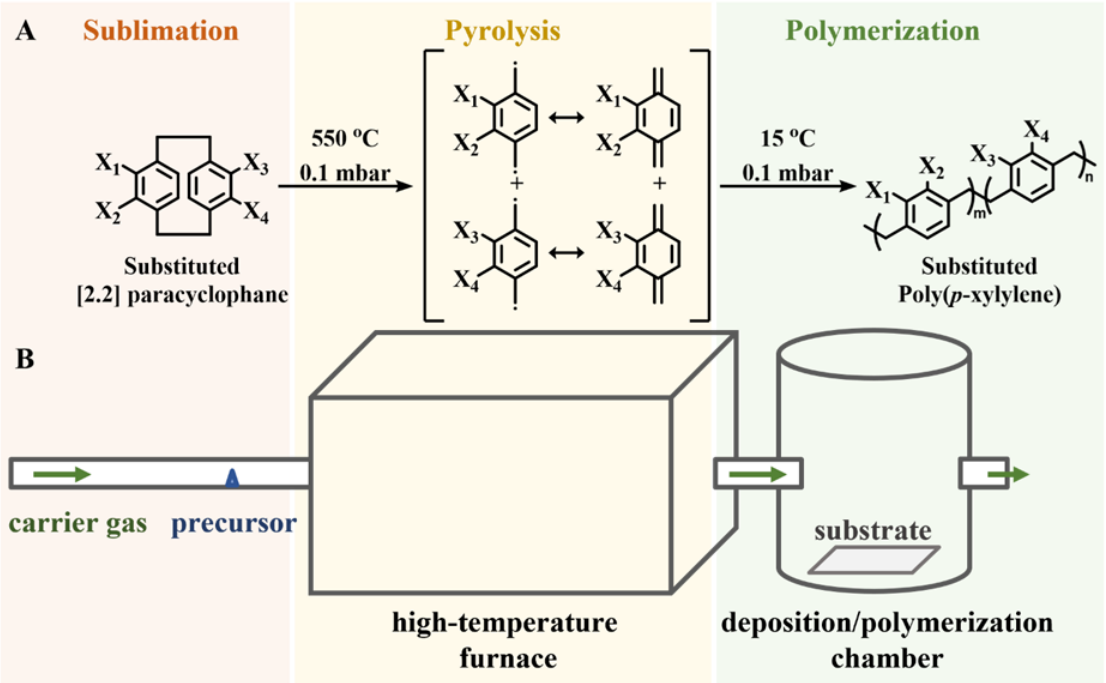

C

	(1)	(2)	(3)	(4)	(5)	(6)	(7)	(8)	(9)	(10)	(11)	(12)
X_1 =	H	Br	Br	Cl	Cl	$(CO)_2O$	$COCF_3$	CH_2NH_2	NH_2	CH_2OH	COC_2H_5	CH_2OCH_3
X_2 =	H	H	H	H	H		H	H	H	H	H	H
X_3 =	H	H	Br	Cl	H	$(CO)_2O$	H	H	H	H	H	H
X_4 =	H	H	H	H	H		H	H	H	H	H	H

Scheme 3-1: a) Polymerization process of substituted [2,2]paracyclophanes. b) Schematic illustration of CVD polymerization process. c) Table of polymer **1 - 12** that deposited via CVD polymerization.

To investigate the inhibition of Ru substrates, 12 different substituted poly(*p*-xylylene) (PPX) precursors were utilized to deposited on flat Ru and Si substrates via CVD polymerization. All substrates operated in this work have natural oxidation layers. The reaction of polymerization is shown in Scheme 3-1A and the CVD polymerization process is illustrated in Scheme 3-1B. Guided by previous published area-selective CVD polymerization principles,[27] the selected substituted PPX contains a wide range of side functional groups, including amines,[98], [99] alcohols,[99],

[100] aldehydes,[73] anhydrides,[101] and ketones.[53], [101] The list of deposited polymers is shown in Scheme 3-1C. As we mentioned before, the term area-selectivity is used to compare the deposition abilities on two or more different substrates. The thickness of CVD polymer films on Ru and Si were measured by ellipsometer, as shown in Figure 3-1, so that the area-selective can be defined by the equation of selectivity (S) (Eq. 3-1) which compare the thickness difference on different substrates. The equation of selectivity (S) is named below.

$$S = \frac{|\text{thickness}_{\text{sub1}} - \text{thickness}_{\text{sub2}}|}{\text{thickness}_{\text{sub1}} + \text{thickness}_{\text{sub2}}} \qquad (3\text{-}1)$$

S ranges between 0 and 1.0 and the polymer shows more area-selectivity on the substrate pair if S is closer to 1.0. Based on the ellipsometer results, polymer selectivity can be summarized into four categories. 1) If the polymer cannot be deposited on one of the substrates, but can polymerization on the other, we call this kind of polymer an area-selective material. For area-selective polymers, their S is usually higher than 0.95. 2) If the polymer can be deposited on both substrates but with significant thickness difference, they are defined as partial area-selective polymers. Under these circumstances, their S is between 0.85 and 0.95. 3) The same as partial-area selective polymer, but with less thickness difference. These polymers are called semi-area selective. Their S is usually between 0.1 to 0.85. 4)The last one is non-area selective materials, which have almost identical thicknesses on both substrates with S no large than 0.10.

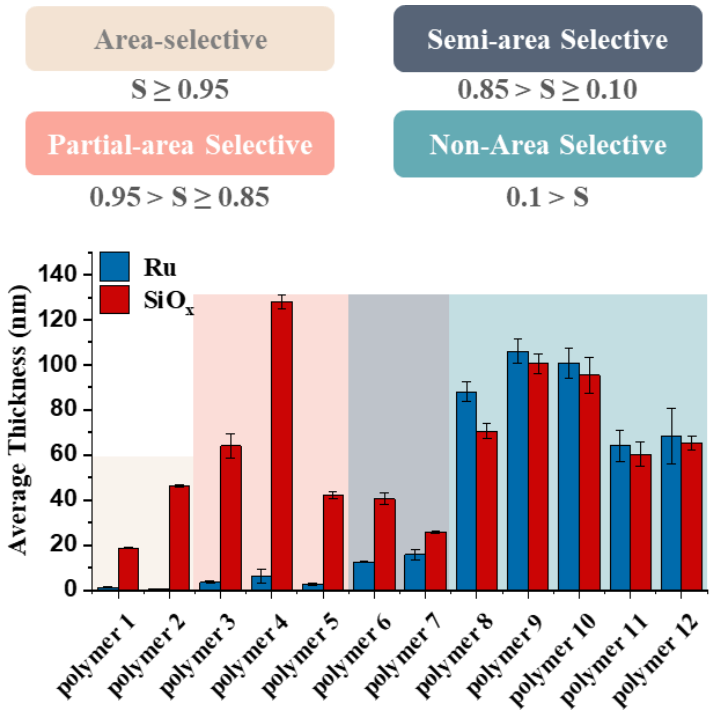

Figure 3-1: Average thickness of polymer **1 - 12** on Ru (blue) and SiOx (red) substrates. Values are shown in average ± SD, n = 3.

Because of the nature of X-ray Photoelectron Spectroscopy (XPS), which can detect the chemical composition of the top 10-nm materials, we used it as a confirmation of the ellipsometry results (Table 3-1). The thickness of materials can be roughly identified depending on if the Ru substrates can be detected or not. The XPS results are consistent with the ellipsometry, together with the calculated S of each polymer shown in Table 3-1.

Table 3-1: Measured XPS results of 20 mg polymer **1-12** deposit on Ru substrates and their selectivity results. The selectivity results were calculated based on ellipsometer data, n = 5.

Polymer	**XPS (observed)**		**Selectivity (S)**
	Ru	Polymer film	
1	✓	×	0.98
2	✓	×	0.97
3	✓	✓	0.91
4	✓	✓	0.89
5	✓	✓	0.89
6	✓	✓	0.53
7	×	✓	0.23
8	×	✓	0.10
9	×	✓	0.03
10	×	✓	0.03
11	×	✓	0.03
12	×	✓	0.02

After categorizing the 12 polymers by their selective property, more focus is put on the partial-area selective polymers (polymer **3-5**). Do these polymer coatings become non-area selective if they are deposited with sufficient weight to limit the influence of the substrate? Under these

circumstances, five different precursors of polymer **1-5** (polymer **1** and **2** are used as control) were polymerized on four different substrates, including Si, Gold (Au), Copper (Cu), and Ru. 20 mg (Figure 3-2A) and 40 mg (Figure 3-2B) of each material were used as the feeding amount of each precursor. All polymerizations were processed under identical experimental conditions. When using 20 mg precursors, only polymer **1** revealed area-selectivity on Au substrates, while the rest were all non-selective on Au, compared with deposition on Si substrates. All monomers showed area selectivity on Cu substrates. This confirmed with previous studies that Cu (1.81 J/m^2)[102] has higher surface energy than Au (1.51 J/m^2)[102] and Si ({111}, 1.14 J/m^2).[103] Among all metal substrates, only Ru demonstrated partial-area selectivity as the other metal substrates were either selective or non-selective. This is because Ru has the highest surface energy (3.0 J/m^2) [104], and even for polymers that can be deposited on its surface, the deposition rate is very slow until a conformal polymer coating is formed. Meanwhile, polymer **1**, PPX with no side functional group, has the highest selective ability within five substituted PPX. However, once the amount of the precursors increased to about 40 mg of three partial-area selective polymers on Ru (polymer **3-5**), polymer **4** and **5**, both have chlorine as side functional groups, became non-area selective on Ru. Polymer **3** still maintained its partial-area selectivity on Ru regardless of the increasing feeding amount. This might be due to a higher selectivity of polymer **3** than polymer **4** and **5**. The results indicate that there is also a mass threshold for each precursor to switch between area-selectivity and non-selectivity. This threshold is changing based on precursor species, substrate type, and deposition conditions (deposition temperature or working pressure). Knowing the mass threshold of each precursor and substrate pair can help to design different nanostructures under varied deposition conditions.

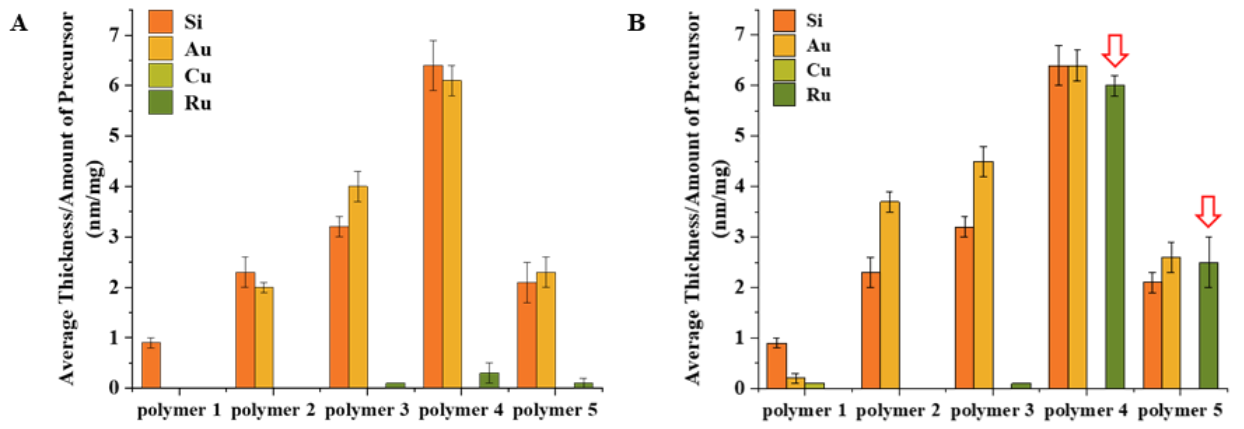

Figure 3-2: Average thickness of unit amount of polymer **1-5** precursors on Si (orange), Au (yellow), Cu (light green), and Ru (dark green) substrates, with (a) 20mg and (b) 40mg deposition. Values are shown in average ± SD, n = 3.

Ru patterned Si substrates were utilized to examine the proximity effect of area-selective CVD. Given that the focus of this work is directed toward microelectronic and nanoelectronics applications, a variety of line patterns were investigated as Ru-on-Si substrates. The key parameters for these patterns are feature thickness and spacing between the center of each line denoted as 80/200 (nm) for a line width of 80 nm and a spacing of 200 nm in this work. Made through controlled etching, Ru thickness is held constant at 25 nm though some Si is lost to the etching process (leading to an additional ca. 20 nm of depth between features). The morphology of the substrate surface was confirmed by scanning electron microscopy (SEM) in Figure 3-3.

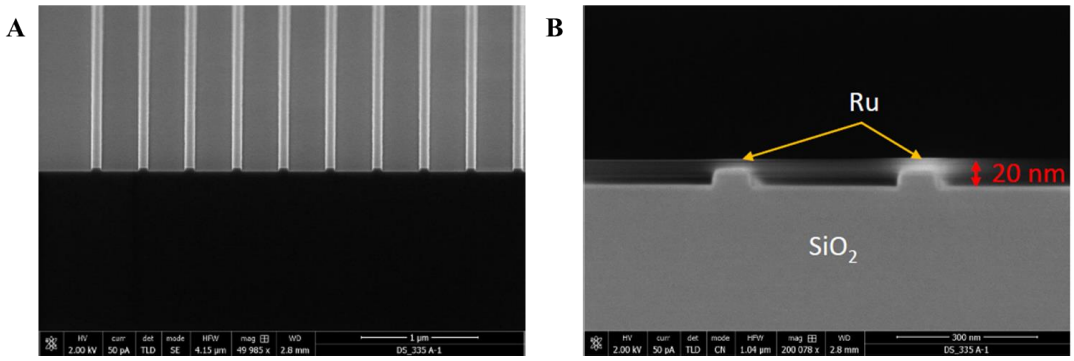

Figure 3-3: Surface geometry of Ru patterned substrates. (a) top-down SEM image of substrate. (b) cross-section SEM image of substrate.

10 mg of area-selective (polymer **5**, poly[(chlorine-*p*-xylylene)-*co*-(*p*-xylylene)]) and non-area selective (polymer **10**, poly[(hydroxymethyl-*p*-xylylene)-*co*-(*p*-xylylene)]) polymers were deposited on the patterned substrates by CVD polymerization. Here, the feeding amount of polymer **5** precursors was 10 mg, lower than the 20 mg used in the previous screening study. With this low amount of precursors, polymer **5** reveals S = 1.0, indicating area selectivity. After deposition, cross-section STEM was performed to detect the morphology of polymer layers on different surfaces of patterned substrates. Deposition of polymer **10** (non-selective) on 80/200 nm line patterns were shown in Figure 3-4A and B. In Figure 3-4A, polymer **10** coating fully covered both Si and Ru area with a S = 0.03, demonstrating its non-area selectivity on substrates with complex geometry. However, within the zoom-in image in Figure 3-4B, polymer aggregation at the corner of structures cannot be entirely ruled out. It has been observed in related systems that (strong) anisotropic surface energy can affect the diffusion of reactive species during deposition and polymerization.[105] Further work is warranted to fully elucidate the underlying mechanism. Then the thickness of polymer **10** on Si and Ru was calculated based on these STEM images, as shown in Table 3-2. The polymer thickness on Ru was measured in the middle area of Si surface, avoiding the aggregation effects. The results address the same thickness on different substrates

and reveal that CVD polymerization can still form conformal polymer layers on patterned substrates. Besides, the STEM images of polymer **5** coating on patterned substrates were shown in Figure 3-4C and D. The fact that there is no residual on Ru top surface validates the area-selectivity of polymer **5** on three-dimensional nanostructure. Similarly, polymer aggregation at the corner region is also observed in Figure 3-4D. Unlike the current ASD processes which usually need an afterward cleaning process to remove the possible nuclei on non-target areas, as these unwanted materials might cause the loss of area-selectivity, here we introduce a new possible vapor deposition solution by area-selective CVD polymerization. [22]

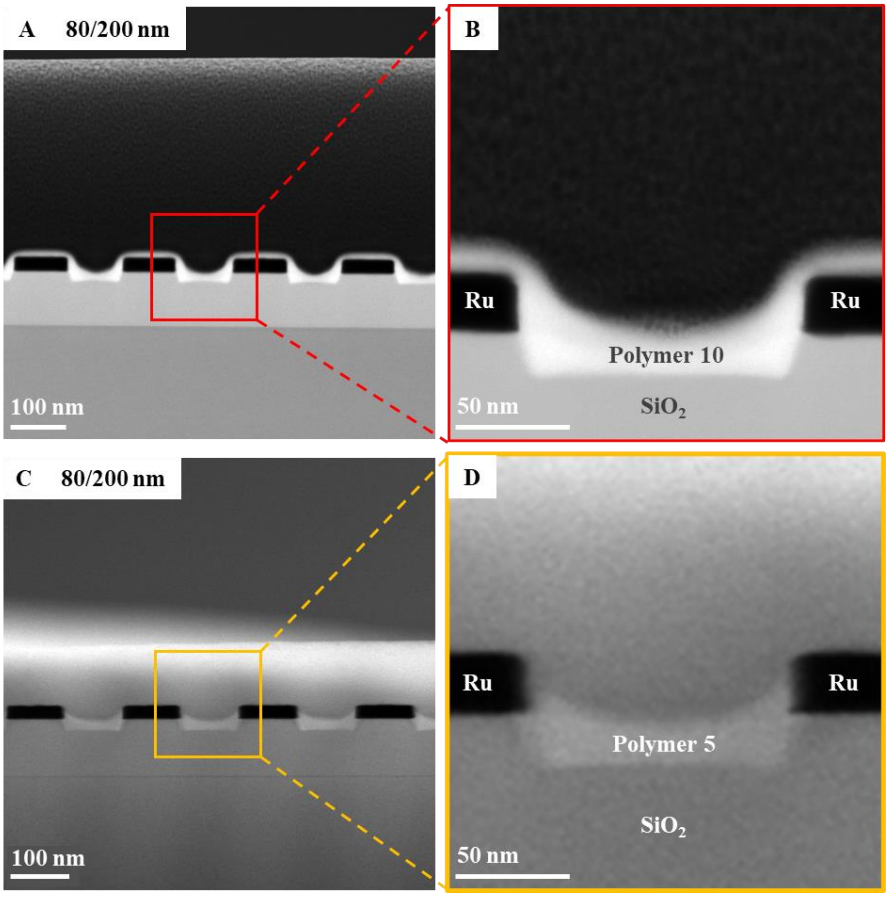

Figure 3-4: Cross-section STEM images of 10mg (a) polymer **10** and (c) polymer **5** deposition on 80/200 nm Ru patterned Si substrates. (b) and (d) are zoom-in images of (a) and (c), respectively.

Table 3-2: Polymer thickness on different substrate regions. Value = average ± SD, n = 5.

Polymer	**Polymer 10**	**Polymer 1**	**Polymer 5**
Filling shape	Conformal	Non-conformal	Non-conformal
Polymer thickness on SiO_x	13.5±0.9 nm	19.4±0.4 nm	18.5±0.3 nm
Polymer thickness on Ru	14.4 ±0.2 nm	-	-

Nevertheless, in order to meet the requirement of small-scale selective deposition, area-selective deposition on different feature/spacing size of patterned substrates were measured. 10 mg of polymers **5** were deposited on patterned substrates with different feature/spacing sizes (80/200 nm and 2/5 μm), as shown Figure 3-5. Our previous results suggest that polymer **5** is a partial-area selective polymer (20 mg). Here, its area-selectivity was tested on a larger feature size (2/5 μm) and polymer **1**, which proved to have higher selectivity, were utilized on smaller feature size (40/100 nm and 60/200 nm) as shown in Figure 3-6. The STEM images in Figure 3-5 and 3-6 address that selective polymers remain their selectivity on patterned substrates, regardless of the feature size.

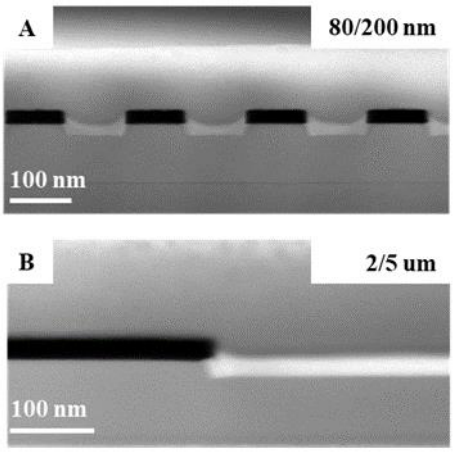

Figure 3-5: Cross-section STEM images of 10mg polymer **5** (PPX-Cl) deposition on (a) 80/200 nm and (b) 2/5 μm Ru patterned Si substrates.

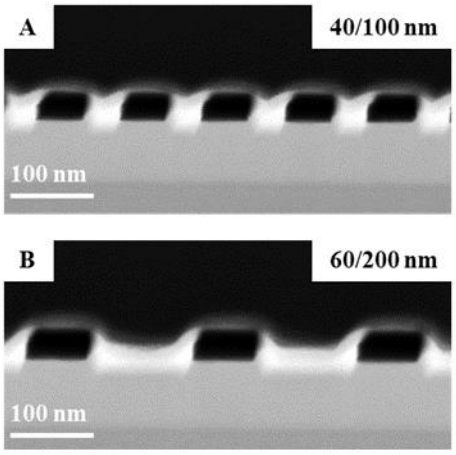

Figure 3-6: Cross-section STEM images of 10mg polymer **1** (PPX-N) deposition on (a) 40/100 nm and (b) 60/200 nm Ru patterned Si substrates.

3.4 Conclusion

In summary, we report Ru as a prohibitive metal substrate for some of the functional PPX deposition. As the surface energy of Ru is higher between the usual metal substrates that we tested (Cu and Au),[102], [103], [106] partial-area selective deposition was observed on Ru substrates

under common CVD process conditions. This indicates that the feeding amount of polymer precursors also plays a critical role in deciding polymer selectivity and can be controlled to grow different nanostructures by needs. Furthermore, our results first indicate that the cross-section images of area-selective deposition on patterned substrates by CVD polymerization. The fact that there are no residuals of area-selective polymers on the Ru surface shows the potential use of area-selective CVD as a bottom-up technology to grow nanostructures. In a previous study, we find out that besides mass, deposition conditions, including working pressure and deposition temperature, can also transfer selectivity. Further study will be focused on the selectivity control on Ru patterned subtracts based on those controllable CVD parameters.

Chapter 4 CVD-Based Reactive Polymer Coatings for Engineered Biological Applications

The materials shown in this section were adapted from the following peer-reviewed journal article with permission:

- Horowitz, J. A., **Zhong, X.**, DePalma S. J., Ward Rashidi, M. R., Baker, B. M., Lahann, J., Forrest S. R., "Printable Organic Electronic Materials for Precisely Positioned Cell Attachment". Langmuir 2021, 37(5), 1874–1881.

4.1 Overview

In Chapter 4, bio-orthogonal polymer coatings prepared by CVD polymerization of functional [2,2]paracyclophanes were used to engineer biological applications.

- In Section 4.2, we address a fabrication method for precisely positioned cell attachment, applying chemical vapor deposition (CVD)-initiated atom transfer radical polymerization (ATRP) reaction.
- In Section 4.3, we demonstrate the ability to utilize the CVD-based copolymer coatings as a reactive gene-therapy vehicle to immobilize multiple biomolecules of interest for bone regeneration application.

4.2 Printable Materials for Precisely Positioned Cell Attachment

4.2.1 Introduction and Background

Since the 1960s, there has been increasing interest in engineering biological interfaces for biotechnological applications, based on cell-surface interaction. [107], [108] Previous research has revealed the application of polymer brushes to either prevent non-specific protein adsorptions[44] or precisely recognize and bind to specific proteins[45], [46] by controlling the brush composition. Polymer brushes are special macromolecular structures with polymer chains densely tethered to another polymer chain or the surface of ideal substrates via a stable covalent or non-covalent bond linkage.[106] Polyethylene glycol (PEG)-based compounds are often considered biologically inert as they do not mediate interactions with most proteins,[109], [110] are a popular choice for preventing the attachment of extracellular matrix (ECM) adhesion proteins. Surface-initiated atomic transfer radical polymerization (ATRP) has been used most widely to form PEG-based polymer brushes, as this method is compatible with a wide range of different functional monomers.[49] However, as a surface modification method, ATRP still requires initial surface modification to introduce initiator groups to the substrates, allowing the following polymerization process.

Chemical vapor deposition (CVD) polymerization is one of the common surface modification protocols to deposit various side functional groups onto a wide range of different substrate materials.[27] The CVD polymerization process shows promising features, such as ultra-thin polymer layers with pinhole-free coverage, tunable chemistry and geometry, and conformal coatings.[1], [3], [18], [26] Herein, in this work, we introduce a new process whereby using biocompatible poly(hydroxymethyl-*p*-xylylene) (PPX-HM) coating, which is readily deposited using CVD polymerization, to attach ATRP initiators on the substrate surface by initiation

reaction. Subsequently, antifouling polyethylene glycol methacrylate (PEGMA) polymer brushes are selectively grown in the spaces between adhesion points. Fibronectin attaches only to the non-polymer brush area, enabling the selective attachment of murine fibroblasts (NIH3T3). Our results addressed a high throughput, reproducible, and highly selective tissue production method for therapeutic and research applications, using a CVD-based ATRP process.

4.2.2 Experimental Methods

Chemical Vapor Deposition (CVD) Polymerization:

Silicon substrates with a natural oxide film (1 cm^2) are sequentially cleaned with 1:100 Tergitol in deionized (DI) water, acetone, isopropanol, and ultraviolet-ozone plasma. Next, a layer of PPX-HM is grown by CVD using the Gorham process (Scheme 4-1A).[76] The PPX-HM precursor is homolytically cleaved in a furnace with zones set at 450, 550, and 560 °C. The substrate is kept at 15 °C during deposition, allowing the reactive pyrolysis products to polymerize on its surface. The CVD system is pumped to 8 mtorr and then purged with 20 standard cubic centimeters per minute (sccm) of Ar, resulting in a pressure of 0.08 torr. The deposition is at a rate of 0.1 Å/s, resulting in a 15−20 nm thick layer of PPX-HM, as measured by ellipsometry.

Atom Transfer Radical Polymerization (ATRP) Reaction:

Following vapor phase deposition and patterning, samples are placed in a vacuum desiccator with four glass slides. Triethylamine is placed on each of two glass slides and 2-bromoisobutyryl bromide (30 μL on each glass slide) on the other two. The reaction, occurring overnight (approximately 18 h), attaches 2-bromoisobutyryl onto the hydroxymethyl group of PPX-HM (Scheme 4-1B). 2-bromoisobutyryl does not form on regions of PPX-HM covered by deposited organic electronic material. PEGMA polymer brushes are then grown via an atom transfer radical

polymerization (ATRP) reaction where a mixture of 4 g of PEGMA, 7 mg of $CuBr_2$, and 20 mg of CuBr, in 10 mL of DI water is reacted with 30 mg of 2,2'-bipyridyl in 10 mL of DI water. The reaction occurs over 90 min, growing PEGMA polymer brushes to a height of 20−30 nm off of the acetyl bromide groups on PPX-HM (Scheme 4-1C).[54] X-ray photoelectron spectroscopy (XPS) and Fourier transform infrared spectroscopy (FTIR) spectra of the PEGMA brush growth process are provided in Figure 4-1.

Surface Characterization:

Fourier transform infrared (FTIR) spectrometry measurements were performed using a Thermo Nicolet 6700 spectrometer with a grazing angle accessory on a 20 nm thick film of PPX-HM deposited onto cleaned Au substrates.

XPS measurements were performed with a monochromatic Kratos Axis Ultra X-ray photoelectron spectrometer on 20 nm thick small-molecule films and PPX-HM deposited onto cleaned Si substrates. The Al X-ray gun emission current was 8 mA with a 14 kV high-temperature anode in a sample-analysis chamber at 10−8 torr. Sample charging was corrected assuming 284.8 eV as C 1s binding energy.

Fibronectin Attachment (performed by Samuel DePalma):

Alexa Fluor 555-labeled fibronectin or unlabeled fibronectin is coated onto the samples at a concentration of 50 μg/mL in prebuffered saline (PBS) solution (Scheme 4-1F). The fibronectin-coated samples are incubated for 1 h and rinsed to remove excess solution. Murine fibroblasts (NIH3T3) are cultured at 37 °C and 5% CO_2 in Dulbecco's Modified Eagle Medium (DMEM) containing 1% penicillin/streptomycin, L-glutamine, and 10% bovine serum. The culture media is

aspirated, and substrates are rinsed twice with PBS, followed by the addition of 0.5 mL of 0.05% trypsin−EDTA (ethylenediamine tetra-acetic acid). The cultures are incubated at 37 °C for 5 min, causing the cells to detach from the surface. Trypsin is deactivated by adding 1.5 mL of culture media to each well, and the cell solution is transferred to a 15 mL tube. Cells are seeded at a density of 12,000 or 10,000/cm^2 and incubated overnight, after which they are fixed in 4% paraformaldehyde for 10 min and rinsed twice with PBS. The samples are treated with 4',6-diamidino-2-phenylindole (DAPI) to image nuclei blue and with Alexa Fluor 488-labeled phalloidin to image F-actin. All fluorescent images are taken with a laser-scanning confocal microscope (Zeiss LSM800).

Confocal Imaging (performed by Samuel DePalma):

Silicon substrates with patterned cells and fibronectin are placed on glass microscope slides, with the patterned surface facing the glass. The microscope slides are flipped and placed in the Zeiss LSM800 confocal microscope such that the patterned surface faces the laser and lens to image the sample surface. The laser wavelengths used are 405 nm to image DAPI, 488 nm to image Alexa Fluor 488, and 555 nm to image Alexa Fluor 555.

4.2.3 Results and Discussion

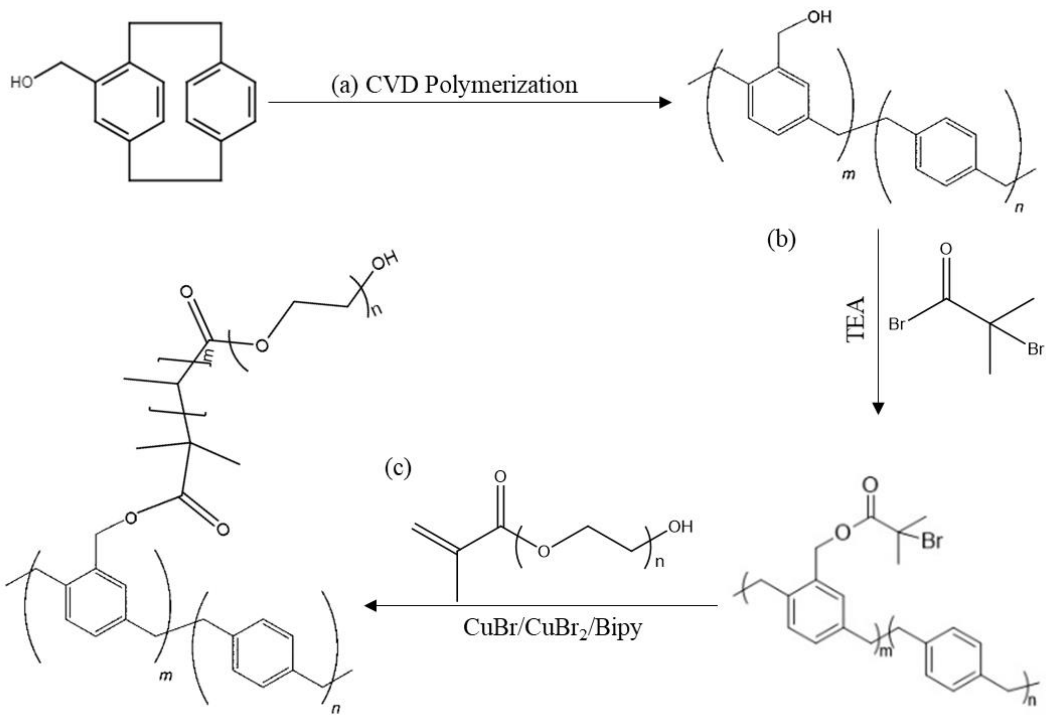

Scheme 4-1: Polymerization process flow of polymer brushes. Si substrate is coated with (a) poly(hydroxymethyl-*p*-xylylene) (PPX-HM) by chemical vapor deposition (CVD) polymerization. (b) Initiator reaction in a vacuum desiccator forms acetyl bromide on the hydroxymethyl group of PPX-HM. (c) PEGMA polymer brushes are grown from acetyl bromide by an atomic transfer radical polymerization reaction in solution.

The whole substrate preparation contains three parts: deposition of PPX-HM, initiation reaction on the PPX-HM surface, and growth of PEGMA brushes by surface initiated-ATRP. After the CVD polymerization process, organic materials, CBP, DBP, and rubrene, were deposited through TEM grids to make patterns on the PPX-HM surface. They were utilized to confirm the initiation reaction which only happens on the PPX-HM surface. The XPS results in Figure 4-1 compare the presence of Br for the different reaction steps. After the initial deposition of DBP, CBP, rubrene, or PPX-HM, there is no Br on the samples (Figure 4-1A). Following the

immobilization of the bromine-containing ATRP initiator, two characteristic Br signals are visible on samples coated with PPX-HM, but not on the control samples coated with DBP, CBP, or rubrene (Figure 4-1B). This clear contrast indicates successful covalent immobilization, rather than non-specific adsorption. Following the ATRP reaction, Br is ultimately consumed during extended chain propagation, and the two Br signals are no longer visible in the XPS spectra (Figure 4-1C). These results demonstrate that acetyl bromide groups are selectively formed on PPX-HM surfaces. Because PEGMA polymer brushes require initiation from these acetyl bromide groups, the polymer brushes can be patterned selectively onto PPX-HM patches, and will not form on surfaces covered with DBP, CBP, or rubrene. The corresponding FTIR spectra confirm the chemical reaction scheme used to modify the PPX-HM films. The characteristic bands of the PPX-HM film (Figure 4-1D) include -OH (3360 cm^{-1}) and C-H (2846, 2915, 2962 cm^{-1}) stretching vibrations. After the ATRP initiator immobilization, characteristic signals of the strong C=O (1731 cm^{-1}) and C-O-C (1159 cm^{-1}) stretching vibrations are observed (Figure 4-1E), indicating a successful reaction of the hydroxyl groups of the PPX-HM films with the acetyl bromide groups of the ATRP

initiator. After the ATRP initiator reaction (Figure 4-1f), the strong bands indicative of the C-O-C stretching vibrations are broadened and a slight shift to higher wavenumbers is observed.

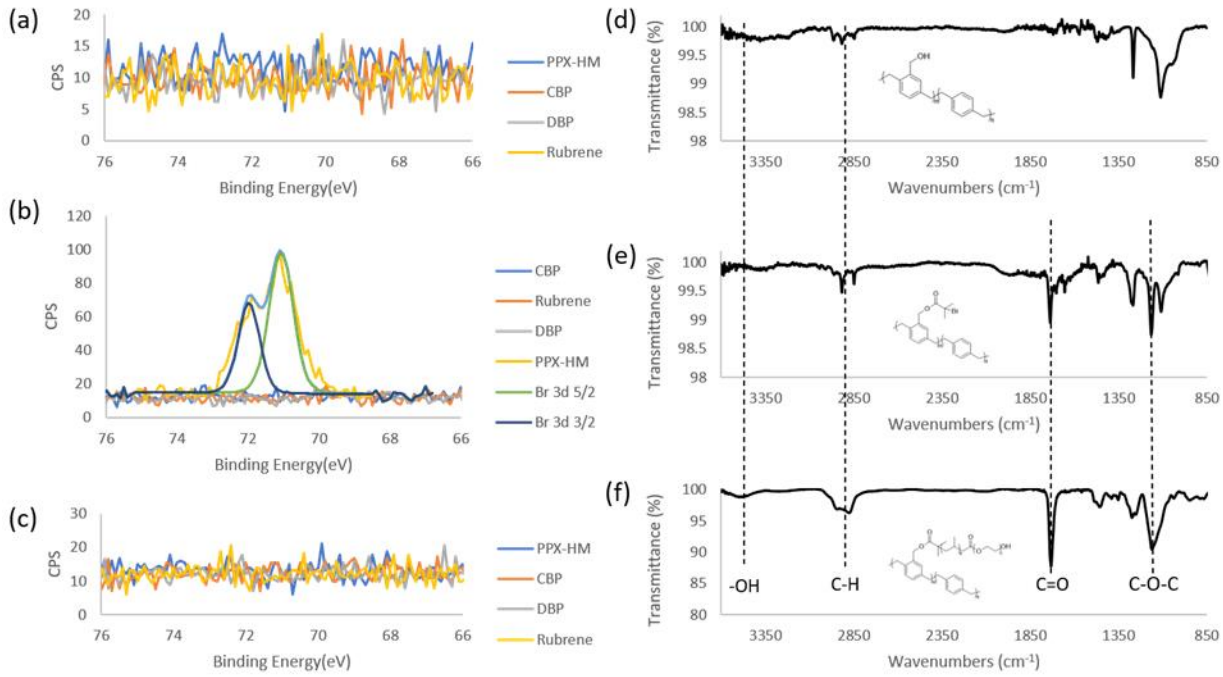

Figure 4-1: XPS spectra of Br 3d for PPX-HM (yellow), CBP (blue), and DBP (gray). (a) Before, and (b) after the reaction with the ATRP initiator. The green and dark blue lines in (b) indicate the corresponding PPX-HM, while the flat blue and grey lines indicate no Br on CBP or DBP. (c) The XPS spectra after ATRP polymerization. The FT-IR spectra of PPX-HM are given (d) before and (e) after the reaction with the ATRP initiator. (f) FT-IR spectra of PEGMA polymer brushes on the PPX-HM surfaces after ATRP.

After that, the Baker group (Department of Biomedical Engineering, University of Michigan) evaluated the attachment of biomolecules on designed patterned substrates. They found that fibronectin shows considerable adhesive selectivity, which is only attached within the hexagon array of DBP material. This confirms that PEGMA brushes are able to inhibit the adhesion of cells in their regions, and consequently, fibronectin or cells may attach only on organic materials surface. On this basis, a simple process can be engineered to control the precise adhesion of cells,

combining CVD initiated-ATRP and other vapor phase deposition methods. Details of the experimental procedures and results can be found in [100].

4.2.4 Conclusion

We have demonstrated a simple, high-yield, and biocompatible process for the selective attachment of fibroblasts using common, vacuum-deposited thin polymer coatings combined with ATRP reaction to growing PEGMA brushes, which can inhibit fibronectin attachment outside of the desired adhesion regions. The process diverges from previous micropatterning techniques in two significant ways. First, CVD polymerization has been confirmed as an efficient surface modification method for a wide range of different substrate materials.[2], [27], [53], [75] In this case, this CVD initiated-ATRP approach establishes a generic surface engineering protocol that is widely applicable to a range of materials. Second, with designed adhesion points, this fabrication method can be employed for the purpose of cell adhesion, allowing for the optimization of parameters for a particular cell chemistry or scaffold attachment application. This technique can also be modified to achieve higher yield and scalability, ultimately allowing for the design of biological tissue *in vitro* or *in vivo*.

4.3 Gene Delivery via Reactive CVD Co-polymer Coating for Enhanced Cell Communication

4.3.1 Introduction and Background

Gene therapy is a common treatment method for human genetic diseases, such as hemophilia,[111] infectious disease,[112] and cancer,[113]–[115] by introducing genetic materials/information into specific cells, showing growing promise.[116] Viral plasmids are now designed to maintain the coding aspects for packaging and delivery of the gene of interest, while rendered incapable of replication, allowing us to utilize the highly efficient transduction mechanism of the virus and limiting safety risks. Selection genes and fluorescent markers can be added to the plasmid as well, which are additional tools for *in vitro* and *in vivo* studies. The scope of use of viral gene delivery significantly increases with the aforementioned materials and viral technology improvements.

Cell-cell communication is necessary for tissue homeostasis, coordination, and synchronization of various cell behaviors in 2D and 3D. The most rapid form of cell-cell communication is gap junction intracellular communication (GJIC), which is mediated through connexon channels. These channels allow passage of small molecules under 1-2 kDa,[117] such as ions and secondary messengers, and thus are important for both mechanical and chemical signal propagation. One of the most ubiquitous connexins is Connexin 43 (Cx43), which is present in a variety of cells including cardiomyocytes, and endothelial cells and is the most prevalent connexin in bone, expressed in Mesenchymal Stem Cells (MSCs) as well as osteoblasts and osteoclasts.[118], [119] Deletion of Cx43 leads to poor bone formation, reduced osteoclast function, and reduced MSC differentiation while upregulating Cx43 and gap junction intracellular communication (GJIC) leads to increased Mesenchymal Stem Cells (MSCs) differentiation *in-*

vitro and bone formation *in-vivo*.[120] Thus Cx43 upregulation can be used as a tool to improve the necessary function of numerous cell types found in bone. Exogenous gene delivery via a lentivirus encoding GJA1, the gene for Cx43, can be used to modulate GJIC.

To ensure low toxicity, high efficiency, and long-term expression of genetic therapeutics, viral vectors for gene replacement can be directly injected into the patient for local treatment[121] or transduced to the targeted cells before being reintroduced in the patient.[122] However, these methods have disadvantages, including increasing risks to the patient and large cell numbers and critical sterilization conditions requirements.[123] Implant placements show high potential for efficiency as a gene delivery method, by avoiding the risk of virus dispersion and infection of surrounding tissue. Moreover, as implants enable the therapeutics to be localized on the engineering biomaterials surface, it can highly increase the transduction efficiency and reduce the administration dose.[124], [125] At present, several physical methods have been used to enhance biomolecule-biomaterial conjugation, such as surface adsorption,[125] physical entrapment/encapsulation,[126] and affinity binding,[127] which often use organic solvents that can pose potential cytotoxicity. Another concern of physical methods is that physical interactions are generally weak, causing biomolecule release.[51] Therefore, chemical reactions by solvent-free methods present a strong potential to enhance the retention of biomolecules by modifying the surface of biomaterials with highly specific functional groups for the molecule of interest.

Chemical vapor deposition (CVD) polymerization is a surface modification method that uses reactive functional poly(*p*-xylylene) (PPX) for surface engineering of various biomaterials. By accommodating different reactive functional groups into their chemical structure, these substituted PPX coatings offer an applicable strategy for the specific covalent immobilization of biomolecules while maintaining their biocompatibility.[10], [11], [52] In our previous research, a thin polymer

layer with ester groups was generated on three-dimensional biomaterials surface by CVD polymerization, such as polylactic-co-glycolic acid (PLGA), polycaprolactone (PCL), and titanium (Ti), to bind anti-adenovirus antibody[124], [128], [129] The designed adenoviral vector was further conjugated through antigen-antibody reaction. This procedure provides an effective method for direct gene delivery in a more controlled and temporal manner. Our previous studies also reported the potential of bio-orthogonal CVD co-polymer coatings for precise immobilization of multiple biomolecules[10], [11], [52] or establishing biological signaling gradient for further biochemical modification after deposition.[130]

In this study, a lentivirus delivering GJA1 was bound to a titanium (Ti) surface using a CVD copolymer coating and was used to increase GJIC in MSCs. To improve MSC binding and future targeting in heterogeneous environments, DPIYALSWSGMA (DPI), an MSC-binding peptide discovered via phage display against clonally derived human MSCs known to form bone *in-vivo*[131] was microprinted onto the copolymer-coated surface. The objective of this study was to develop a co-polymer coating, which binds viral particles and peptides to a surface to enhance cell-cell communication among MSCs. Such modified coatings then are used for purposes of enhancing MSC differentiation, and tissue coordination and be used as coatings on bone implants.

4.3.2 Experimental Methods

Chemical Vapor Deposition (CVD) Polymerization

Titanium substrates were manufactured from 1.0 inch x 0.02 inch (diameter x thickness) titanium discs by slicing 1 cm x 1 cm substrates using a Computerized Numerical Control (CNC) machine. A layer of co-polymer was deposited on titanium substrates via a custom-built CVD system as shown in Scheme 4-2. The synthesis of 4-(3,4-Dibromomaleimide)[2.2]paracyclophane and 4-pentafluorophenyl-[2.2]paracyclophane used in this study were described elsewhere. A 1:1

molar mixture of two precursors was sublimated into a gas phase at the right end of the CVD tube which was about 100 ^{o}C. Inert gas Ar, with 20 sccm flow rate, carried them into the pyrolysis zone where the furnace was about 550 ^{o}C. Subsequently, the reactive species were transferred into the deposition zone, with substrates on a rotating stage set to about 15 ^{o}C. The wall of the deposition chamber was adjusted to 120 ^{o}C to prevent residual deposition. The absolute pressure of the system was controlled at 0.1 mbar.

Surface Characterization via X-ray Photoelectron Spectroscopy (XPS)

XPS results were measured by monochromatic Axis Ultra X-ray photoelectron spectrometer (Kratos Analyticals, UK) with Al Kα X-ray source at 160 eV and 20 eV for survey and high-resolution spectra, respectively. All spectra were calibrated with a binding energy of C 1s at 285 eV.

Immobilization of Anti-lentivirus Antibody

The polymer coated Ti substrates were sterilized in 70% ethanol for 1 hr after CVD polymerization. Each sample was then added to 1ml 10ug/ml solution of anti-lentivirus antibody (anti-VSV-G antibody) in phosphate-buffered saline (PBS) and incubated on a stage rotator at 4 °C. After overnight incubation, PBS was used to rinse samples 5 times (5 mins per time) to remove the non-immobilized primary antibody.

Verification of Anti-lentivirus Antibody Binding

After incubation in primary antibody solution and rinsed by PBS, the samples were then incubated in DPBS solution containing 10μ/ml AlexaFluor 488 Goat anti-Mouse IgG secondary antibody (Invitrogen, Inc.), 0.02% (v/v) Tween20 and 0.1% (w/v) bovine serum albumin (Sigma-Aldrich, Inc.) for 1 hour under room temperature, followed by 5 x 5 min PBS rinses. Afterward, fluorescence microscopy (EVOS M7000) and ImageJ were used to quantify and compare the fluorescence signals obtained on polymer-coated and uncoated substrates.

Immobilization of Peptide

Cysteine functionalized DPI peptide was synthesized by Proteomics & Peptide Synthesis Core, University of Michigan. Microcontact printing (μCP) was used here to immobilize the peptide on antibody-attached polymer surfaces. PDMS stamps were created as described elsewhere. After oxidizing for 10 mins by UV-ozone, the stamps inked with peptide solution (10 μg/ml in PBS) were kept in contact with the surface of the sample for 4 hr. After stamps removal, the patterned samples were rinsed thoroughly with PBS and deionized water. The immobilization reaction in solution without using μCP with the same reaction condition was the same as described above.

Lentivirus Immobilization (performed by Merjem Mededovic)

After immobilizing both antibody and peptide on coated Ti, the samples were incubated in lentivirus solution (3 x 106 particles in 1 ml PBS) at 4oC for 24 hrs. The samples were then rinsed thoroughly with PBS 5 times.

Cell Culture, Transduction, and Attachment to the Material (performed by Merjem Mededovic)

Human mesenchymal stem cells (MSC) (RoosterBio Inc) were added to lentivirus and peptide co-presented samples and control samples at a density of 10,000 cells per well. Each sample was placed in an individual well in a 12-well plate and incubated for 72 h in growth media (RoosterBio Inc). All studies are performed on cells in passages 3 to 5. Live cell nuclei were stained with Hoechst 33342 and subsequently, fluorescence microscopy (EVOS M7000) and ImageJ were used to quantify and compare the fluorescence of eGFP obtained on the sample and controls.

For viral transduction, cells were seeded at 2.0 - 3.0 x105 cells per well of 6 well plates 24h prior to transduction. On the day of transduction, viral stock solution (107 cfu/ml) is added to fresh DMEM supplemented with 10% FBS to ensure MOI of interest given the seeded number of cells. Cells are incubated at 37°C for 24 hours, and the media is replaced with RoosterNourish (RoosterBio Inc) media. Imaging and protein expression analysis are performed 72 hours after media exchange.

4.3.3 Results and Discussion

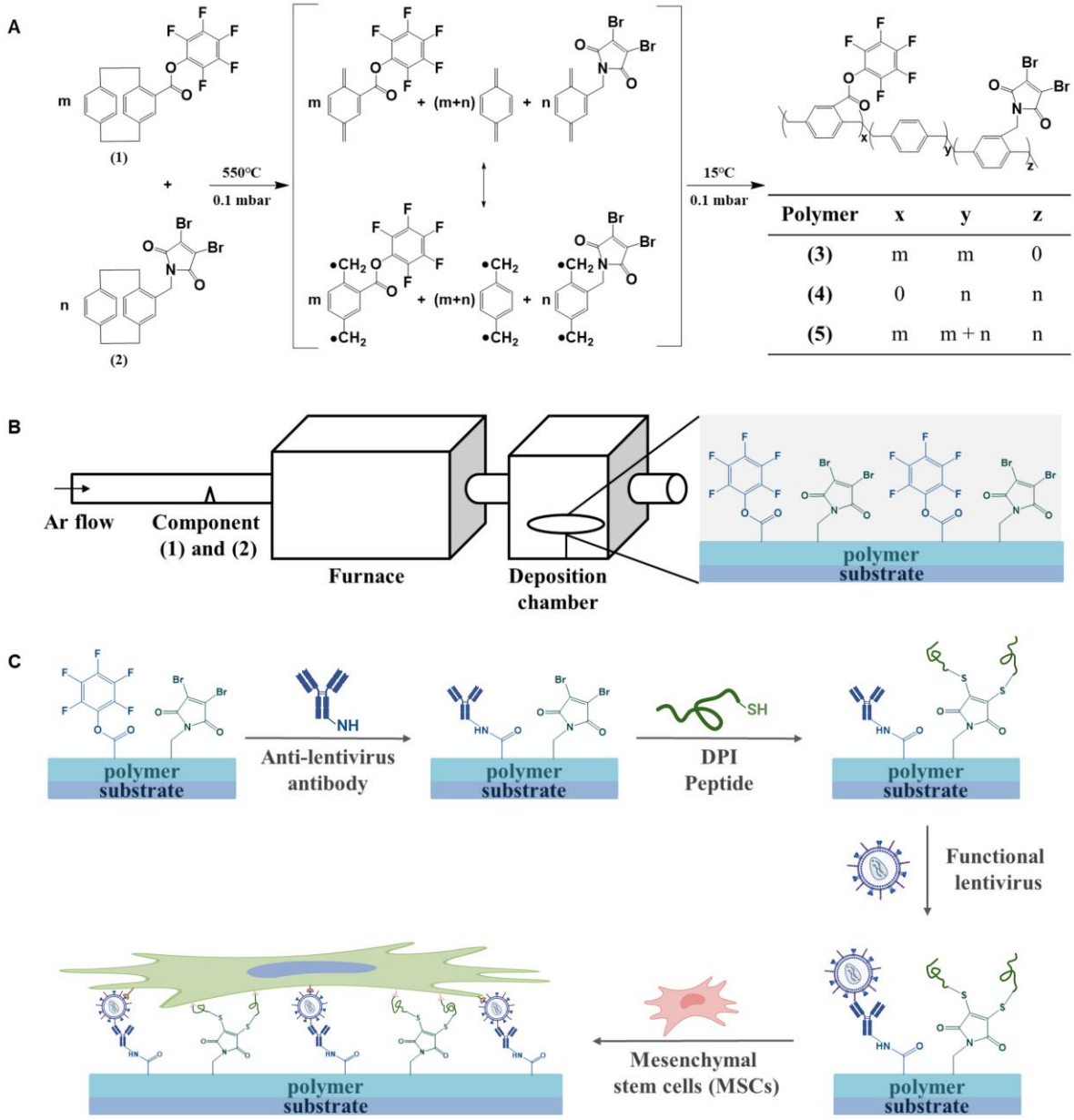

Polymer	x	y	z
(3)	m	m	0
(4)	0	n	n
(5)	m	m + n	n

Scheme 4-2: Process of coating assembly. (a) CVD copolymerization of [2.2]paracyclophanes with pentafluorophenyl ester (precursor **1**) and dibromomaleimide groups (precursor **2**). (b) Copolymerization process in a custom-made CVD system. (c) Co-immobilization process of lentivirus and DPI peptide.

A co-polymer coating was engineered as a bio-orthogonal film to immobilize viral vector and peptide simultaneously, influenced by click chemistry reactions.[132] Pentafluorophenyl ester was selected to immobilize viral vectors by active ester and amine reactions,[8] while cysteine residues on synthesized peptide offer access to thiol groups that react rapidly with maleimides.[133]The mixed precursors of 4-pentafluorophenyl-[2.2]paracyclophane (**1**) and 4-(3,4-dibromomaleimide)-[2.2]paracyclophane (**2**) were co-polymerized on titanium (Ti) substrates, following the chemical reaction shown in Scheme 4-2A. This polymerization process was performed in a custom-made chemical vapor deposition (CVD) system (Scheme 4-2B). The precursors were selected due to their specific side functional groups, which can bio-orthogonally immobilize different molecules with covalent bonding. Poly[4-(3,4-dibromomaleimide)-*p*-xylylene-*co*-*p*-xylylene] (**3**) and poly[(4-pentafluorophenyl ester-*p*-xylylene)-*co*-(*p*-xylylene)] (**4**) are polymers that only have one of the two functional groups. The XPS results shown in Figure 4-2A indicate the elemental composition of the top 10 nm of the sample after depositing 20 mg of Polymer **3**. They were in line with the atomic percentages that were calculated based on the chemical formula of polymer **3**, supporting the attachment of polymer on the Ti surface after CVD polymerization. The same method was used to confirm the presence of the polymer **4** coating on the Ti substrate. The table shown in Figure 4-2B reveals that the experimental chemical composition was in reasonable agreement with the theoretical chemical structure of polymer **4**. FT-IR has routinely been used to confirm the existence of known polymers by identifying special side functional groups. The FT-IR spectrum shown in Figure 4-2C reveals a characteristic band signal of C=O group at 1716 cm^{-1}. Moreover, the presence of symmetric and asymmetric C-H stretching modes were confirmed by the characteristic bands at 2855, 2927, and 3038 cm^{-1}, indicating the existence of benzene group

in the material surface. As a result, both FT-IR and XPS confirmed the presentence of polymer **4** on the Ti substrate after CVD polymerization.

A

Elements	C 1s						O 1s	F 1s
(Chemical states)	C-C/H	C-C=O	C-O	C-F	O-C=O	π→π*		
B.E [eV]	285.0	285.7	286.6	288.1	289.2	291.5	533.0	688.0
Calculated values [at%]	50	3.3	3.3	16.7	3.3	-	6.7	16.7
Experimental values [at%]	48.3 ±1.5	3.4 ±0.1	3.6 ±0.2	17.2 ±0.6	2.9 ±0.3	2.1 ±0.2	6.1 ±0.6	16.4 ±0.7

B

Elements	C 1s	O 1s	Br 3p	N 1s
B.E [eV]	285.0	533.0	185.0	401.0
Calculated Values [at%]	80.8	7.7	7.7	3.8
Experimental values [at%]	82.7 ± 1.2	7.1 ± 0.6	7.0 ± 0.5	3.2 ± 0.2

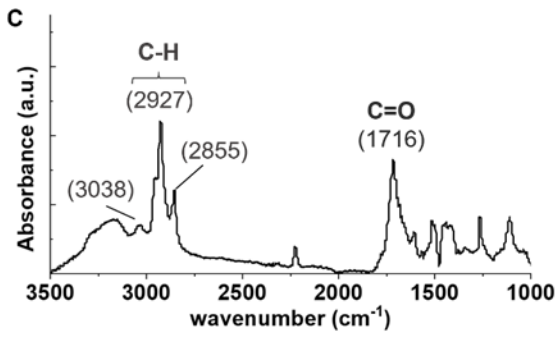

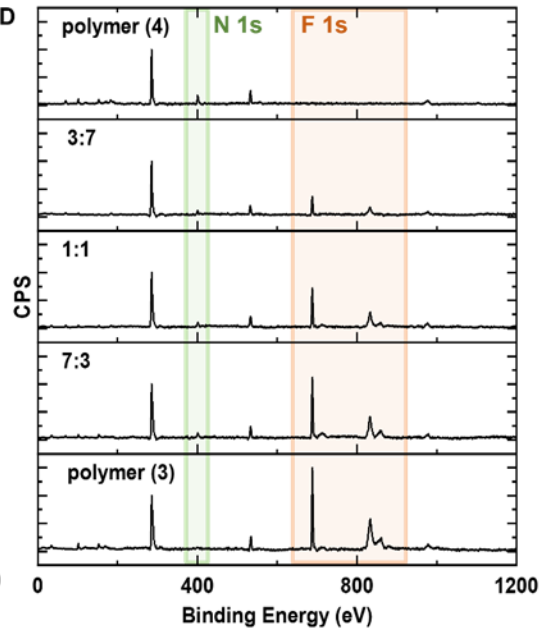

Figure 4-2: Chemical characterization of CVD samples. (a) XPS analysis of titanium discs coated with polymer 3. (b) XPS analysis of titanium discs coated with polymer 4. (c) FT-IR spectrum of polymer 4. (d) XPS spectra of copolymer with different molar ratios.

After confirming the existence of polymer **3** and **4**, mixed precursors of different molar ratios were deposited on Ti surfaces and measured by XPS, as shown in Figure 4-2D. Here, the ratios labeled in the figure reflect the ratios of the mole number of precursor 2 to the mole number of precursor 1. Besides, all XPS spectra were normalized by the peak area of C 1s for the convenience of comparing the atomic percentage of each element in different ratios of co-polymers. From top

to bottom, the usage of precursor 2 was decreasing as the usage of precursor 1 increased, reflecting the decreasing of N 1s peak area (stands for dibromomaleimide group) and the increase of F 1s peak area (stands for pentafluorophenyl ester group). The result shows that we can design the ratio between different side functional groups on the surface by changing the molar ratio of the precursors. A 1:1 mixture of precursors was used in this study to deposit co-polymer coatings.

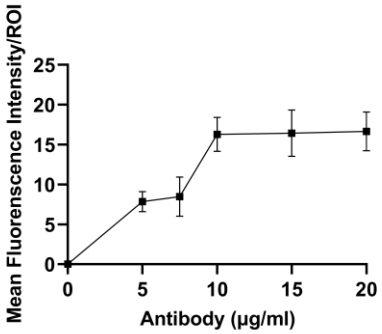

Figure 4-3: Saturation curve of antibody conjugation on CVD-coated Ti films. AlexaFluor 488 Goat anti-Mouse IgG secondary was conjugated on Ti films. Values are reported as means ± SD, n = 5.

Anti-lentivirus antibody was immobilized via ester reaction with amines, which were carried by CVD coating and antibody, respectively. To test the capacity of antibody conjugation, as well as find out the saturation point of antibody, different concentration varied from 5 µg/ml to 20 µg/ml was used. AlexaFluor 488 Goat anti-Mouse IgG secondary antibody was used as a model antibody, confirming the conjugation of primary antibody on CVD films via immunofluorescence. Saturation of the CVD functional groups was observed at antibody levels above 10 µg/well (Figure 4-3). After determining optimal antibody amounts, lentivirus was added to the sample surface. To verify the function of CVD polymer coatings, polymer-coated and non-polymer substrates were also used. Higher mean fluorescence intensity on polymer-coated Ti was higher than the one without CVD coating (Figure 4-4A), confirming higher binding of antibodies on the polymer-

coated substrates. It is critical to emphasize, even though the IgG antibody also contains an amine group, under our conjugation conditions, IgG antibodies bind only in the presence of the primary antibodies, as shown in Figure 4-4A. More lentivirus was observed to be attached to polymer-coated Ti surface than non-polymer substrate in Figure 4-4B, confirming the binding between anti-lentivirus and lentivirus, which can be a benefit for further material transformation. The transduction efficiency (TE) is determined from the fraction of fluorescent or antibiotic-resistant cells in the population, which reflects the efficiency of cell communication. TE of cell communication in the supernatant was utilized as a positive control, as the free virus can always find a way to bind to cells freely in 3-D. The TE in the region of interest on different samples was calculated and shown in Figure 4-4C. The results show that CVD-coated Ti samples have higher TE than all the other negative controls, confirming the function of CVD-coated Ti on biomolecule immobilization. Besides, no significant TE difference was found between supernatant samples and CVD-coated samples, indicating the surface modification methods did not affect the virus binding to the cells. Moreover, the TE of samples that incubated after 5 days was also calculated and was compared with the 3-day result, shown in Figure 4-4D. It indicates that the substrates were still functional after long-time incubation.

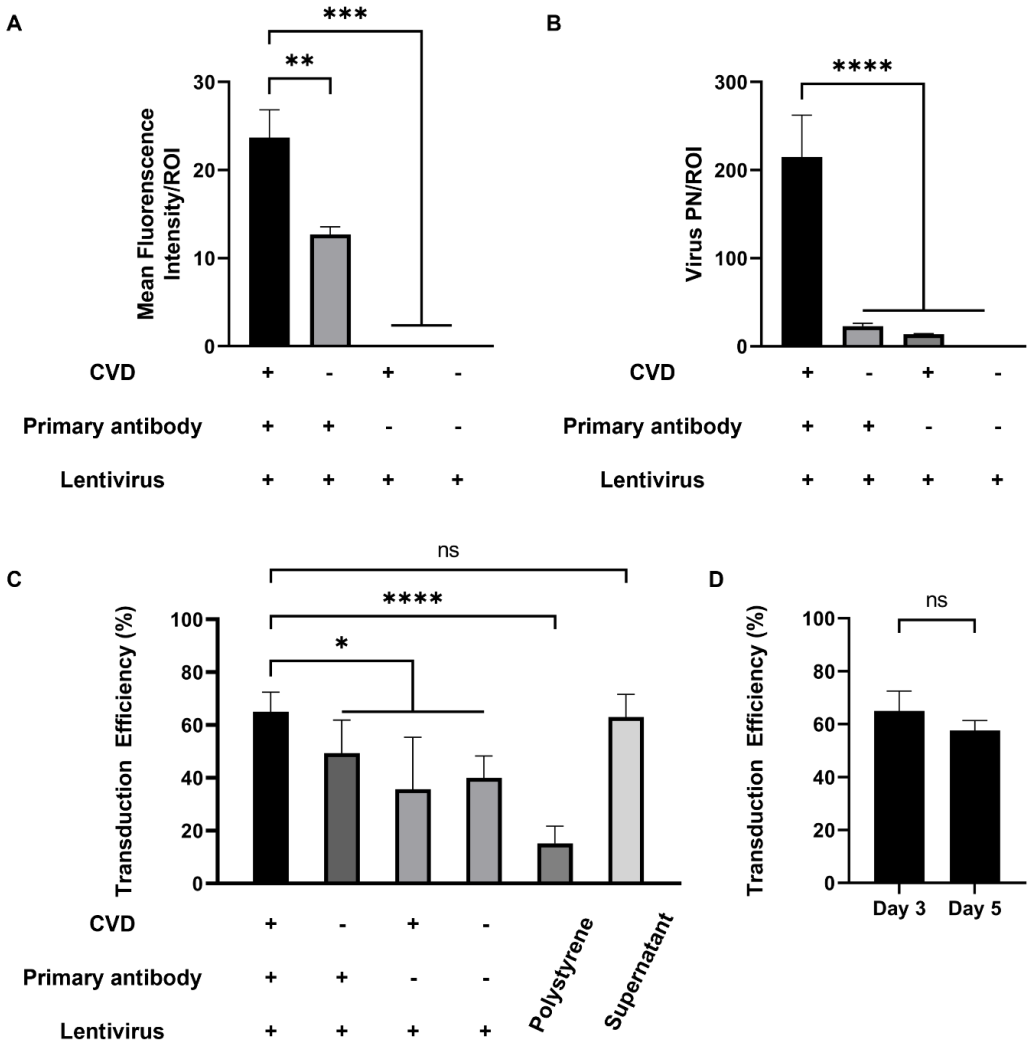

Figure 4-4: Viral binding and transduction confirmation. (a) Mean fluorescence intensity within the region of interest (ROI) of polymer-coated and non-coated discs with/without following incubation in anti-lentivirus antibody and Alexa fluor 488-conjugated secondary antibody. (b) Quantification of viral particle number (PN) on different samples by SEM imaging. (c) Transduction efficiency (%) of lentivirus on different sample surfaces/solutions after 3 days incubation. (d) Transduction efficiency (%) of lentivirus on polymer-coated Ti samples after 3 days (left) and 5 days (right) incubation. Values are reported as means ± SD, n = 5. ROI = 50μm^2. *: < 0.5; **: < 0.05; ***:< 0.005; ***: <0.0005.

We then evaluated the function of the MSCs-binding peptide after immobilization. To confirm the simultaneous surface conjugation of both the peptide and antibody was feasible, microcontact

printing (μCP) was used to enable the interaction between the peptide and reactive substrate surface (Scheme 4-1C). μCP is the process that protein can be transferred from an engineered PDMS stamp to a substrate and has been widely used to produce arrays of biologically active proteins quickly and easily.[134] Material surface topology, such as roughness, is a critical parameter that affects the cellular response, such as adhesion and stabilization.[135] Previous research found an increase in histone acetylation in MSCs grown on μCP modified surfaces, which is an important epigenetic modification that can increase gene expression.[136] Therefore, μCP is utilized in this study to enhance the adhesion and viability of MSCs.[137] TRITC-conjugated peptides were utilized to confirm the binding efficiency of μCP methods. 100 mg/ml TRITC-peptide in PBS solution was prepared as ink to print onto copolymer-coated Ti sample surfaces. The peptide was immobilized onto copolymer coating through the rapid reaction between the thiol group and maleimides. The same peptide system was used as a control method to assess the peptide binding onto the surfaces in the solution. Figure 4-5 demonstrates clear fluorescence patterns on the sample surface after μCP (Figure 4-5B), while rarely fluorescence peptide had been detected by solution immobilizing method (Figure 4-5A), indicating that μCP provides a more intimate contact between peptide and surface that enables a higher efficiency compared with the reaction in solution. After that, the TE in the region of interest for samples that bond with peptide, scramble peptide, and no peptide was calculated. As shown in Figure 4-6A, the DPI peptide that was immobilized via μCP increased the TE from 60% to 82%. Moreover, there was a 2.7x fold increase in cell binding with μCp immobilized peptide samples as shown in Figure 4-6B, confirming the MSC-binding function of DPI peptide.

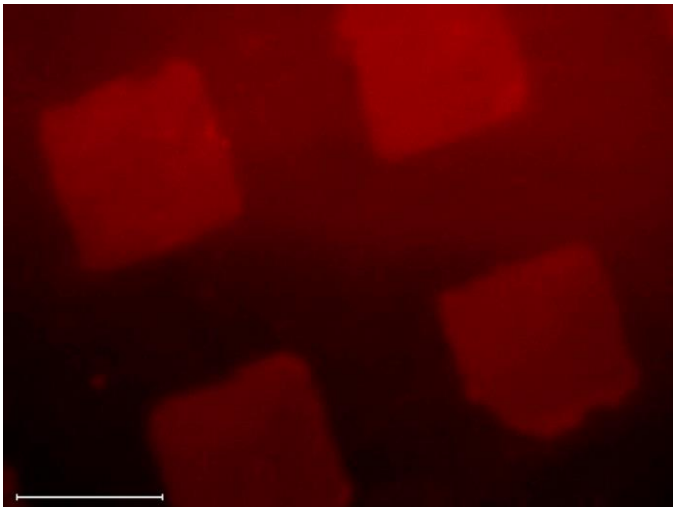

Figure 4-5: Fluorescence image of TRITC-DPI-GGC peptide binding on CVD-coated substrates, using μCP for 4 hr at room temperature. Scale bar = 275 nm.

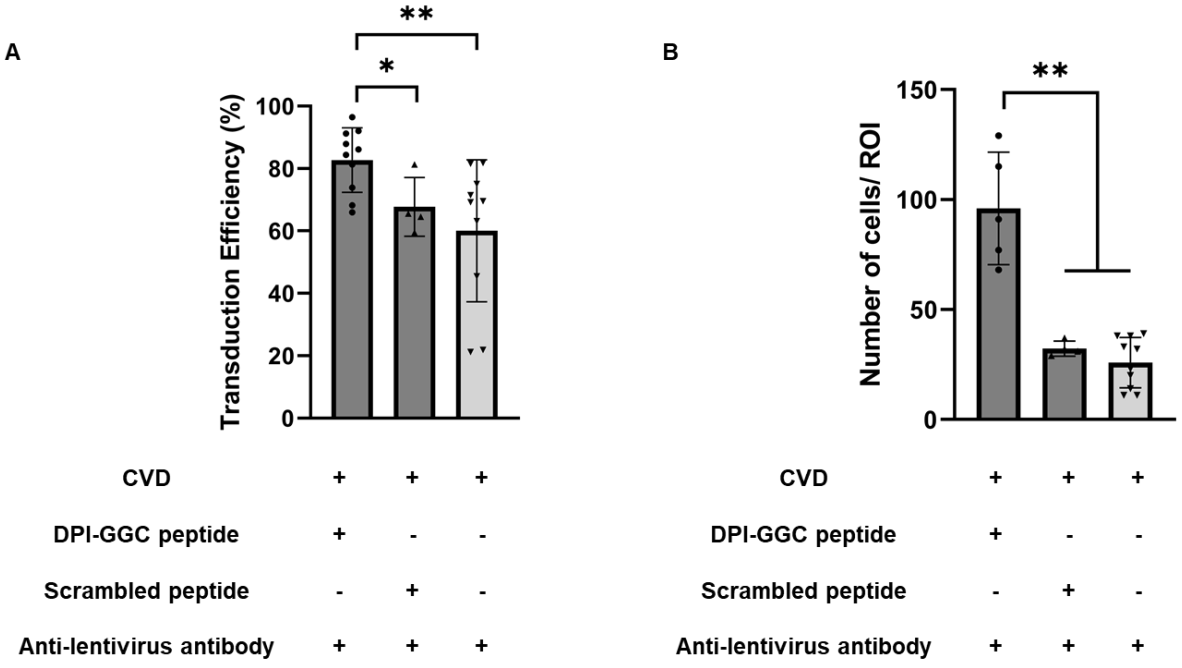

Figure 4-6: Effect of MSC bonding peptide on viral transduction. (a) Transduction efficiency (%) and (b) the number of cells on samples with DPI peptide, with scrambled peptide, and without peptide. Values are reported as means ± SD. ROI = 50μm^2. *: < 0.5; **: < 0.05

4.3.4 Conclusion

Immobilized lentivirus particles transduce MSCs at a comparable level to lentiviral particles in suspension, both at levels above 60%, a common benchmark for lentivirus transduction efficiency (TE). If any components of the coating are missing, the TE falls below the benchmark. Transduction is followed by a 2x fold increase in Cx43 expression and a 1.8x fold increase in cell communication. When DPI, the MSC binding peptide, is microprinted onto the surface, as opposed to adsorbed onto the coating, the number of cells attached to the surface increases 3x fold. With the addition of DPI, the TE increases allowing for a lower multiplicity of infection (MOI), which is beneficial for cell health and genetic stability. These results confirmed the usage of CVD polymer coatings as a transferred biomaterial and its ability to precisely immobilize different biomolecules.

These data demonstrate the utility of gene delivery coating with immobilized biomolecules to recruit and bind target cell populations to the surface. This co-immobilization approach reduced the drawbacks of gene therapy, poor TE, and off-target effects, thus broadening the utility of lentiviral gene therapy for a variety of tissue engineering purposes. Future work includes using the coating to amplify MSC differentiation, and its use *in vivo* as a coating on orthopedic internal fixation devices to expedite bone fracture healing.

Chapter 5 Conclusion and Future Direction

5.1 Conclusion

The work described in this dissertation serves as an extension to previous work on CVD polymerization described in [9], [27], [44], [128], [129]. Specifically, this dissertation further addressed the mechanistic studies into interfacial interactions, utilizing reactive poly(*p*-xylylene) coating. In Chapter 2, the fundamental mechanism of area-selective CVD polymerization was analyzed. It addressed that working pressure and deposition temperature have an effect on the deposition process. These two thermodynamic parameters have the ability to switch selective properties. Deposition of area-selective polymer on unfavored substrates revealed that the monomer follows the same deposition/polymerization behavior under suitable deposition conditions. Furthermore, Chapter 4 addressed that mass is also an influencing parameter of selectivity and demonstrated the ability of area-selective CVD polymerization onto 3-D complex geometries, suggesting the potential use of area-selective CVD as a bottom-up fabrication strategy. Moreover, this dissertation also demonstrated the use of CVD polymer coating as a surface modification method for biological applications. Chapter 4 describes the ability of CVD polymerization to form an initiator coating, followed by an ATRP process to form polymer brushes that prevent the adhesion of cells. Besides that, Chapter 4 also introduced a bio-orthogonal polymer film that is copolymerized by CVD polymerization, allowing simultaneously the precise conjugation of multiple functional biomolecules. Lentivirus and MSC-binding peptides can be co-presented on this polymer surface and worked together for efficient viral-based gene delivery therapy.

5.2 Future Direction

5.2.1 Future Mechanism Study Directions for Area-selective CVD

Temperature, pressure, and mass study on patterned substrates

It has been demonstrated in Chapter 2 and 3 that deposition temperature, working pressure, and feeding mass are all parameters influencing the area-selective property of functional PPX. However, only flat substrates were used to detect the area-selective properties. In order to study the effects of these engineering parameters on 3-D nanostructures with complex geometry, different deposition conditions should be used in future studies to evaluate their influence and extend the application from flat substrates to hybrid substrates consisting of two or more materials in close proximity to each other with complex geometries. Meanwhile, it will be essential to understand the mechanism of CVD polymerization on 3-D geometry and compare it with the 2-D mechanism that we described in this dissertation.

Height study of polymer on patterned substrates

In Chapter 3, the feature size or spacing of patterned substrates has been demonstrated does not affect the selectivity of polymers on the 3-D nano-structure surfaces. However, polymer films that were deposited on the substrates were lower than the height of metal substrates. To investigate if the reactive monomer/polymer would diffuse from one substrate surface to another, a future prospect would be to examine the area-selectivity of polymer films on patterned substrates with higher thickness than the pattern height.

Screening of effects of substituted PPX side-functional groups

The previous study has demonstrated that the side functional groups of substituted PPX have a function on the selective property. The side functional groups on PPX have been found to help form different films, including hydrophilic films,[138] hydrophobic films,[139] superhydrophobic films,[139] pattern chemical groups on surfaces,[11] linear chemical gradients of multiple monomers,[140] photo-patternable coatings,[141] and as a means of promoting further bio-functionalization.[11] In this case, a future outlook would be to screen the interaction between different side functional groups and metal substrates and provide an operating guidance of area-selective deposition.

5.2.2 Future Directions for Bio-orthogonal CVD Polymer Coatings

Developing a 3-D matrix for cell precisely adhesion

As shown in Chapter 4.2,[100] a 2-D biomaterial fabrication strategy has been developed by combining the CVD-initiated ATRP and OVJP process, which can be used to decide the adhesion points of cells. We can also extend this strategy into the 3-D matrix to mimic the real extracellular matrix environment with surface modification for the precise adhesion of cells. Lahann Lab has recently demonstrated a modified electrospinning process, 3-D jet writing, which offers customizable pore geometries and scalability of scaffolds.[142] A future outlook would be to apply our fabrication strategy to different scaffolds and examine their use in biological applications.

Developing 3-D biomaterial for gene therapy

Reactive co-poly(*p*-xylylene) coatings prepared by CVD polymerization can be utilized to surface modify and conjugate biomolecules on a broad range of materials, as demonstrated in Chapter 4.3. However, the flat substrates used in this work limited the application of biomaterial

in biomedical applications that require biomaterials with different shapes. A future study would be to examine the coating process on 3-D materials, such as Ti rods with small diameters, in *in-vitro* and *in-vivo* studies to apply CVD-based gene delivery therapy to different biomedical applications.

Bibliography

[1] M. Wang *et al.*, 'CVD Polymers for Devices and Device Fabrication', *Advanced Materials*, vol. 29, no. 11, p. 1604606, Mar. 2017

[2] J. L. Yagüe, A. M. Coclite, C. Petruczok, and K. K. Gleason, 'Chemical Vapor Deposition for Solvent-Free Polymerization at Surfaces', *Macromol Chem Phys*, vol. 214, no. 3, pp. 302–312, Feb. 2013

[3] P. Kovacik, M. Wang, N. Chen, D. Han Kim, H. Sojoudi, and K. K. Gleason, 'Polymer Thin Films and Surface Modification by Chemical Vapor Deposition: Recent Progress', *Annu. Rev. Chem. Biomol. Eng*, vol. 7, pp. 373–93, 2016

[4] W. F. Gorham, 'A New, General Synthetic Method for the Preparation of Linear Poly-p-xylylenes', *JOURNAL OF POLYMER SCIENCE: PART A-1*, vol. 4, pp. 3027–3039, 1966.

[5] X. Wang *et al.*, 'Room Temperature Resistive Volatile Organic Compound Sensing Materials Based on a Hybrid Structure of Vertically Aligned Carbon Nanotubes and Conformal oCVD/iCVD Polymer Coatings', *ACS Sens*, vol. 1, no. 4, pp. 374–383, Apr. 2016

[6] M. H. Gharahcheshmeh, K. K. Gleason, M. H. Gharahcheshmeh, and K. K. Gleason, 'Device Fabrication Based on Oxidative Chemical Vapor Deposition (oCVD) Synthesis of Conducting Polymers and Related Conjugated Organic Materials', *Adv Mater Interfaces*, vol. 6, no. 1, p. 1801564, Jan. 2019

[7] M. H. Gharahcheshmeh, M. M. Tavakoli, E. F. Gleason, M. T. Robinson, J. Kong, and K. K. Gleason, ‘Tuning, optimization, and perovskite solar cell device integration of ultrathin poly(3,4-ethylene dioxythiophene) films via a single-step all-dry process’, *Science Advance*, vol. 5, no. eaay0414, 2019

[8] X. Deng and J. Lahann, ‘Orthogonal surface functionalization through bioactive vapor-based polymer coatings’, *J Appl Polym Sci*, vol. 131, no. 14, Jul. 2014

[9] X. Deng, T. W. Eyster, Y. Elkasabi, and J. Lahann, ‘Bio-orthogonal polymer coatings for co-presentation of biomolecules’, *Macromol Rapid Commun*, vol. 33, no. 8, pp. 640–645, Apr. 2012

[10] F. Bally *et al.*, ‘Co-immobilization of Biomolecules on Ultrathin Reactive Chemical Vapor Deposition Coatings Using Multiple Click Chemistry Strategies’, *ACS Appl Mater Interfaces*, vol. 5, pp. 9262–9268, 2013

[11] X. Deng, C. Friedmann, and J. Lahann, ‘Bio-orthogonal “Double-Click” Chemistry Based on Multifunctional Coatings’, *Angewandte Chemie*, vol. 123, no. 29, pp. 6652–6656, 2011

[12] Y. Xia and G. M. Whitesides, ‘Soft Lithography’, *Annu. Rev. Mater. Sci*, vol. 28, no. 1, pp. 153–184, Nov. 1998

[13] A. Kumar and G. M. Whitesidesa, ‘Features of gold having micrometer to centimeter dimensions can be formed through a combination of stamping with an elastomeric stamp and an alkanethiol “ink” followed by chemical etching’, *Appl. Phys. Lett*, vol. 63, no. 14, pp. 2002–2004, 1993.

[14] H. Y. Chen and J. Lahann, ‘Fabrication of discontinuous surface patterns within microfluidic channels using photodefinable vapor-based polymer coatings’, *Anal Chem*, vol. 77, no. 21, pp. 6909–6914, Nov. 2005

[15] H. Y. Chen, M. Hirtz, X. Deng, T. Laue, H. Fuchs, and J. Lahann, 'Substrate-independent dip-pen nanolithography based on reactive coatings', *J Am Chem Soc*, vol. 132, no. 51, pp. 18023–18025, Dec. 2010,

[16] S. G. Im, B. S. Kim, L. H. Lee, W. E. Tenhaeff, P. T. Hammond, and K. K. Gleason, 'A Directly Patternable, Click-Active Polymer Film via Initiated Chemical Vapor Deposition', *Macromol Rapid Commun*, vol. 29, no. 20, pp. 1648–1654, Oct. 2008

[17] M. T. Raimondi, S. M. Eaton, M. M. Nava, M. Laganà, G. Cerullo, and R. Osellame, 'Two-photon laser polymerization: From fundamentals to biomedical application in tissue engineering and regenerative medicine', *Journal of Applied Biomaterials and Functional Materials*, vol. 10, no. 1. Wichtig Publishing Srl, pp. 56–66, 2012

[18] S. J. Yu *et al.*, 'Initiated Chemical Vapor Deposition: A Versatile Tool for Various Device Applications', *Adv Eng Mater*, vol. 20, no. 3, p. 1700622, Mar. 2018

[19] J. Kim *et al.*, 'Chemically Tunable Organic Dielectric Layer on an Oxide TFT: Poly(p-xylylene) Derivatives', *ACS Appl Mater Interfaces*, vol. 13, p. 43133, 2021

[20] X. Deng *et al.*, 'Orthogonal surface functionalization through bioactive vapor-based polymer coatings', *J Appl Polym Sci*, vol. 131, no. 14, Jul. 2014

[21] G. N. Parsons, 'Functional model for analysis of ALD nucleation and quantification of area-selective deposition', *Citation: Journal of Vacuum Science & Technology A*, vol. 37, p. 20911, 2019

[22] G. N. Parsons and R. D. Clark, 'Area-Selective Deposition: Fundamentals, Applications, and Future Outlook', *Chemistry of Materials*, vol. 32, no. 12, pp. 4920–4953, 2020

[23] W. L. Gladfelter, 'Reviews Selective Metallization by Chemical Vapor Deposition', *Chem. Mater*, vol. 5, pp. 1372–1388, 1993.

[24] K. F. J. Kathleen M. Vaeth, ‘Selective Growth of Poly(p-phenylene vinylene) Prepared by Chemical Vapor Deposition’, *Advanced Materials*, vol. 11, no. 10, pp. 814–820, 1999

[25] K. M. Vaeth and K. F. Jensen, ‘Transition metals for selective chemical vapor deposition of parylene-based polymers’, *Chemistry of Materials*, vol. 12, no. 5, pp. 1305–1313, 2000

[26] K. Y. Suh, R. Langer, and J. Lahann, ‘Fabrication of elastomeric stamps with polymer-reinforced sidewalls via chemically selective vapor deposition polymerization of poly(p-xylylene)’, *Appl Phys Lett*, vol. 83, no. 20, p. 4250, Nov. 2003

[27] H. Y. Chen, J. H. Lai, X. Jiang, and J. Lahann, ‘Substrate-Selective Chemical Vapor Deposition of Reactive Polymer Coatings’, *Advanced Materials*, vol. 20, no. 18, pp. 3474–3480, Sep. 2008

[28] J. B. Fortin and T. M. Lu, ‘A model for the chemical vapor deposition of poly(para-xylylene) (parylene) thin films’, *Chemistry of Materials*, vol. 14, no. 5, pp. 1945–1949, 2002

[29] I. J. Lee and M. Yun, ‘Island nucleation and growth dynamics during submonolayer vapor deposition polymerization’, *Macromolecules*, vol. 43, no. 12, pp. 5450–5454, Jun. 2010

[30] R. Chau, ‘Process and Packaging Innovations for Moore’s Law Continuation and beyond’, *Technical Digest - International Electron Devices Meeting, IEDM*, vol. 2019-December, Dec. 2019

[31] M. Hoffmann, S. Slesazeck, and T. Mikolajick, ‘Progress and future prospects of negative capacitance electronics: A materials perspective’, *APL Mater*, vol. 9, no. 2, p. 020902, Feb. 2021

[32] M. Altissimo, ‘E-beam lithography for micro-/nanofabrication’, *Biomicrofluidics*, vol. 4, no. 2, p. 026503, Jun. 2010

[33] S. Ravi-Kumar, B. Lies, X. Zhang, H. Lyu, and H. Qin, ‘Laser Ablation of Polymers: A Review’, *Procedia Manufacturing*, vol. 34, pp 316-327, 2019

[34] T. Gao *et al.*, ‘Template synthesis of single-crystal Cu nanowire arrays by electrodeposition’, *Appl. Phys. A*, vol. 73, pp. 251–254, 2001

[35] Z. H. Hua *et al.*, ‘CoFe2O4 nanowire arrays prepared by template-electrodeposition method and further oxidization’, *J Alloys Compd*, vol. 427, no. 1–2, pp. 199–203, Jan. 2007

[36] L. Zhang *et al.*, ‘Molecular Beam Epitaxy of Two-Dimensional Vanadium-Molybdenum Diselenide Alloys’, *ACS Nano*, vol. 14, no. 9, pp. 11140–11149, Sep. 2020

[37] G. Boddeti *et al.*, ‘Review on nanomaterials: Synthesis and applications’, *Mater Today Proc*, vol. 18, pp. 2182–2190, 2019

[38] N. Abid *et al.*, ‘Synthesis of nanomaterials using various top-down and bottom-up approaches, influencing factors, advantages, and disadvantages: A review’, *Adv Colloid Interface Sci*, vol. 300, p. 102597, Feb. 2022

[39] G. N. Parsons and R. D. Clark, ‘Area-Selective Deposition: Fundamentals, Applications, and Future Outlook’, *Chemistry of Materials*, vol. 32, no. 12, pp. 4920–4953, 2020

[40] M. C. Barr *et al.*, ‘Direct Monolithic Integration of Organic Photovoltaic Circuits on Unmodified Paper’, *Advanced Materials*, vol. 23, no. 31, pp. 3500–3505, Aug. 2011

[41] J. Kim *et al.*, ‘Chemically Tunable Organic Dielectric Layer on an Oxide TFT: Poly(p-xylylene) Derivatives’, *Cite This: ACS Appl. Mater. Interfaces*, vol. 13, p. 43133, 2021

[42] D. J. Siegwart, J. K. Oh, and K. Matyjaszewski, ‘ATRP in the design of functional materials for biomedical applications’, *Progress in Polymer Science (Oxford)*, vol. 37, no. 1, pp. 18–37, 2012

[43] T. Chen, I. Amin, and R. Jordan, ‘Patterned polymer brushes’, *Chem Soc Rev*, vol. 41, no. 8, pp. 3280–3296, Mar. 2012

[44] R. Kumar, A. Welle, F. Becker, I. Kopyeva, and J. Lahann, ‘Substrate-Independent Micropatterning of Polymer Brushes Based on Photolytic Deactivation of Chemical Vapor Deposition Based Surface-Initiated Atom-Transfer Radical Polymerization Initiator Films’, 2018

[45] S. Waichman *et al.*, ‘Functional immobilization and patterning of proteins by an enzymatic transfer reaction’, *Anal Chem*, vol. 82, no. 4, pp. 1478–1485, Feb. 2010

[46] J. E. Gautrot, W. T. S. Huck, M. Welch, and M. Ramstedt, ‘Protein-resistant NTA-functionalized polymer brushes for selective and stable immobilization of histidine-tagged proteins’, *ACS Appl Mater Interfaces*, vol. 2, no. 1, pp. 193–202, Jan. 2010

[47] M. Weck, J. J. Jackiw, R. R. Rossi, P. S. Weiss, and R. H. Grubbs, ‘Ring-opening metathesis polymerization from surfaces’, *J Am Chem Soc*, vol. 121, no. 16, pp. 4088–4089, Apr. 1999

[48] M. K. Brinks and A. Studer, ‘Polymer brushes by nitroxide-mediated polymerization’, *Macromolecular Rapid Communications*, vol. 30, no. 13. pp. 1043–1057, Jul. 01, 2009

[49] X. Jiang, H. Y. Chen, G. Galvan, M. Yoshida, and J. Lahann, ‘Vapor-based initiator coatings for atom transfer radical polymerization’, *Adv Funct Mater*, vol. 18, no. 1, pp. 27–35, Jan. 2008

[50] K. A. Kyburz and K. S. Anseth, ‘Synthetic Mimics of the Extracellular Matrix: How Simple is Complex Enough?’, *Ann Biomed Eng*, vol. 43, no. 3, pp. 489–500, Mar. 2015

[51] Y. Zeng, J. Hoque, and S. Varghese, ‘Biomaterial-assisted local and systemic delivery of bioactive agents for bone repair’, *Acta Biomater*, vol. 93, pp. 152–168, Jul. 2019

[52] F. Xie *et al.*, 'Degradable Polymers Backbone-Degradable Polymers Prepared by Chemical Vapor Deposition', *Angewandte Chemie*, vol. 129, pp. 209–213, 2017

[53] Y. Elkasabi, H. Y. Chen, and J. Lahann, 'Multipotent polymer coatings based on chemical vapor deposition copolymerization', *Advanced Materials*, vol. 18, no. 12, pp. 1521–1526, Jun. 2006

[54] X. Jiang, H. Y. Chen, G. Galvan, M. Yoshida, and J. Lahann, 'Vapor-based initiator coatings for atom transfer radical polymerization', *Adv Funct Mater*, vol. 18, no. 1, pp. 27–35, Jan. 2008

[55] C. Cheng *et al.*, 'Advances in preparation, mechanism and applications of graphene quantum dots/semiconductor composite photocatalysts: A review', *J Hazard Mater*, vol. 424, p. 127721, Feb. 2022

[56] R. G. Hobbs, N. Petkov, and J. D. Holmes, 'Semiconductor Nanowire Fabrication by Bottom-Up and Top-Down Paradigms', *Chem. mater.*, vol. 24, no. 11, pp. 1975–1991, 2012

[57] G. N. Parsons, 'Functional model for analysis of ALD nucleation and quantification of area-selective deposition', *Journal of Vacuum Science & Technology A*, vol. 37, no. 2, p. 020911, Mar. 2019

[58] A. J. M. , M. M. J. M. , & L. J. Mackus, 'Area-selective atomic layer deposition for bottom-up fabrication of nanoelectronics', *Nevac Blad*, vol. 58, no. 2, pp. 32–34, 2020.

[59] F. Grillo *et al.*, 'Area-selective deposition of ruthenium by area-dependent surface diffusion', *Chemistry of Materials*, vol. 32, no. 22, pp. 9560–9572, Nov. 2020

[60] M. F. J. Vos *et al.*, 'Area-Selective Deposition of Ruthenium by Combining Atomic Layer Deposition and Selective Etching', *Chemistry of Materials*, vol. 31, no. 11, pp. 3878–3882, Jun. 2019

[61] A. J. M. Mackus, M. J. M. Merkx, and W. M. M. Kessels, 'From the Bottom-Up: Toward Area-Selective Atomic Layer Deposition with High Selectivity', *Chemistry of Materials*, vol. 31, no. 1, pp. 2–12, 2019

[62] M. J. M. Merkx, T. E. Sandoval, D. M. Hausmann, W. M. M. Kessels, and A. J. M. Mackus, 'Mechanism of Precursor Blocking by Acetylacetone Inhibitor Molecules during Area-Selective Atomic Layer Deposition of SiO2', *Chem. Mater*, vol. 32, p. 3345, 2020

[63] J.-O. Carlsson and J.-O. Carlsson, 'Selective vapor-phase deposition on patterned substrates', *Critical Reviews in Solid State and Material Sciences*, vol. 16, no. 3, pp. 161–212, 1990

[64] F. Bally-Le Gall *et al.*, 'Free-Standing Nanomembranes Based on Selective CVD Deposition of Functional Poly-p-xylylenes', *ACS Nano*, vol. 9, no. 2, pp 1400–1407, 2015

[65] K. M. Vaeth, R. J. Jackman, A. J. Black, G. M. Whitesides, and K. F. Jensen, 'Use of Microcontact Printing for Generating Selectively Grown Films of Poly(p-phenylene vinylene) and Parylenes Prepared by Chemical Vapor Deposition', *Langmuir*, vol. 16, no. 22, pp. 8495–8500, 2000.

[66] K. M. Vaeth and K. F. Jensen, 'Transition metals for selective chemical vapor deposition of parylene-based polymers', *Chemistry of Materials*, vol. 12, no. 5, pp. 1305–1313, 2000

[67] W. E. Tenhaeff and K. K. Gleason, 'Initiated and Oxidative Chemical Vapor Deposition of Polymeric Thin Films: iCVD and oCVD', *Adv. Funct. Mater.*, vol. 18, pp 979–992, 2008

[68] S. J. Yu *et al.*, 'Initiated Chemical Vapor Deposition: A Versatile Tool for Various Device Applications', *Adv. Eng. Mater.*, vol. 20, no. 1700622, 2018

[69] Y. Zhang *et al.*, 'Poly-para-xylylene enhanced Fe-based amorphous powder cores with improved soft magnetic properties via chemical vapor deposition', *Mater Des*, vol. 191, Jun. 2020

[70] J. Lahann, 'Vapor-based polymer coatings for potential biomedical applications', *Polym Int*, vol. 55, no. 12, pp. 1361–1370, Dec. 2006

[71] H. Y. Chen, Y. Elkasabi, and J. Lahann, 'Surface modification of confined microgeometries via vapor-deposited polymer coatings', *J Am Chem Soc*, vol. 128, no. 1, pp. 374–380, Jan. 2006

[72] / Langmuir, H.-Y. Chen, and J. Lahann, 'Designable Biointerfaces Using Vapor-Based Reactive Polymers', *Langmuir*, vol. 27, no. 1, pp. 34–48, 2011

[73] H. Nandivada, H. Y. Chen, and J. Lahann, 'Vapor-based synthesis of poly[(4-formyl-p-xylylene)-co-(p-xylylene)] and its use for biomimetic surface modifications', *Macromol Rapid Commun*, vol. 26, no. 22, pp. 1794–1799, Nov. 2005

[74] H. Nandivada, H. Y. Chen, L. Bondarenko, and J. Lahann, 'Reactive Polymer Coatings that "Click"', *Angewandte Chemie International Edition*, vol. 45, no. 20, pp. 3360–3363, May 2006

[75] M. E. Alf *et al.*, 'Chemical vapor deposition of conformal, functional, and responsive polymer films', *Advanced Materials*, vol. 22, no. 18, pp. 1993–2027, May 2010

[76] W. F. Gorham, 'A New, General Synthetic Method for the Preparation of Linear Poly-p-xylylenes', *Journal of Polymer Science Part A-1: Polymer Chemistry*, vol. 4, no. 12, pp 3027-3039, 1966

[77] H. Y. Chen, J. H. Lai, X. Jiang, and J. Lahann, ‘Substrate-selective chemical vapor deposition of reactive polymer coatings’, *Advanced Materials*, vol. 20, no. 18, pp. 3474–3480, Sep. 2008

[78] J. B. Fortin and T. M. Lu, ‘A model for the chemical vapor deposition of poly(para-xylylene) (parylene) thin films’, *Chemistry of Materials*, vol. 14, no. 5, pp. 1945–1949, 2002

[79] S. A. Kukushkin and A. v Osipov, ‘NEW PHASE FORMATION ON SOLID SURFACES AND THIN FILM CONDENSATION’, *Prog Surf Sci*, vol. 51, no. 1, p. 107, 1996.

[80] H. van Bui, F. Grillo, and J. R. van Ommen, ‘Atomic and molecular layer deposition: off the beaten track’, *Chemical Communications*, vol. 53, no. 1, pp. 45–71, 2017

[81] W. van Assche and S. B. Yakubovich, ‘Multiple orthogonal polynomials associated with Macdonald functions’, *Integral Transform Spec Funct*, vol. 9, no. 3, pp. 229–244, 2000

[82] J. J. Senkevich and S. B. Desu, ‘Poly(chloro-p-xylylene)/SiO2 multilayer thin films deposited near-room temperature by thermal CVD’, *Thin Solid Films*, vol. 322, no. 1–2, pp. 148–157, Jun. 1998

[83] S. Y. Lee, N. Mettlach, N. Nguyen, Y. M. Sun, and J. M. White, ‘Copper oxide reduction through vacuum annealing’, *Appl Surf Sci*, vol. 206, no. 1–4, pp. 102–109, Feb. 2003

[84] N. Setter *et al.*, ‘Ferroelectric thin films: Review of materials, properties, and applications’, *J Appl Phys*, vol. 100, no. 5, p. 051606, Sep. 2006

[85] Y. Fu, H. Du, W. Huang, S. Zhang, and M. Hu, ‘TiNi-based thin films in MEMS applications: a review’, *Sens Actuators A Phys*, vol. 112, no. 2–3, pp. 395–408, May 2004

[86] G. Ozaydin-Ince, A. M. Coclite, and K. K. Gleason, ‘CVD of polymeric thin films: applications in sensors, biotechnology, microelectronics/organic electronics, microfluidics, MEMS, composites and membranes’, *Rep Prog Phys*, vol. 75, no. 1, Jan. 2012

[87] R. Chau, ‘Process and Packaging Innovations for Moore’s Law Continuation and Beyond’, in *2019 IEEE International Electron Devices Meeting (IEDM)*, 2019.

[88] J. del Barrio and C. Sánchez-Somolinos, ‘Light to Shape the Future: From Photolithography to 4D Printing’, *Advanced Optical Materials*, vol. 7, no. 16, Aug. 01, 2019

[89] Y. Chen, ‘Nanofabrication by electron beam lithography and its applications: A review’, *Microelectron Eng*, vol. 135, pp. 57–72, Mar. 2015

[90] J. R. Puryear, J. K. Yoon, and Y. T. Kim, ‘Advanced fabrication techniques of microengineered physiological systems’, *Micromachines*, vol. 11, no. 8, Aug. 01, 2020

[91] H. Xu, V. Kosma, E. Giannelis, C. K. Ober, and K. Sakai, ‘EUV photolithography: resist progress and challenges’, Mar. 2018

[92] D. M. D. A. J. P. D. and R. B. O. H. Elibol, ‘Integrated nanoscale silicon sensors using top-down fabrication’, *Appl Phys Lett*, vol. 83, no. 22, 2003

[93] G. Yoo *et al.*, ‘An effective, cost-efficient extraction method of biomass from wet microalgae with a functional polymeric membrane’, *Green Chemistry*, vol. 16, no. 1, pp. 312–319, 2014

[94] R. Clark *et al.*, ‘Perspective: New process technologies required for future devices and scaling’, *APL Mater*, vol. 6, no. 5, p. 058203, May 2018

[95] T. Moss and A. Greiner, ‘Functionalization of Poly(para-xylylene)s—Opportunities and Challenges as Coating Material’, *Adv Mater Interfaces*, vol. 7, no. 11, Jun. 2020

[96] H. Y. Chen and J. Lahann, ‘Designable biointerfaces using vapor-based reactive polymers’, *Langmuir*, vol. 27, no. 1, pp. 34–48, Jan. 2011

[97] J. N. Hilfiker *et al.*, ‘Survey of methods to characterize thin absorbing films with Spectroscopic Ellipsometry’, *Thin Solid Films*, vol. 516, no. 22, pp. 7979–7989, Sep. 2008

[98] M. Koenig *et al.*, ‘Molecular Changes in Vapor-Based Polymer Thin Films Assessed by Characterization of Swelling Properties of Amine-Functionalized Poly-p-xylylene’, *Macromol Chem Phys*, vol. 221, no. 19, p. 2000213, Oct. 2020

[99] J. Lahann, D. Klee, and H. Höcker, ‘Chemical vapour deposition polymerization of substituted [2.2]paracyclophanes’, *Macromol Rapid Commun*, vol. 19, no. 9, pp. 441–445, Sep. 1998

[100] J. A. Horowitz *et al.*, ‘Printable Organic Electronic Materials for Precisely Positioned Cell Attachment’, *Langmuir*, vol. 37, no. 5, pp. 1874–1881, Feb. 2021

[101] J. Lahann *et al.*, ‘Reactive polymer coatings: A platform for patterning proteins and mammalian cells onto a broad range of materials’, *Langmuir*, vol. 18, no. 9, pp. 3632–3638, Apr. 2002

[102] H. L. Skriver and N. M. Rosengaard, ‘Surface energy and work function of elemental metals’, *Phys Rev B*, vol. 46, no. 11, p. 7157, Sep. 1992

[103] C. Messmer and J. C. Bilello, ‘The surface energy of Si, GaAs, and GaP’, *J Appl Phys*, vol. 52, no. 7, p. 4623, Aug. 1998

[104] M. Y. Chou and J. R. Chelikowsky, ‘Structural properties of the Ru(0001) surface’, *Phys Rev B*, vol. 35, no. 5, p. 2124, Feb. 1987

[105] M. Salvalaglio, R. Backofen, A. Voigt, and F. Montalenti, ‘Morphological Evolution of Pit-Patterned Si(001) Substrates Driven by Surface-Energy Reduction’, *Nanoscale Res Lett*, vol. 12, 2017

[106] C. Feng and X. Huang, ‘Polymer Brushes: Efficient Synthesis and Applications’, *Acc Chem Res*, vol. 51, no. 9, pp. 2314–2323, Sep. 2018

[107] S. B. Carter, ‘Haptotactic islands: A method of confining single cells to study individual cell reactions and clone formation’, *Exp Cell Res*, vol. 48, no. 1, pp. 189–193, Oct. 1967

[108] S. D. Hauschka and I. R. Konigsberg, ‘The influence of collagen on the development of muscle clones.’, *Proc Natl Acad Sci U S A*, vol. 55, no. 1, pp. 119–126, Jan. 1966

[109] Q. Yu, Y. Zhang, H. Wang, J. Brash, and H. Chen, ‘Anti-fouling bioactive surfaces’, *Acta Biomater*, vol. 7, no. 4, pp. 1550–1557, Apr. 2011

[110] A. Agarwal, E. Luria, X. Deng, J. Lahann, and H. Hess, ‘Landing rate measurements to detect fibrinogen adsorption to non-fouling surfaces’, *Cell Mol Bioeng*, vol. 5, no. 3, pp. 320–326, Sep. 2012

[111] C. E. Walsh, ‘Gene therapy Progress and Prospects: Gene therapy for the hemophilias’, *Gene Therapy 2003 10:12*, vol. 10, no. 12, pp. 999–1003, May 2003

[112] B. A. Bunnell and R. A. Morgan, ‘Gene therapy for infectious diseases’, *Clin Microbiol Rev*, vol. 11, no. 1, pp. 42–56, 1998

[113] I. A. McNeish, S. J. Bell, and N. R. Lemoine, ‘Gene Therapy Progress and Prospects: cancer gene therapy using tumour suppressor genes’, *Gene Therapy 2004 11:6*, vol. 11, no. 6, pp. 497–503, Feb. 2004

[114] R. Vile, S. J. Russell, and N. R. Lemoine, ‘Cancer gene therapy: hard lessons and new courses’, *Gene Therapy 2000 7:1*, vol. 7, no. 1, pp. 2–8, Jan. 2000

[115] D. Kerr, ‘Clinical development of gene therapy for colorectal cancer’, *Nature Reviews Cancer 2003 3:8*, vol. 3, no. 8, pp. 615–622, Aug. 2003

[116] A. S. Sawhney *et al.*, ‘The Basic Science of Gene Therapy’, *Science (1979)*, vol. 260, no. 5110, pp. 926–932, 1993

[117] R. Civitelli, E. C. Beyer, P. M. Warlow, A. J. Robertson, S. T. Geist, and T. H. Steinberg, ‘Connexin43 mediates direct intercellular communication in human osteoblastic cell networks.’, *J Clin Invest*, vol. 91, no. 5, pp. 1888–1896, May 1993.

[118] F. Lecanda *et al.*, ‘Gap junctional communication modulates gene expression in osteoblastic cells’, *Mol Biol Cell*, vol. 9, no. 8, pp. 2249–2258, Oct. 1998

[119] M. Ransjö, J. Sahli, and A. Lie, ‘Expression of connexin 43 mRNA in microisolated murine osteoclasts and regulation of bone resorption in vitro by gap junction inhibitors’, *Biochem Biophys Res Commun*, vol. 303, no. 4, pp. 1179–1185, Apr. 2003

[120] R. A. Rosselló, Z. Wang, E. Kizana, P. H. Krebsbach, and D. H. Kohn, ‘Connexin 43 as a signaling platform for increasing the volume and spatial distribution of regenerated tissue’, *Proc Natl Acad Sci U S A*, vol. 106, no. 32, pp. 13219–13224, Aug. 2009

[121] M. Grossman *et al.*, ‘Present address for Successful ex vivo gene therapy directed to liver in a patient with familial hypercholesterolaemia’, 1994

[122] A. Fraldi, M. Serafini, N. C. Sorrentino, B. Gentner, A. Aiuti, and M. E. Bernardo, ‘Gene therapy for mucopolysaccharidoses: In vivo and ex vivo approaches 10 Technology 1004 Medical Biotechnology’, *Ital J Pediatr*, vol. 44, Nov. 2018

[123] R. T. Franceschi, ‘Biological approaches to bone regeneration by gene therapy’, *J Dent Res*, vol. 84, no. 12, pp. 1093–1103, Dec. 2005

[124] Y. Zhang *et al.*, 'The effects of Runx2 immobilization on poly (ε-caprolactone) on osteoblast differentiation of bone marrow stromal cells in vitro', *Biomaterials,* vol. 31, no. 12, pp. 3231–3236, Apr. 2010

[125] M. Mehta, K. Schmidt-Bleek, G. N. Duda, and D. J. Mooney, 'Biomaterial delivery of morphogens to mimic the natural healing cascade in bone', *Advanced Drug Delivery Reviews,* vol. 64, no. 12, pp 1257-1276, 2012

[126] M. Geiger, R. H. Li, and W. Friess, 'Collagen sponges for bone regeneration with rhBMP-2', *Advanced Drug Delivery Reviews,* vol. 55, pp. 1613–1629, 2003

[127] S. Spriano, S. Yamaguchi, F. Baino, and S. Ferraris, 'A critical review of multifunctional titanium surfaces: New frontiers for improving osseointegration and host response, avoiding bacteria contamination', *Acta Biomater,* vol. 79, pp. 1–22, 2018

[128] S. Maekawa *et al.*, 'BMP Gene-Immobilization to Dental Implants Enhances Bone Regeneration', *Adv Mater Interfaces,* vol. 9, no. 22, p. 2200531, Aug. 2022

[129] J. Hao *et al.*, 'Multigrowth Factor Delivery via Immobilization of Gene Therapy Vectors', *Adv Mater,* vol. 28, no. 16, p. 3145, Apr. 2016

[130] Y. M. Elkasabi, J. Lahann, and P. H. Krebsbach, 'Cellular transduction gradients via vapor-deposited polymer coatings', *Biomaterials,* vol. 32, no. 7, pp. 1809–1815, Mar. 2011

[131] H. Ramaraju, S. J. Miller, and D. H. Kohn, 'Dual-functioning peptides discovered by phage display increase the magnitude and specificity of BMSC attachment to mineralized biomaterials', *Biomaterials,* vol. 134, pp. 1–12, Jul. 2017

[132] M. G. F. and K. B. S. Hartmuth C. Kolb, 'Click Chemistry: Diverse Chemical Function from a Few Good Reactions', *Angew. Chem. Int. Ed.*, vol. 40, pp. 2004–2021, 2001.

[133] A. Ross *et al.*, 'Selective and reversible binding of thiol-functionalized biomolecules on polymers prepared via chemical vapor deposition polymerization', *Langmuir*, vol. 31, no. 18, pp. 5123–5129, May 2015

[134] S. Alom Ruiz and C. S. Chen, 'Microcontact printing: A tool to pattern', *Soft Matter*, vol. 3, no. 2. pp. 168–177, 2007

[135] L. Larsson, S. P. Pilipchuk, W. V. Giannobile, and R. M. Castilho, 'When epigenetics meets bioengineering—A material characteristics and surface topography perspective', *Journal of Biomedical Materials Research - Part B Applied Biomaterials*, vol. 106, no. 5. John Wiley and Sons Inc., pp. 2065–2071, Jul. 01, 2018

[136] Y. Li *et al.*, 'Biophysical Regulation of Histone Acetylation in Mesenchymal Stem Cells', *Biophys J*, vol. 100, no. 8, pp. 1902–1909, Apr. 2011

[137] P. Lagonegro *et al.*, 'Osteoblasts preferentially adhere to peaks on micro-structured titanium', *Dent Mater J*, vol. 37, no. 2, pp. 278–285, 2018

[138] J. P. Seymour, Y. M. Elkasabi, H. Y. Chen, J. Lahann, and D. R. Kipke, 'The insulation performance of reactive parylene films in implantable electronic devices', *Biomaterials*, vol. 30, no. 31, pp. 6158–6167, 2009

[139] Y. Elkasabi *et al.*, 'Partially fluorinated poly-p-xylylenes synthesized by CVD polymerization', *Chemical Vapor Deposition*, vol. 15, no. 4–6, pp. 142–149, 2009

[140] Y. Elkasabi and J. Lahann, 'Vapor-based polymer gradients', *Macromol Rapid Commun*, vol. 30, no. 1, pp. 57–63, 2009

[141] H. Y. Chen and J. Lahann, 'Fabrication of discontinuous surface patterns within microfluidic channels using photodefinable vapor-based polymer coatings', *Anal Chem*, vol. 77, no. 21, pp. 6909–6914, 2005

[142] Jordahl JH, Solorio L, Sun H, Ramcharan S, Teeple CB, Haley HR, Lee KJ, Eyster TW, Luker GD, Krebsbach PH, Lahann J. ‘3D Jet Writing: Functional Microtissues Based on Tessellated Scaffold Architectures.’ *Adv Mater.*, vol. 30, no. 14, Apr. 2018